

Aus dem Institut für Neuropathologie  
der Medizinischen Fakultät Charité – Universitätsmedizin Berlin

**DISSERTATION**

**Spermidine-induced autophagy and its effect on Alzheimer´s  
disease pathogenesis in mice**

**Die Auswirkung der Spermidin-induzierten Autophagie auf die  
Pathogenese der Alzheimer Erkrankung im Mausmodell**

zur Erlangung des akademischen Grades  
Doctor of Philosophy (PhD)

vorgelegt der Medizinischen Fakultät  
Charité – Universitätsmedizin Berlin

von

**Kiara Freitag**

aus Düsseldorf

Datum der Promotion: 30.11.2023



# CONTENT

<b>CONTENT</b>	<b>3</b>
<b>TABLE OF FIGURES</b>	<b>4</b>
<b>LIST OF ABBREVIATIONS</b>	<b>5</b>
<b>ABSTRACT</b>	<b>6</b>
<b>ZUSAMMENFASSUNG</b>	<b>7</b>
<b>1 INTRODUCTION</b>	<b>9</b>
<b>2 METHODS</b>	<b>15</b>
<b>3 RESULTS AND DISCUSSION</b>	<b>19</b>
<b>4 CONCLUSION AND OUTLOOK</b>	<b>32</b>
<b>5 REFERENCES</b>	<b>35</b>
<b>6 EIDESSTATTLICHE VERSICHERUNG</b>	<b>39</b>
<b>7 ANTEILSERKLÄRUNG</b>	<b>40</b>
<b>8 AUSZUG JOURNAL SUMMARY LIST</b>	<b>41</b>
<b>9 PUBLIKATION</b>	<b>42</b>
<b>10 LEBENSLAUF</b>	<b>68</b>
<b>11 PUBLIKATIONSLISTE</b>	<b>69</b>
<b>12 DANKSAGUNG</b>	<b>70</b>

## TABLE OF FIGURES

<b>Figure M1.</b> Summary of hypothesis.	<b>13</b>
<b>Figure M2.</b> iPSC-derived microglia differentiation protocol.	<b>17</b>
<b>Figure M3.</b> No effect of spermidine on the amount of IBA1-positive microglia and the microglial degradation of insoluble A $\beta$ plaques.	<b>21</b>
<b>Figure M4.</b> Spermidine targets oligodendrocytes.	<b>23</b>
<b>Figure M5.</b> Spermidine reverts AD-associated proteome in microglia of APPPS1 mice.	<b>26</b>
<b>Figure M6.</b> Spermidine reverts proteomic changes in activated microglia <i>in vitro</i> .	<b>29</b>
<b>Figure M7.</b> Spermidine exhibits anti-inflammatory effects in human iPSC-derived microglia.	<b>31</b>
<b>Figure M8.</b> Graphical abstract of thesis findings.	<b>32</b>

## LIST OF ABBREVIATIONS

A $\beta$	Amyloid beta
AD	Alzheimer's disease
ATP	Adenosine triphosphate
DAM	Disease-associated microglia
EAE	Experimental autoimmune encephalomyelitis
IL	Interleukin
iPSC	Induced pluripotent stem cells
LPS	Lipopolysaccharide
MACS	Magnetic activated cell sorting
NF- $\kappa$ B	Nuclear factor 'kappa-light-chain-enhancer' of activated B-cells
OPC	Oligodendrocyte progenitor cells
poly I:C	Polyriboinosinic:polyribocytidilic acid
TNF- $\alpha$	Tumor necrosis factor alpha

## ABSTRACT

Alzheimer's disease (AD), the most common cause of dementia, is not only characterized by extracellular amyloid  $\beta$  ( $A\beta$ ) plaque formation and neurofibrillary tangles deposition, but also by microglia- and astrocyte-mediated neuroinflammation. In the last decade, impairment of autophagy has been found to be yet another important feature of AD linking neuroinflammation and  $A\beta$  pathology.

The nutritional supplement spermidine is a known autophagy activator which has been shown to induce longevity in various model organisms. Here, we investigated spermidine's therapeutic potential in the AD-like mouse model APPPS1. Oral treatment with spermidine resulted in a reduction of neurotoxic soluble  $A\beta$  at both early and late stages of pathology in APPPS1 mice. Subsequent single nuclei sequencing of hemispheres of spermidine-treated APPPS1 mice and H<sub>2</sub>O controls revealed that spermidine affected disease-associated microglia by increasing migratory and phagocytic genes. Spermidine also altered the transcriptome of oligodendrocytes. Similar to microglia, spermidine modified genes associated with anti-inflammation, proliferation, transcription and the cytoskeleton and additionally reduced heat shock response genes in oligodendrocytes. *In vitro* treatment of activated microglia, astrocytes and oligodendrocytes with spermidine reduced the release of cytokines dose-dependently, thus confirming the anti-inflammatory properties of spermidine. To complement the transcriptomics approach, a proteomics analysis of isolated microglia from spermidine-treated APPPS1 mice was performed. Spermidine reversed AD-associated changes in APPPS1 mice by promoting anti-inflammatory, cytoskeletal, autophagic and endocytic effects. An in-depth assessment of the anti-inflammatory effects of spermidine in microglia *in vitro* elucidated that spermidine targeted NF- $\kappa$ B-mediated cytokine transcription upon LPS/ATP, poly I:C and  $A\beta$  stimulation as well as the assembly of the NLRP3 inflammasome, thus reducing the release of IL-1 $\beta$  and IL-18. The anti-inflammatory effects of spermidine were further substantiated by a spermidine-mediated CNS-wide reduction in cytokine levels in the hemispheres of APPPS1 mice at late stages of the pathology. As a translational approach, activated microglia derived from human induced pluripotent stem cells were treated with spermidine validating the anti-inflammatory effects of spermidine.

Taken together, spermidine reduced glial-mediated neuroinflammation and induced cell migration, autophagy and  $A\beta$  degradation in microglia of APPPS1 mice resulting in reduced levels of soluble  $A\beta$ . Thus, spermidine supplementation presents an intriguing approach that should be further validated in AD patients.

## ZUSAMMENFASSUNG

Die Alzheimer-Krankheit (AD), eine der häufigsten Ursache für Demenz, ist nicht nur durch die Bildung von extrazellulären Amyloid  $\beta$  (A $\beta$ )-Plaques und der Ablagerung von neurofibrillären Tangles gekennzeichnet, sondern auch durch eine von Mikroglia und Astrozyten vermittelte Neuroinflammation. Im letzten Jahrzehnt wurde die Beeinträchtigung der Autophagie als ein weiteres Merkmal für die Alzheimer-Krankheit identifiziert, welches die Neuroinflammation und A $\beta$ -Pathologie miteinander verbindet.

Das Nahrungsergänzungsmittel Spermidin ist ein bekannter Autophagie-Aktivator, welcher in verschiedenen Modellorganismen Langlebigkeit induziert. Hier haben wir den therapeutischen Effekt von Spermidin im AD-ähnlichen Mausmodell APPPS1 untersucht. Die orale Behandlung mit Spermidin führte zu einer Reduktion des neurotoxischen löslichen A $\beta$  in der frühen und späten Pathologie der APPPS1 Mäuse. Die Einzel-Nukleus RNA-Sequenzierung von Hemisphären der mit Spermidin behandelten APPPS1 Mäuse und H<sub>2</sub>O-Kontrollen ergab, dass Spermidin krankheitsassoziierte Mikroglia durch Erhöhung von Migrations- und Phagozytosegenen beeinflusst. Spermidin veränderte auch das Transkriptom von Oligodendrozyten. Ähnlich wie in Mikroglia modifizierte Spermidin auch in Oligodendrozyten Gene, die mit Entzündungshemmung, Proliferation, Transkription und dem Zytoskelett in Verbindung stehen und reduzierte zusätzlich Hitzeschockreaktionsgene. In-vitro-Behandlung von aktivierten Mikroglia, Astrozyten und Oligodendrozyten mit Spermidin verringerte die Freisetzung von Zytokinen dosisabhängig und bestätigte die entzündungshemmenden Wirkung von Spermidin. Neben der Transkriptomanalyse wurde eine Proteomanalyse von isolierten Mikroglia aus Spermidin behandelten APPPS1 Mäusen durchgeführt. Spermidin kehrte die AD-assoziierten Veränderungen in APPPS1 Mäusen um, indem es entzündungshemmende, zytoskelettale, autophagische und endozytische Effekte förderte. Eine tiefgreifende Analyse der entzündungshemmenden Wirkung von Spermidin in Mikroglia *in vitro* ergab, dass Spermidin gezielt die NF- $\kappa$ B-vermittelte Zytokintranskription nach LPS/ATP, poly I:C und A $\beta$  Stimulation sowie das NLRP3-Inflammasom hemmte und so die Freisetzung von IL-1 $\beta$  und IL-18 reduzierte. Die entzündungshemmende Wirkung von Spermidin wurden durch eine ZNS-weite Reduktion der Zytokinspiegel in den Hemisphären der mit Spermidin behandelten APPPS1 Mäuse weiter untermauert. Als translationaler Ansatz wurden aktivierte Mikroglia aus menschlichen induzierten pluripotenten Stammzellen mit Spermidin behandelt, welches ebenfalls eine entzündungshemmende Wirkung von Spermidin zeigte.

Zusammenfassend reduzierte Spermidin die gliavermittelte Neuroinflammation und induzierte Zellmigration, Autophagie und den A $\beta$ -Abbau in Mikroglia von APPPS1 Mäusen, was zu einer Reduktion der löslichen A $\beta$ -Konzentration führte. Somit stellt die Spermidin-Supplementierung einen faszinierenden Ansatz dar, welcher in Zukunft weiter an Alzheimer-Patienten getestet werden sollte.

# 1 INTRODUCTION

## 1.1 Hallmarks of Alzheimer's disease

Dementia challenges our public health majorly by affecting increasing numbers of elderly people worldwide. The most prevalent cause of dementia is Alzheimer's disease (AD), in which patients suffer from progressive cognitive and functional deficits due to the degeneration of neurons in the cerebral cortex. Until today, the cure of AD by preventing AD onset or delaying AD progression still presents an urgent unmet clinical need.

AD is characterized by the aggregation of amyloid- $\beta$  ( $A\beta$ ) peptides in extracellular amyloid plaques and the formation of intracellular neurofibrillary tangles consisting of hyperphosphorylated MAP tau <sup>1</sup>. Next to these long-standing classical hallmarks of AD, in the last decades also neuroinflammation became a well-known characteristic of AD progression. Whilst neuroinflammation in form of increased cytokine levels has been found in AD patients with increasing pathology, yet accumulating data indicate that immune actions might also be sufficient for causing AD. Systemic immune challenges through the viral mimic polyriboinosinic:polyribocytidilic acid (poly I:C) induced an AD-like pathology including  $A\beta$  plaques, microglia activation and tau aggregation in wild type mice <sup>2</sup>.

Microglia are myeloid-derived resident immune cells important for the clearance and immunomodulation in the brain. Nowadays, microglia are thought to be involved in two substantial aspects of AD: the removal or failure of removal of extracellular  $A\beta$  by phagocytosis <sup>3</sup> and the production and release of cytokines resulting in progressive neuroinflammation. By means of single-cell RNA sequencing (sc-RNAseq), so-called disease-associated microglia (DAM) were identified as an AD-specific subset of microglia that are in an activated and transcriptionally distinct state. In addition to neuroinflammatory and phagocytotic changes, DAM also exhibit numerous alterations in microglial metabolism <sup>4</sup>. Although sc-RNAseq has provided valuable and detailed transcriptional knowledge of the microglial state in AD mouse models and patients, the extent to which microglial activation is beneficial or exacerbates AD is still debated. The early migratory and phagocytic response of microglia to  $A\beta$  is rather considered neuroprotective. In contrast, the chronic proinflammatory response to  $A\beta$  is characterized by a reduction in phagocytosis, migration and physiological functions leading to a neurotoxic microglia phenotype at later disease stages. To interfere with AD progression, it thus may be important to keep microglia in a balanced phagocytic and degradative state to prevent neuron loss. Next to microglia, also

astrocytes transform into a reactive phenotype, which directly affects neuronal networks and synaptic communication, thus potentially contributing to a decline in cognition in AD. Reducing astrogliosis has been shown to reveal beneficial effects on cognition <sup>5</sup>. Since myelin loss can be observed in AD as well <sup>6</sup>, restoring homeostasis in all glial cells may be required for halting or slowing the progression of AD.

## 1.2 Autophagy in AD

A highly conserved degradative pathway and quality control system, known to be defective in AD patients, is autophagy <sup>7</sup>. Macroautophagy, here referred to as autophagy, is involved in the degradation of large, long-lived proteins and organelles, in cellular remodelling and survival during nutrient starvation <sup>8</sup>. Apart from maintaining the cell homeostasis by mediating degradation, autophagic proteins act as inducers and suppressors of many different factors including inflammatory cytokines <sup>9</sup>. The autophagic cascade can be initiated by multiple stimuli such as Toll-like receptor signalling, which results in the nucleation of a double membrane. BECN1 is the key modulator for the vesicle nucleation by recruiting lipids and proteins to this autophagic membrane <sup>10</sup>. In the elongation and closure stage leading to the formation of the autophagosome, two ubiquitin like conjugation systems (ATG12-ATG5-ATG16L and ATG4B-ATG3-ATG7) contribute to the conjugation of cytosolic LC3-I to phosphatidylethanolamine to form the membrane-binding LC3-II <sup>11-13</sup>. After closing, the autophagosome fuses with late endosomes and afterwards with a lysosome leading to degradation of the cargo by acidification of the autolysosome <sup>14</sup>. Accumulating evidence demonstrates that autophagy is dysfunctional in AD patients and may therefore also contribute to the progression of the disease. Dysfunctional autophagosomes were shown to accumulate in neuronal dendrites due to defective axonal transport in rodent AD models <sup>15,16</sup>. In addition, several autophagic proteins such as BECN1 were found to be downregulated in the brains of AD patients <sup>17,18</sup>. Interestingly, growing evidence shows that autophagy increases very early in AD pathology, most likely a neuroprotective response to the appearance of A $\beta$  <sup>19</sup>. With the progression of disease pathology, the autophagy flux declines and autophagy degradation becomes compromised <sup>20</sup>. Nowadays, autophagy is thought to modulate two important A $\beta$ -related pathways. First, autophagy impairment in ATG7 KO mice resulted in increased accumulation of intraneuronal A $\beta$  and reduced extracellular A $\beta$  plaques indicating that autophagy is required for A $\beta$  secretion to protect from cognitive impairment <sup>21,22</sup>. Second, many studies show that autophagy is required for A $\beta$  clearance. Increased autophagy in a knock-in AD mouse model

interfering with the interaction of BECN1 and Bcl-2 reduced A $\beta$  plaques and improved cognition, while BECN1 KO AD mice showed the opposite effect <sup>17,23</sup>.

### 1.3 Context of the presented research

While the importance of autophagy for the functionality of neurons was shown in multiple studies, its effect on glial metabolism and neuroinflammation was rather unknown. In a previous study within our group, we studied the effect of autophagy impairment in BECN1<sup>+/-</sup> mice on the neuroinflammatory response of microglia. Our *in vitro* studies revealed that BECN1<sup>+/-</sup> microglia expressed an increased number of inflammasomes resulting in an enhanced release of IL-1 $\beta$  and IL-18 upon LPS/ATP stimulation. Increased levels of IL-1 $\beta$  were also found in BECN1<sup>+/-</sup> APPPS1 mice, indicating that selective autophagy degrades the NLRP3 inflammasome, thus regulating the neuroinflammatory response of microglia <sup>24</sup>. Meanwhile, also other autophagy-related mechanisms for microglia endocytosis of A $\beta$  were found to play a role in AD. Next to autophagy, also LC3-associated endocytosis (LANDO) protected from microglial activation, inflammation and neurotoxic A $\beta$  accumulation in an AD mouse model <sup>25</sup>. The TAM system with the receptor kinases AXL and MER was recently shown to be essential for A $\beta$  engulfment and recognition by microglia <sup>26</sup>. In summary, the maintenance of functional degradative pathways such as autophagy, LANDO and TAM-associated phagocytosis seems to be a key aspect in order to protect from AD-associated neuroinflammation and neurotoxic A $\beta$  pathology.

### 1.4 Spermidine in health and disease

As we identified autophagy impairment in microglia as an essential driver of neuroinflammation and neuroinflammation is known to promote AD pathology, we set out to pursue a therapeutic approach and to study the effect of autophagy induction on glial metabolism in AD.

Spermidine is a body-endogenous polyamine and dietary supplement, which induced autophagy in multiple tissues upon administration in aged yeast, flies, worms, mammalian cells and mice <sup>27</sup>. Although the exact mechanism underlying the autophagy induction by spermidine still remains to be elucidated, spermidine interfered with the activity of acetyltransferases such as EP300 suggesting that spermidine induces autophagy by decreasing acetylation <sup>28</sup>. Intracellularly, spermidine has pleiotropic effects ranging from

transcription to protein synthesis as well as differentiation, cell proliferation, apoptosis and tissue regeneration. The intracellular bioavailability of spermidine is determined by cellular biosynthesis, synthesis of intestinal microbiota or nutritional uptake as well as catabolism and excretion. Interestingly, spermidine concentrations in multiple tissues decline in aging humans and model organisms <sup>27</sup>, potentially resulting in a decline in autophagy observed in patients with neurodegenerative diseases such as AD.

Numerous studies revealed protective effects of spermidine administration on the manifestation of cardiac aging, metabolic syndrome and cancer in various model organisms <sup>27</sup>. Besides, spermidine also increased in the life span of yeast, flies, worms, human cells and mice <sup>29-31</sup>, making it an interesting candidate for the preventive treatment of age-associated pathologies.

Regarding neurological diseases, spermidine showed neuroprotective effects in Huntington's disease and Parkinson's disease rat models <sup>32</sup> or in murine models of accelerated aging <sup>33</sup>. Similarly, supplementation with spermidine ameliorated neuroinflammation and clinical scores in mice with experimental autoimmune encephalomyelitis (EAE) <sup>34</sup>. A few studies also revealed anti-inflammatory effects of spermidine in myeloid cells. For instance, LPS-induced cytokine release by macrophages or the microglial cell line BV2 was dampened upon spermidine treatment *in vitro* <sup>35,36</sup>. However, little was known on the effect of spermidine on microglia and to our knowledge, the effect of spermidine on other glial cells such as astrocytes and oligodendrocytes was not studied so far. The effect of spermidine in the brain was mostly studied with a focus on neurons revealing an improvement of age-related synaptic alterations and cognition in *Drosophila* and mice upon spermidine treatment <sup>37,38</sup>. Spermidine also improved spontaneous regeneration of axons after peripheral lesion of the dorsal root ganglion neurons <sup>39</sup> as well as age-associated deterioration of hippocampal mossy fiber (MF-CA-3) synaptic transmission and plasticity <sup>40</sup>. Additionally, spermidine reduced tau fibrillization and oligomerization *in vitro* and dysregulating the polyamine metabolism by overexpression of AZIN2 increased tau pathology in tau PS19 mice <sup>41</sup>. Notably, it was recently shown that orally supplemented spermidine can indeed cross the blood-brain barrier and might therefore directly affect the cells in the brain <sup>38</sup>.

Based on all the existing data, spermidine might provide a promising therapeutic agent to tackle neuroinflammation, glial-associated changes and A $\beta$  pathology in AD.

## 1.5 Aims and methodological insights

Thus, the aim of this thesis was to elucidate the effects of spermidine on AD pathology and neuroinflammation with a specific focus on glial cells. The following objectives were pursued (Fig. M1):

**Aim 1:** Investigating effects of spermidine on the A $\beta$  pathology in APPPS1 mice

**Aim 2:** Unbiased transcriptomic and proteomic analysis of spermidine-treated APPPS1 mice

**Aim 3:** Elucidating effects of spermidine on AD-associated neuroinflammation in APPPS1 mice

**Aim 4:** Investigating the underlying anti-inflammatory mechanisms of spermidine using *in vitro* model systems

**Aim 5:** Transferring murine findings into human context by using human iPSC-derived microglia

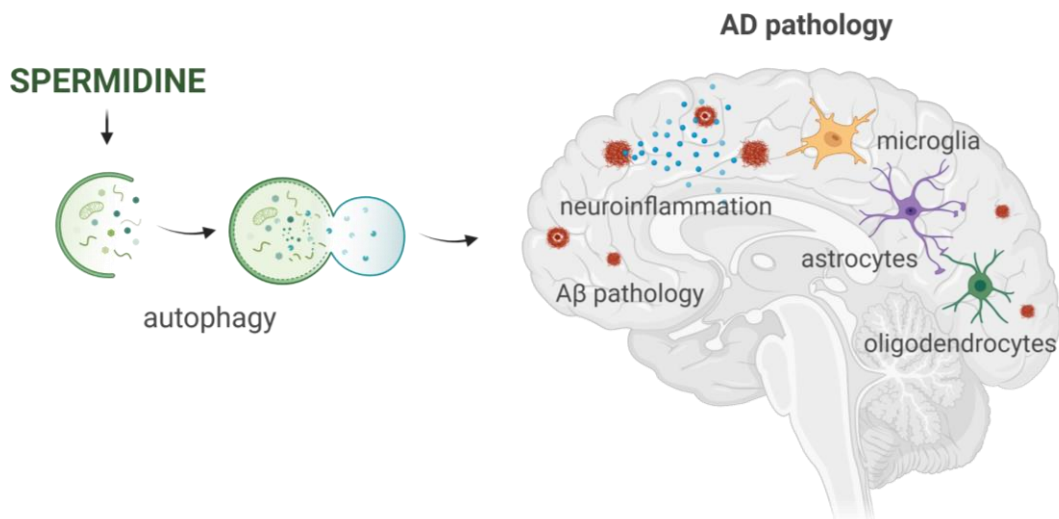


**Figure M1.** Summary of hypothesis. The effects of spermidine-mediated autophagy induction were investigated on AD pathology including the main hallmarks, A $\beta$  pathology and neuroinflammation. Furthermore, the effect on microglia, astrocytes and oligodendrocytes was determined. The figure was self-created with Biorender.com.

To give further insights into the methodology, the reasoning for the model systems chosen to assess these objectives are summarized here. Whether A $\beta$  or tau is the main driver of AD is still highly debated with literature supporting both hypotheses. In this thesis, we focused on the effects of spermidine on the amyloid pathology. The amyloid hypothesis is supported by the fact that all mutations resulting in early-onset AD occur in the A $\beta$  generation pathway. Furthermore, soluble A $\beta$ 42 from brains of AD patients was found to induce synaptic toxicity

and reduce long-term potentiation. Human A $\beta$  also induced hyperphosphorylation of tau and caused neuronal dystrophy<sup>1</sup>. As the effect of spermidine on A $\beta$  pathology *in vivo* was not investigated yet, we decided to study the effect of spermidine in the A $\beta$  expressing mouse model APPPS1. We received the protocol for the oral treatment with 3 mM spermidine via the drinking water from our collaborator Prof. Dr. Stephan Sigrist, who previously found beneficial effects of spermidine on hippocampal neurons and cardiac functions using this protocol<sup>40</sup>. The oral treatment via the drinking water offers the advantage of an easy administration and a continuous treatment over a long period of time to investigate the effects on AD development.

The APPPS1 mouse model is a common AD-like model, which carries the transgenes for the human APP with the Swedish mutation along with PSEN1 containing a L166P mutation the main risk genes for familial or early onset AD. APPPS1 mice consequently develop a strong A $\beta$  pathology including neuroinflammation at a late disease stage, with the amyloidosis starting early at 6-8 weeks of age in the cerebrum<sup>42</sup>. This model enabled us to investigate the effects of spermidine in a strong A $\beta$  pathology model and its effects on A $\beta$ -driven neuroinflammation.

For the analysis of the effects of spermidine, the newest state-of-the-art technologies ranging from single nuclei sequencing with the 10x Genomics platform, sensitive cytokine and A $\beta$  MesoScale Discovery panels and liquid chromatography tandem mass spectrometry combined with classic well-established methods as immunohistochemistry, western blot and RT-qPCR analysis were used. Additionally, a side-by-side analysis of spermidine-mediated effects on glial cells *in vivo* with in-depth mechanistic pathway analysis using primary glial cultures *in vitro* was performed.

## 2 METHODS

Methods, which were extensively described in the published manuscript <sup>43</sup>, were not repeated here, meaning only methods of additional experiments are mentioned in this section.

### *Quantification of IBA1-positive plaque-associated microglia cells*

Fixed hemispheres were cryosectioned as described in the publication <sup>43</sup>, permeabilized with TBS and 0.2% Triton X-100 for 10 min and blocked with TBS and 10% goat serum (NGS) for 1 h, before incubation with the anti-4G8 antibody specific for A $\beta$  (1:1,000 dilution, Covance, SIG39320) and the microglia specific antibody IBA1 (1:500 dilution, Wako, 019-19741) for 48 h at 4°C in TBS with 5% NGS. The secondary antibodies Alexa Fluor 488 goat anti-mouse IgG (H+L) (1:500 dilution, Invitrogen, A11001) and Alexa Fluor 647 goat anti-rabbit IgG (H+L) (1:500 dilution, Invitrogen, A21244) were added for 2 h at RT. Images were taken on a Leica TCS SP5 confocal laser scanning microscope. Three regions of 10 serial coronal sections were imaged per animal using a step size of 1  $\mu$ m for each z-stack confocal image.

As previously described <sup>44</sup>, maximum projections of the confocal stacks were used to quantify the expression levels of IBA1 and 4G8 positive plaques, radial intensity profiles, cell numbers and distances to the nearest plaque. The quantification was performed by the Advanced Medical Bioimaging Core Facility (AMBIO, Dr. Niclas Gimber, Charité-Universitätsmedizin Berlin) in an automated manner using custom-written ImageJ macros (segmentation) <sup>45</sup> and python scripts (radial profiles and other statistics), which were uploaded to GitHub (<https://github.com/ngimber/AlzheimersWorkflow>). The median from all images per animal was calculated. The displayed data represents the mean and SEM of all animals from one group. In the histogram, the data were binned image-wise and histograms and radial intensity profiles were normalized (divided by its own integral) and then pooled as mentioned above. Histogram-based thresholding (Otsu binarization) <sup>46</sup> followed by watershed segmentation of the Euclidean distance map of the binary image was used for the segmentation of nuclei from blurred DAPI channels (Gaussian blur, sigma = 720 nm) using ImageJ. Cell bodies were approximated from the nuclear region by a dilation of 10 pixels (3.6  $\mu$ m). Plaques were segmented from the blurred 4G8 channel (Gaussian blur, sigma = 7.2  $\mu$ m) with subsequent histogram-based thresholding (based on the method from Ridler and Calvard <sup>47</sup>, "default" auto-threshold function from ImageJ) by regarding only objects above 720  $\mu$ m<sup>2</sup> as plaques.

For the quantification of the IBA1 expression levels, the mean intensities within segmented cell bodies were used. IBA1-positive/-negative cells were classified by auto-thresholding (Otsu's method on all cell-specific expression levels within one image). For the subsequent analyses only IBA1-positive cells were used (e.g. radial intensity profiles, cell numbers and distances to the nearest plaque). For each microglia cell, we determined the size of the nearest plaques using the segmented regions mentioned above. We calculated radial intensity profiles for all channels around the center of mass of the segmented nucleus.

#### *Isolation and culture of oligodendrocytes*

Neonatal mice were sacrificed by decapitation, the brain dissected and the hemispheres dissociated into a single cell suspension using the Neural Tissue Dissociation kit (P) (Miltenyi Biotec, 130-092-628) in C-tubes (Miltenyi, 130-096-334) on a gentleMACS Octo Dissociator with Heaters (Miltenyi Biotec, 130-096-427). Afterwards, the brain cell suspension was labelled with O4 microbeads (Miltenyi Biotec, 130-093-634), strained and passed through MS columns (Miltenyi Biotec, 130-042-201) placed on an OctoMACS™ manual separator. Subsequently, oligodendrocytes were collected by column flushing and cultured in MACS® Neuro Medium (Miltenyi Biotec, 130-093-570) supplemented with 50 U/ml penicillin/streptomycin (Sigma, P0781-20ML), 2 % NeuroBrew-21 (Miltenyi Biotec, 130-093-566), 0.25 % L-Glutamine (0.5 mM; Thermo Fisher, 25030-024), 5 ng/ml human FGF-2 and 10 ng/ml human PDGF-AA. Half of the medium was changed every other day and oligodendrocytes were treated with IL-1 $\beta$  (10 ng/ml, Miltenyi Biotec, 130-094-053), poly I:C (50  $\mu$ g/ml, InVivoGen, tlr-picw-250), TNF- $\alpha$  (10 ng/ml, Miltenyi Biotec, 130-101-687) or TGF- $\beta$ 3 (2 ng/ml, Miltenyi Biotec, 130-094-007) after 6 days in culture. Cells were pre-treated with the indicated concentration of spermidine for 2 h and the above mentioned stimuli were added to the medium for another 24 h.

#### *ATP measurement*

To measure the ATP production within microglia cells, we used the ATP Assay Kit (Abcam, ab83355) and followed the manufacturer's instructions. In brief, cells were treated with 30  $\mu$ M and 100  $\mu$ M spermidine for 6 h and harvested by scraping. 300,000 cells per condition were lysed with the provided ATP assay buffer followed by a deproteinization by precipitation using 2 M potassium hydroxide and 4 M perchloric acid. The deproteinized sample was mixed with an ATP reaction mix and the fluorescent signal of each sample was measured in duplicates. The ATP concentration was calculated using a standard curve and the background fluorescence was subtracted.

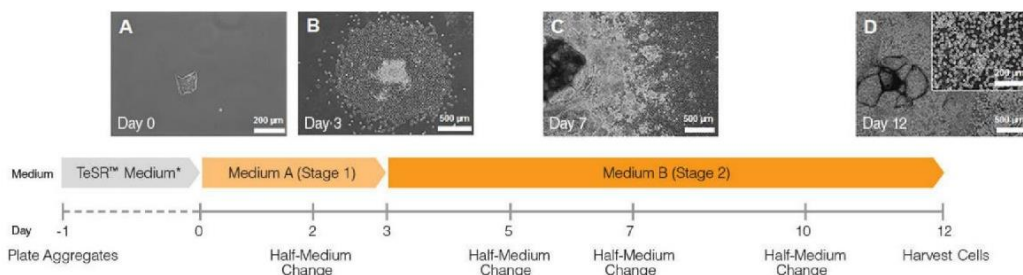
### Proteomics of *in vitro* cultures

Neonatal microglia were pre-treated with 30  $\mu$ M spermidine for 2 h. Afterwards, 1  $\mu$ g/ml LPS (Sigma, L4391-1MG) was added for 3 h followed by 2 mM ATP (Sigma Aldrich, A6419-5 g) for 45 min. 300,000 cells were pelleted and further processed for mass spectrometry as described in the published manuscript <sup>43</sup>.

### iPSC-derived microglia differentiation

For the differentiation of human induced pluripotent stem cells (iPSCs) into hematopoietic stem cells and the subsequent differentiation into microglia, the manufacturer's protocol of three kits provided by StemCell technologies were followed with a few adjustments (STEMdiff™ Hematopoiesis Kit (05310), STEMdiff™ Microglia Differentiation Kit (100-0019), STEMdiff™ Microglia Maturation Kit (100-0020)). In brief, 16-40 colonies of iPSCs per well were differentiated into hematopoietic stem cells using the provided Medium A for 3 days, followed by the second stage of differentiation using Medium B for an additional 9 days (Fig. M2a).

#### a STEMdiff™ Hematopoietic Kit



#### b STEMdiff™ Microglia Differentiation and Maturation Kit

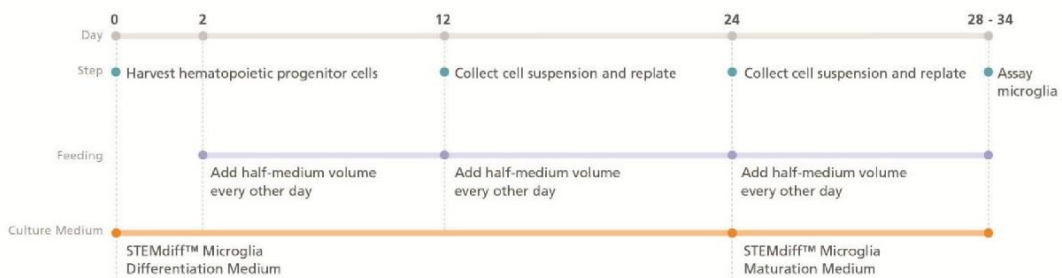


**Figure M2.** iPSC-derived microglia differentiation protocol. Human iPSCs were differentiated into hematopoietic stem cells and the subsequent differentiation into microglia using the following kits: STEMdiff™ Hematopoiesis Kit (05310), STEMdiff™ Microglia Differentiation Kit (100-0019), STEMdiff™ Microglia Maturation Kit (100-0020). The figure was adapted from the Kit manuals of StemCell technologies.

At day 12 hematopoietic cells were harvested by pipetting them up and down and subsequently seeded at a density of  $1 \times 10^5$  cells in Matrigel®-coated 6-well plates in the provided microglia differentiation medium. After 12 days of differentiation, cell suspension was collected, cells pelleted and reseeded in the same 6 well plates and differentiated for another 12 days. After the microglia differentiation for 24 days, microglia maturation was induced by collecting the cells and reseeding them into the same 6-well plate at a density of  $10^6$  cells/well using microglia maturation medium (Fig. M2b). After 4 days microglia were collected and 50,000 cells per well were seeded into uncoated 96 well plates in maturation medium. The iPSC-derived microglia were differentiated by the MDC Stem Cell Core Facility (Maren Wendt, Dr. Silke Frahm-Barske, Max Delbrück Center for Molecular Medicine Berlin) and further processed by Kiara Freitag on the following day. Microglia were treated with LPS (1  $\mu\text{g/ml}$ ), ATP (2 mM) and spermidine for the indicated periods. The supernatant was collected for ELISA using the IL-6 and IL-1 $\beta$  Human ELISA Kit (88-7066-88, 88-7261-22, ThermoFisher). The protocol described in the method section of the publication <sup>43</sup> was followed.

### *Statistics*

The statistical conditions stated in the manuscript <sup>43</sup> also apply for all additional data presented within this thesis. As controls, spermidine-treated mice were always compared to H<sub>2</sub>O-treated mice, which were housed in parallel to the spermidine cohort. The controls for each specific assay are stated in the respective method section. For *in vitro* experiments, non-treated microglia were used as a reference.

### 3 RESULTS and DISCUSSION

In this section, the main results of the publication<sup>43</sup> are summarized. To avoid redundancy, the figures of the publication are not repeated here and can be found in the publication in section 9. The figure labelling refers to the publication. Further data generated in addition to the published data are embedded in this results section and marked with “M”. Discussion points which were not mentioned in the publication were added to the respective subsection.

#### 3.1 Spermidine affects disease-associated microglia in APPPS1 mice

Oral treatment of APPPS1 mice with 3 mM spermidine starting prior disease onset at 30 days resulted in reduced levels of soluble A $\beta$ 40 at 120 days and in reduced levels of soluble A $\beta$ 40 and A $\beta$ 42 at 290 days (Fig. 1a). Interestingly, spermidine did not affect insoluble A $\beta$  levels or A $\beta$  plaques in size and number (Fig. S1b, c). As the APP production and cleavage machinery and the abundance of A $\beta$ -degrading enzymes was not affected by spermidine (Fig. S1d-g), we suspected that changes in A $\beta$  phagocytosis or degradation might account for the reduction in soluble A $\beta$ .

To receive an unbiased insight into the molecular and transcriptomic changes introduced by spermidine treatment, we performed single-nuclei RNA sequencing (snRNA-seq) of the hemispheres of 180-day-old APPPS1 mice treated with spermidine as well as APPPS1 H<sub>2</sub>O controls and WT H<sub>2</sub>O controls (Fig. 1b). The intermediate time point of 180 days was chosen to gain insights into a pathology state at which A $\beta$  plaques are present for a while, however, the pathology has not reached its end stage yet. The snRNA-seq revealed microglia to show the strongest transcriptomic changes upon spermidine treatment in APPPS1 mice (Fig. 1e). Spermidine affected the homeostatic microglia cluster 1 and the disease-associated AD-specific microglia (DAM) cluster 2. Genes associated with cell motility/ cell migration, phagocytosis, proliferation and transcription/splicing were altered by spermidine in microglia (Fig. 1f). As the most pronounced effects of spermidine detected in a gene set enrichment analysis were on cell migration, microtubule and cell adhesion pathways and the role of spermidine in regulating microglial migration was not described before, we assessed the migratory effects of spermidine *in vitro*. Matching our snRNA-seq findings,

spermidine promoted microglia migration in a scratch wound healing and in a transwell migration assay (Fig. 1h-i). These findings correlate well with very recent data showing that spermidine increased cell migration and proliferation in a porcine intestinal epithelial cell line <sup>48</sup>. During aging and especially pronounced with AD pathology microglia dynamics become impaired, leading to deficient surveillance and chemotaxis <sup>49,50</sup>. Thus, the reversal of AD-associated microglial changes on cell migration by spermidine might maintain microglia in their surveillance mode.

Interestingly, spermidine especially increased the abundance of the DAM-microglia cluster 2 (Fig. 2a) and promoted genes associated with proliferation (Fig. S2k). Even though microgliosis can be observed in AD, it is still debated whether an increase in microglia is beneficial or detrimental. As we found that spermidine increases the motility and phagocytic behavior of these DAM microglia, we rather consider the enlargement of such a population as protective.

To validate that spermidine indeed affects DAM microglia, we stained for the DAM marker and receptor tyrosine kinase AXL and found that the AXL intensity normalized to the IBA1-positive area was increased upon spermidine treatment in APPPS1 mice (Fig. 2c).

In addition, the number of IBA1-positive microglia around 4G8-positive plaques was assessed in the cortex by staining of brain sections of spermidine-treated APPPS1 and H<sub>2</sub>O control mice (Fig. M3a). The number of IBA1-positive cells 30  $\mu$ m around 4G8-positive plaques (Fig. M3b) as well as the total number of IBA1-positive cells were not altered by spermidine treatment in APPPS1 mice (Fig. M3c), supporting the snRNA-seq finding that only the DAM-microglia cell fraction was affected by spermidine. To investigate the amount of 4G8-positive plaque-associated A $\beta$  internalized by IBA1-positive microglia, radial intensity profiling of 4G8 and IBA1 was performed around the center of the nucleus of IBA1-positive microglia at plaques. No difference in the radial plots of spermidine and H<sub>2</sub>O-treated APPPS1 mice were found (Fig. M3d). This data, in correlation with Fig. S1, emphasizes that spermidine indeed did not alter the uptake of insoluble/plaque-based A $\beta$  by microglia and specifically targets the degradation of soluble A $\beta$ . This finding was further underlined by the increased degradation of fluorescently labelled oligomeric A $\beta$ , which we found upon spermidine treatment of primary neonatal microglia (Fig. 2d).

In summary, spermidine seems to keep microglia in an early activated state with protective properties such as increased phagocytosis, cell motility, cell migration and proliferation and thereby potentially induces the degradation of soluble A $\beta$ .

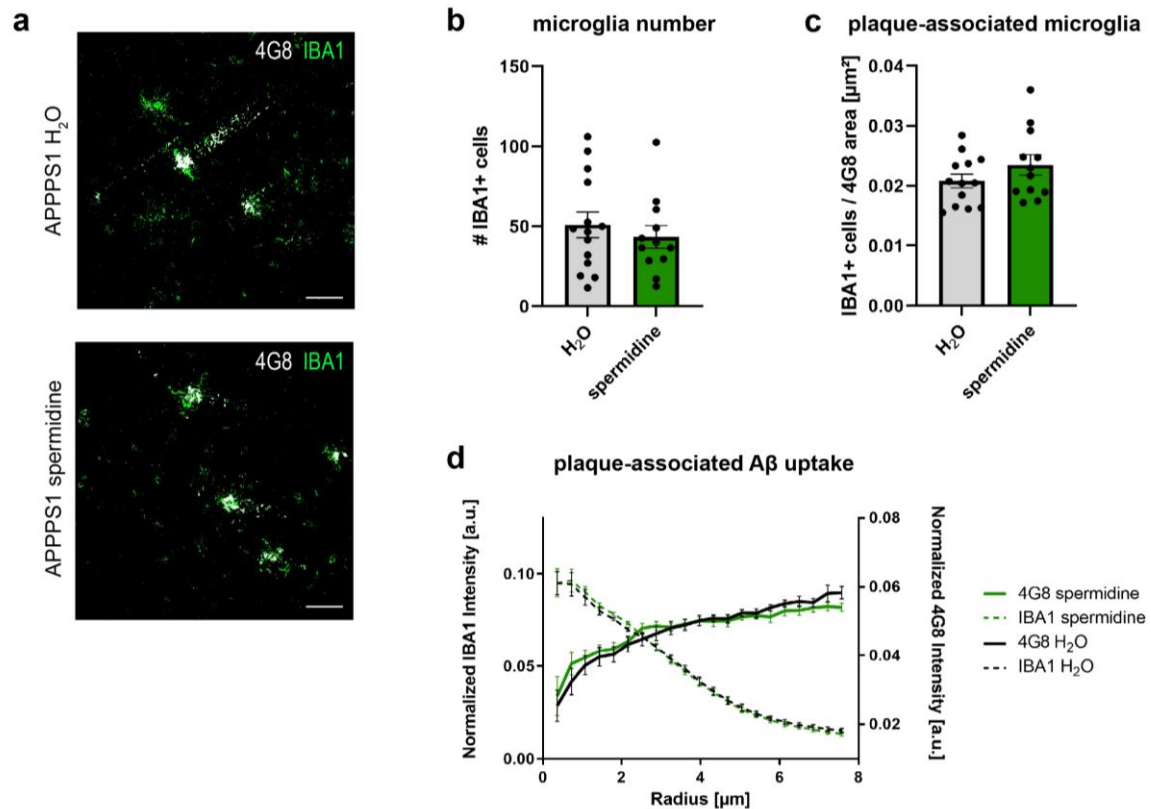


**Figure M3.** No effect of spermidine on the amount of IBA1-positive microglia and the microglial degradation of insoluble A $\beta$  plaques. **(a)** Tissue sections of 290-day-old mice were stained for IBA1 (green) and 4G8 (white). Representative images are shown. Scale bar = 25  $\mu\text{m}$ . The total number of IBA1-positive cells **(b)** and the number of IBA1-positive cells per plaque using a radius of 30  $\mu\text{m}$  around each plaque **(c)** was determined. **(d)** Radial intensity profiles of 4G8 and IBA1 were calculated around the center of the nucleus of plaque-based IBA1-positive microglia;  $n = 12-14$ , two-tailed t-test. The data was quantified by the Advanced Medical Bioimaging Core Facility (Dr. Niclas Gimber, Charité-Universitätsmedizin Berlin). The figure was self-created.

### 3.2 Spermidine targets oligodendrocytes

As mentioned above, the effect of spermidine and autophagy was previously largely studied in neurons with little data on microglia and only very few data on astrocytes and oligodendrocytes. By snRNA-seq, we analyzed the transcriptomic changes upon spermidine treatment in all brain cell populations (Fig. M4a, b). While microglia revealed the most prominent and relevant transcriptomic changes and almost no changes were found in astrocytes, spermidine also affected the transcriptome of oligodendrocytes (Fig. 1e). A breakdown of myelin and the loss of myelin sheath are regarded as one of the initial steps in the early AD pathology which might even appear before the A $\beta$  and tau pathology. Furthermore, impaired repair of oligodendrocyte precursor cells (OPCs) contributes to the progression of the disease pathology, thus indicating that oligodendrocytes also play a

crucial role in AD <sup>6</sup>. Differential gene expression analysis comparing the oligodendrocyte population of spermidine-treated with H<sub>2</sub>O APPPS1 mice revealed alterations in genes involved in heat shock response (*Hsp90aa1*, *Hsp90ab1*, *Cryab*, *Fkbp4*, *St13*, *Dnaja1*), proliferation (*Phlda1*, *Ptma*, *Ghr*, *Orc6*), cytoskeleton/ extracellular matrix (*Fnbp1*, *Colgalt1*), transcription (*Rbfox1*, *Eny2*) and inflammatory processes (*Reep5*) (Fig. M4c, d). Gene set enrichment analysis showed several heat shock response pathways to be downregulated upon spermidine treatment (Fig. M4e). Heat shock response is a protective mechanism induced upon cellular stress and mediated by chaperons, which controls proper protein folding and the neutralization of misfolded proteins. Heat shock proteins as HSP90 were found to be increased in the brains of AD patients in response to accumulating A $\beta$ , however, chronically the heat shock response is downregulated in AD patients and mouse models <sup>12</sup>. The reduction in heat shock response genes in oligodendrocytes might be due to the fact that less cellular stress is induced by soluble A $\beta$  in spermidine-treated APPPS1 mice. Interestingly, HSP90 and REEP5 were shown to induce inflammation <sup>12,51</sup> and were downregulated upon spermidine treatment (Fig. M4d). While microglia are considered the main immune cells of the brain, recently, also so-called disease-associated oligodendrocytes (DOLs) were found to express immune-related transcriptome signatures in the AD-model 5xFAD <sup>52</sup>. To assess whether spermidine might also exert some of its anti-inflammatory effects by affecting oligodendrocytes, we investigated the effect of spermidine on the inflammatory response of oligodendrocytes *in vitro*. Oligodendrocytes positive for the mature marker O4 were isolated from neonatal mice by magnetic activated cell sorting (MACS). In comparison to microglia, oligodendrocytes produce cytokines in response to cytokines released by microglia. We therefore tested which stimuli induced a release of IL-6 in cultured oligodendrocytes. Among the stimuli TNF- $\alpha$ , IL-1 $\beta$ , TGF- $\beta$  and poly I:C, IL-1 $\beta$  triggered the strongest release of IL-6 (Fig. M4f). Co-treatment with 30  $\mu$ M spermidine significantly reduced the IL-1 $\beta$ -induced IL-6 release by oligodendrocytes (Fig. M4g), indicating that spermidine also targets oligodendrocytes-mediated inflammation. Although the effect of spermidine on oligodendrocytes has not yet been described to our knowledge, spermidine protected from demyelination and inflammation in an experimental autoimmune encephalomyelitis (EAE) mouse model <sup>34</sup>. In general, autophagy is essential for the differentiation of oligodendrocytes as well as transporting membrane proteins and lipids to produce new myelin and to compact myelin <sup>53</sup>, thus suggesting that spermidine might affect myelination by the induction of autophagy. To summarize, a common denominator of the effects of spermidine on oligodendrocytes and microglia are the anti-inflammatory properties of spermidine and its effect on proliferation, transcription and cytoskeletal genes.

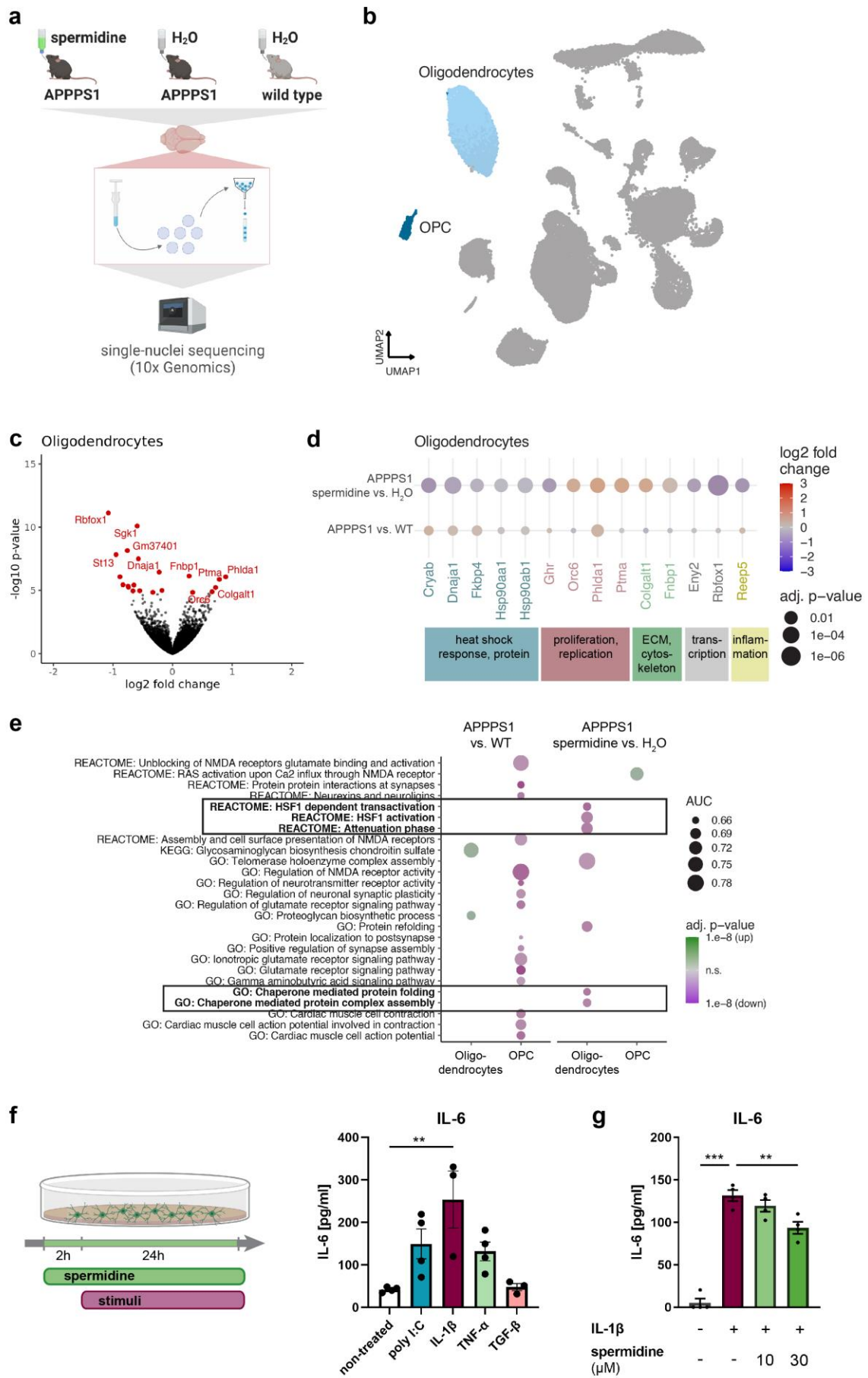


**Figure M4.** Spermidine targets oligodendrocytes.

(See legend on the following page)

**Figure M4.** Spermidine targets oligodendrocytes. **(a)** APPPS1 mice were treated with 3 mM spermidine from 30 days to 180 days of age. FACS-sorted DAPI-stained nuclei of hemispheres from spermidine-treated APPPS1, H<sub>2</sub>O APPPS1 and H<sub>2</sub>O control mice were used for single nuclei sequencing using the 10x Genomics platform (n = 3). The data were analyzed by the Core Unit Bioinformatics (Dr. Benedikt Obermayer, Berlin Institute of Health). Figure was adapted from publication Fig. 1b<sup>43</sup>. **(b)** UMAP embedding and clustering of the snRNA-seq data. The oligodendrocyte and OPC cluster is highlighted. Figure was adapted from publication Fig. 1c<sup>43</sup>. **(c)** Volcano plot of genes differentially expressed in oligodendrocytes of spermidine-treated vs. H<sub>2</sub>O APPPS1 mice are shown. Genes with adj. p-value < 0.01 are highlighted in red and top 5 up- and down-regulated genes are indicated. **(d)** Dot plot for selected genes in a cell-type-specific differential expression analysis between spermidine-treated and H<sub>2</sub>O APPPS1 mice and H<sub>2</sub>O APPPS1 and wild type (WT) mice. Color scale shows log<sub>2</sub> fold change, dot size represents adjusted p value. Associated pathways are color-coded. **(e)** Top gene sets from a gene set enrichment analysis of differential expression between spermidine-treated and H<sub>2</sub>O APPPS1 mice using tmod are shown. **(f)** Neonatal oligodendrocytes isolated by MACS were treated with poly I:C, IL-1 $\beta$ , TNF- $\alpha$  and TGF- $\beta$  for 24 h. **(g)** Neonatal oligodendrocytes were treated with IL-1 $\beta$  and the indicated concentrations of spermidine as depicted in the scheme. IL-6 concentration in the cell supernatant was assessed by ELISA; n = 3 – 4; one-way ANOVA, Dunnett's post hoc test. \* p < 0.05, \*\* p < 0.01, \*\*\* p < 0.001. The graphics in **(a)** and **(f)** were created with Biorender.com (self-created figure).

### 3.3 Spermidine reverts AD-associated proteome in microglia of APPPS1 mice

Autophagy is known to exert a large extent of its effects rather on protein than on transcriptomic level. We previously showed that autophagy is required for the degradation of the inflammasome and thereby for inhibiting the production of IL-1 $\beta$ <sup>24</sup>. To complement our transcriptomics data, we performed liquid chromatography tandem mass spectrometry of microglia isolated from the hemispheres of spermidine-treated APPPS1 mice, APPPS1 H<sub>2</sub>O controls, spermidine-treated wild type mice and wild type H<sub>2</sub>O controls at 180 days (Fig. 3a, Fig. M5a). We specifically focused on microglia for the proteomic screening, as they revealed most of the transcriptomic changes. All differentially expressed proteins found in spermidine-treated APPPS1 mice compared to H<sub>2</sub>O APPPS1 mice were regulate opposite to the changes induced in the APPPS1 mice in comparison to the wild type mice (Fig. 3b, M5b), indicating that spermidine reverted AD-associated changes in the APPPS1 mice. A gene set enrichment analysis revealed that spermidine targeted cytoskeleton, actin and microtubule- as wells as inflammation-associated pathways (Fig. 3c). Spermidine clearly downregulated many cytokine pathways including inflammasome, IL-1 processing and IL-6 signaling pathways (Fig. 3d), correlating with the previously described anti-inflammatory effect of spermidine in an EAE, Multiple sclerosis, mouse model<sup>34</sup>. Furthermore, spermidine enhanced pathways associated with autophagy underlining that spermidine might exert its effects by autophagy induction (Fig. 3d). By direct comparison of the pathways changed in APPPS1 mice with the pathways found to be affected by spermidine treatment, we found

that spermidine treatment reversed the downregulation of actin- and microtubule-associated pathways as well as the upregulation of inflammation, glycolysis, gluconeogenesis and oxidative phosphorylation (Fig. 3e). The subsequent CNS-wide anti-inflammatory effects of spermidine measured by reduced cytokine levels in the hemispheres of APPPS1 mice at 290 days further underlined the protective effects of spermidine in APPPS1 mice (Fig. 3f).

By evaluating the underlying differentially expressed proteins in spermidine-treated APPPS1 mice in comparison to H<sub>2</sub>O control APPPS1 mice, SP110, ORAI1 and MEF2C were among the top upregulated proteins and OSBPL2 among the top downregulated proteins (Fig. M5b). Interestingly, SP110 was downregulated in the APPPS1 mice and its level even increased above that of wild type mice after spermidine treatment (Fig. M5c). SP110 is involved in transcriptional regulation and downregulates multiple immune response and apoptosis-related genes<sup>54</sup> and thus, may account for the anti-inflammatory effects of spermidine. ORAI1 is a calcium modulator and its downregulation by siRNA blocked Angiotensin II-induced autophagy in cardiomyocytes<sup>55</sup>. Thus, autophagy induction by spermidine may be mediated by restoring ORAI1 levels in APPPS1 mice to wild-type levels (Fig. M5d). MEF2C is barely described in microglia, however, as it is dysregulated in Parkinson's disease and its activation required for neuronal survival<sup>56-58</sup>, its upregulation may result in neuroprotective effects of spermidine (Fig. M5e). The Oxysterol Binding Protein Like 2 (OSBPL2) is involved in the intracellular transport of cholesterol from the plasma membrane to the endoplasmic reticulum. Cholesterol transport disturbances are a key hallmark of AD and an upregulation of OSBPL2 was also observed in APPPS1 mice<sup>59</sup>. Since spermidine treatment reduced OSBPL2 to wild type levels, spermidine might also affect AD-associated cholesterol pathway changes (Fig. M5f). Taken together, the observed anti-inflammatory, autophagic and anti-AD associated properties of spermidine found by gene set enrichment analysis are also reflected on single protein level.

Increased glycolytic activity is yet another classical hallmark of microglia activation, as microglia switch their metabolic phenotype from oxidative phosphorylation to glycolysis. The enhanced glucose uptake and glycolytic activity is associated with increased neuroinflammation<sup>60</sup>. Thus, spermidine-induced changes in the glycolytic activity (Fig. 3e) might account for the anti-inflammatory effects resulting in an overall reduction in microglia activation. In line with this, spermidine supplementation partially restored mitochondrial respiration and the number of mitochondria in aged mice and flies<sup>61,62</sup>. To validate the findings on the energy metabolism, we treated neonatal microglia with spermidine for 6 h and measured the intracellular ATP levels by using a luminescence based assay. Spermidine

significantly increased the production of ATP at a concentration of 100  $\mu\text{M}$  (Fig. M5g), underlining the observed proteomics results (Fig. 3). However, to determine the source of ATP and whether glycolysis or oxidative phosphorylation is indeed altered by spermidine, further in-depth analyses are required.

Summarized these data show that spermidine interferes with AD-associated changes at multifarious points to maintain microglial metabolism.

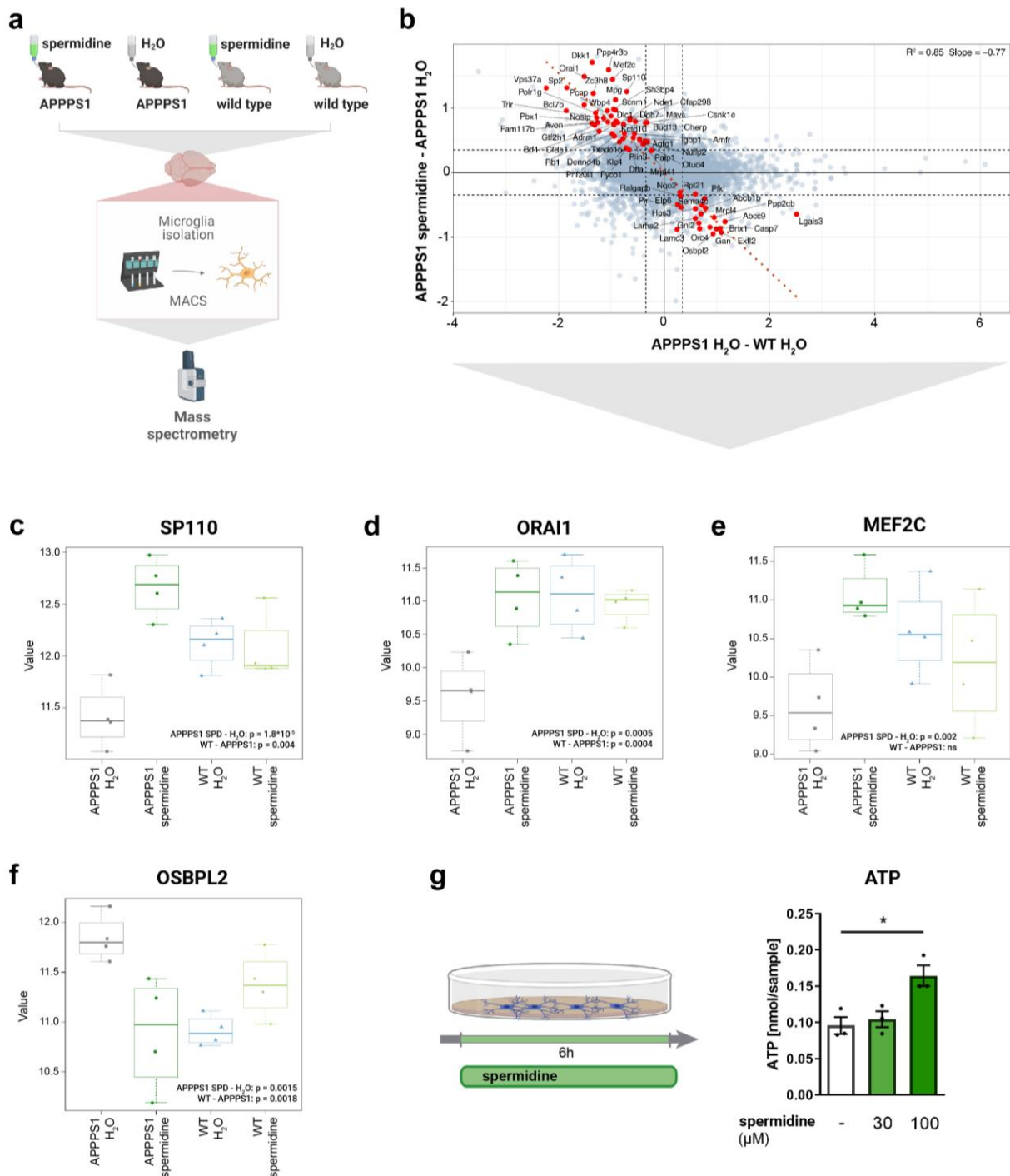


**Figure M5.** Spermidine reverts AD-associated proteome in microglia of APPPS1 mice.

(See legend on the following page)

**Figure M5.** Spermidine reverts AD-associated proteome in microglia of APPPS1 mice. **(a)** Microglia were isolated from 180-day-old male APPPS1 mice by MACS and the proteome analyzed by liquid chromatography tandem mass spectrometry. The data were analyzed by the High-Throughput Mass Spectrometry Core Facility (Dr. Vadim Farztdinov, Charité-Universitätsmedizin Berlin). Figure was adapted from the publication Fig. 3a<sup>43</sup>. **(b)** Protein regulation in contrast 2 (APPPS1 spermidine–APPPS1 H<sub>2</sub>O, y axis) and in contrast 1 (APPPS1 H<sub>2</sub>O,–WT H<sub>2</sub>O, x axis) were compared using a scatterplot. Spermidine-regulated proteins that show an anti-APPPS1 effect were marked in red. Figure was adapted from the publication Fig. 3b<sup>43</sup>. **(c-f)** Selected proteins showing significant differential expression upon spermidine treatment in APPPS1 mice were plotted and the protein regulation compared between APPPS1 H<sub>2</sub>O, APPPS1 spermidine, wild type (WT) H<sub>2</sub>O and WT spermidine. The p-value for the comparison of APPPS1 spermidine (SPD) vs. APPPS1 H<sub>2</sub>O as well as the comparison APPPS1 H<sub>2</sub>O vs. WT H<sub>2</sub>O is shown. n = 4. **(g)** Neonatal microglia were treated with the indicated concentrations of spermidine for 6 h and the ATP content was determined using an ATP Assay Kit (Abcam). n = 3; one-way ANOVA, Dunnett's post hoc test. \* p < 0.05. The figure **(c-g)** were self-created. The graphics in **(a)** and **(g)** were created with Biorender.com.

### 3.4 Spermidine reduces the activity of the NLRP3 inflammasome

As the anti-inflammatory effects of spermidine were among the top-regulated pathways in the proteomics analysis, we performed an in-depth investigation of the underlying pathways using an *in vitro* approach. Spermidine treatment of neonatal microglia activated with different stimuli (LPS/ATP, poly I:C and A $\beta$ ) resulted in a dose-dependent reduction of released cytokines (Fig. 4b-d). Accordingly, spermidine reduced the transcriptional production of cytokines on mRNA level by interfering with the phosphorylation of the transcription factor NF- $\kappa$ B (Fig. 4d-f). Spermidine also significantly reduced the cytokine response of LPS/ATP-treated slice cultures of APPPS1 and wild type mice (Fig. 4a), showing that spermidine can directly interfere with neuroinflammation in these mice. Our *in vitro* analysis revealed that spermidine exerts anti-inflammatory effects with regard to TLR4 (LPS/ATP) and TLR3 (poly I:C)-driven microglia activation as well as TLR3-driven astrocyte activation. Thus, *in vitro* the effect of spermidine seem to be genuine with regard to the stimulus and glial cell type.

Correlating with the proteomics analysis of the spermidine-treated APPPS1 mice, we found that spermidine exerts some of its functions solely on protein level. Spermidine interfered with the assembly of the inflammasome by reducing the number of ASC specks in LPS/ATP-treated microglia (Fig. 5e-f). By inhibiting the activation of the NLRP3 inflammasome, reduced levels of IL-1 $\beta$  and IL-18 were released upon LPS/ATP treatment by microglia (Fig. 5b, c). The NLRP3 inflammasome is a multimeric complex consisting of NLRP3, ASC and CASP1. The assembly and cleavage of Pro-CASP1 is required for the subsequent cleavage of the precursors of IL-1 $\beta$  and IL-18 into its active form. To our knowledge no studies of the effect of spermidine on the inflammasome have been described so far, elucidating a novel

target mechanism of spermidine. However, multiple studies showed that the NLRP3 inflammasome is activated in AD patients and that its absence reduced neuroinflammation as well as A $\beta$  and tau pathology<sup>63,64</sup>. Thus, reducing the NLRP3 inflammasome activity presents an additional way of spermidine to interfere with AD pathology and microglia activation.

### 3.5 Spermidine reverts proteomic changes in activated microglia *in vitro*

To unbiasedly assess which direct effect spermidine has on microglia, we performed liquid chromatography tandem mass spectrometry of microglia treated with LPS/ATP and 30  $\mu$ M spermidine similar to the *in vivo* proteomics analysis shown in Fig. 3 (Fig. M6a). In a principal component analysis (PCA) spermidine treatment of pre-activated neonatal microglia resulted in a distinct clustering of microglia close to non-treated microglia (Fig. M6b). To assess how spermidine modulates the proteome of LPS/ATP-treated neonatal microglia, linear modelling was performed integrating the proteins changing upon spermidine treatment as well as between LPS/ATP-treated and control microglia. Similar to the *in vivo* data, a clear anti-correlation ( $R^2 = 0.977$ ) between the LPS/ATP-mediated and spermidine-mediated effect was observed (Fig. M6c). This underlines the protective effects of spermidine on microglia activation. In total, 826 proteins were differentially regulated by spermidine treatment, which exceeds the number of regulated proteins found *in vivo* (Fig. M6d). To determine which pathways are altered by spermidine treatment, we used a gene-set enrichment analysis (GSEA) with a specific focus on molecular function terms (GO:MF). The top upregulated pathways upon spermidine treatment were mRNA binding and transcription, while also ubiquitin-specific protease binding pathways were found to be upregulated. Ion transporter activity, lipid transport activity as well as IL-6 receptor binding and apolipoprotein pathways were among the downregulated pathways (Fig. M6e). The spermidine-mediated effects on mRNA and transcription correlate well with the observed regulation of the transcription factor NF- $\kappa$ B (Fig. 4d-f), which resulted in a reduced expression of cytokine mRNAs. Again, these results indicate that spermidine may also affect lipid metabolism, making it an interesting avenue for future investigations.

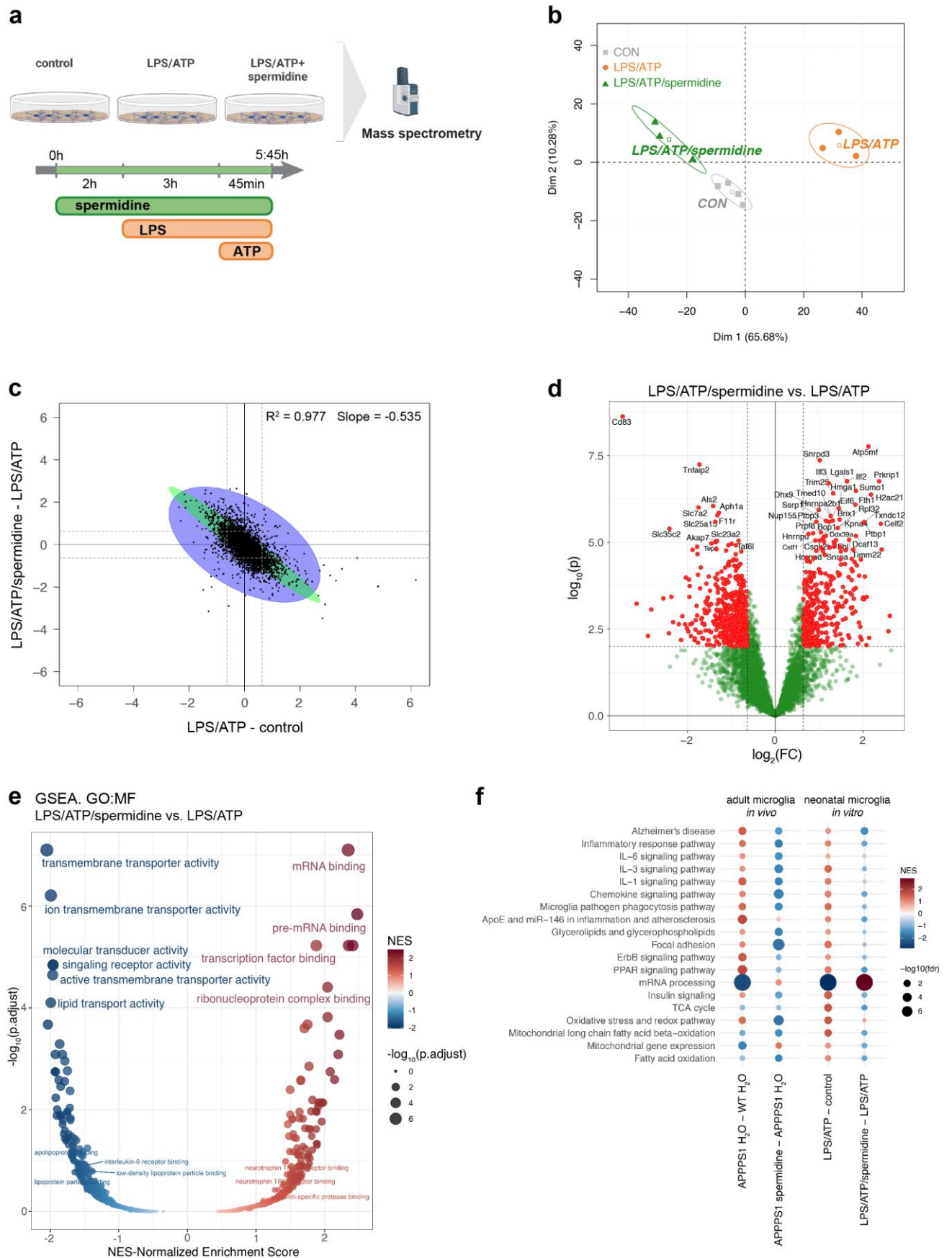


**Figure M6.** Spermidine reverts proteomic changes in activated microglia *in vitro*.  
(See legend on the following page)

**Figure M6.** Spermidine reverts proteomic changes in activated microglia *in vitro*. **(a)** Mass spectrometry of neonatal microglia treated with LPS (1 µg/ml), ATP (2 mM) and spermidine (30 µM) as indicated in the scheme, n = 4. The data were analyzed by the High-Throughput Mass Spectrometry Core Facility (Dr. Vadim Farztdinov, Charité-Universitätsmedizin Berlin). **(b)** PCA plot of data matrix reduced to significantly regulated proteins (alpha = 0.01, FC threshold = 1.55) in the contrast LPS/ATP/spermidine vs. LPS/ATP. **(c)** Scatterplot of protein regulation in contrast (LPS/ATP/spermidine–LPS/ATP, y axis) vs. its regulation in contrast (LPS/ATP–control, x axis). **(d)** Volcano plot of proteins regulated in contrast LPS/ATP/spermidine vs. LPS/ATP. Red dots mark significantly regulated proteins (alpha = 0.01, FC threshold = 1.55). Only the top regulated proteins with p-value < 1E-5 are labelled. **(e)** Volcano plot of GSEA enrichment of GO MF terms. Normalized enrichment score of functional terms is shown on the x-axis, while the y-axis represents the - log<sub>10</sub> of its false discovery rate. Selected terms were labelled. **(f)** Dot plot of selected functional terms from Wiki pathways related to neuroinflammation and degeneration is shown. The comparison of responses to the different stimuli (Aβ in APPPS1 mice and LPS/ATP) and to spermidine in adult microglia *in vivo* and neonatal microglia *in vitro* are shown. The graphic in **(a)** was created with Biorender.com (self-created figure).

To compare how well our LPS/ATP *in vitro* model reflects microglial changes occurring in APPPS1 mice, we performed a comparative gene set enrichment analysis. Plotting the pathway differences of APPPS1 vs. wild type and LPS/ATP vs. non-treated next to each other revealed similar changes regarding neuroinflammation, complement activation, focal adhesion and AD-related pathways. Likewise, the comparisons APPPS1 spermidine vs. APPPS1 H<sub>2</sub>O and LPS/ATP spermidine vs. LPS/ATP revealed very similar effects of spermidine in both model systems. Only few differences in the regulation pattern were found regarding TCA cycle, oxidative stress and redox pathway, fatty acid oxidation and mitochondrial gene expression (Fig. M6f). Since oxidative stress and dysfunction of mitochondria are features of AD largely driven by the brain microenvironment<sup>65</sup> and neonatal microglia were kept in growth medium supplemented with 10% FCS, these features were only targeted by spermidine *in vivo*. All in all, those results indicate the validity of the used *in vitro* models to study neuroinflammation and a robust and consistent effect of spermidine on activated microglia.

### 3.6 Anti-inflammatory properties of spermidine in human iPSC-derived microglia

To transfer our murine findings on the beneficial role of spermidine in microglia into a human context, we differentiated human iPSCs into hematopoietic stem cells and subsequently into human microglia in collaboration with the stem cell core facility (MDC) using kits from stem cell technologies. After 6 weeks of differentiation, microglia were treated with LPS/ATP and spermidine for 5:45 h and the cytokine release into the cell supernatant was measured (Fig. M7a). The iPSC-derived microglia responded well to

LPS/ATP treatment by releasing IL-1 $\beta$  and IL-6, however, no effect of spermidine was observed using the stimulation scheme established of mouse microglia (Fig. M7b, c). Longer incubation with spermidine for 9:45 h significantly reduced the release of IL-6 upon LPS/ATP treatment (Fig. M7b), indicating that the iPSC-microglia require a longer treatment with spermidine to exhibit similar anti-inflammatory effects of spermidine to the mouse microglia. Interestingly, IL-1 $\beta$  levels were not significantly reduced by spermidine treatment, which might be due to the fact that IL-6 and IL-1 $\beta$  have distinct signaling pathways. Although these results are preliminary and need to be repeated independently, these findings suggest that the anti-inflammatory effects of spermidine are genuine and may also be protective in neuroinflammatory diseases in humans.

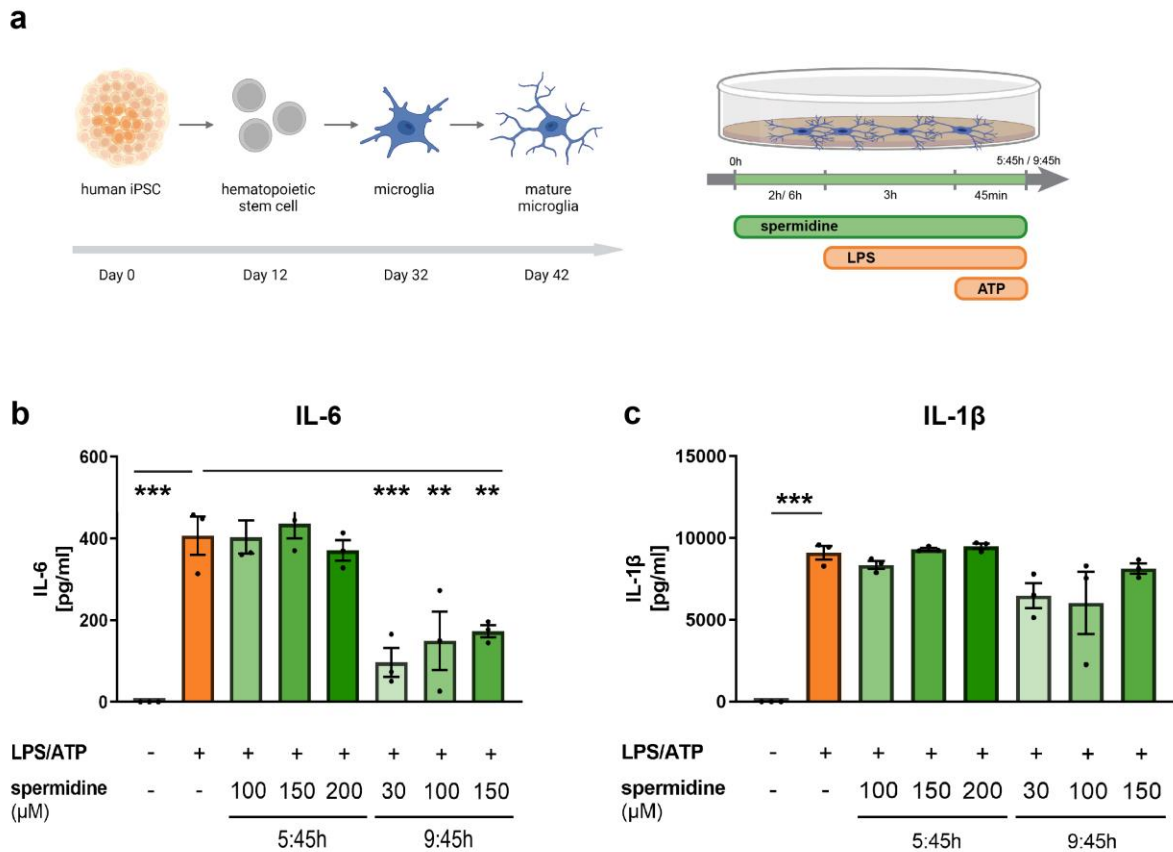


**Figure M7.** Spermidine exhibits anti-inflammatory effects in human iPSC-derived microglia. **(a)** Human iPSCs were differentiated into hematopoietic stem cells and subsequently into microglia. Finally, microglia were matured and treated at day 42 with LPS (1  $\mu$ g/ml) and ATP (2 mM) and the indicated concentrations of spermidine as depicted in the scheme. **(b-c)** IL-6 and IL-1 $\beta$  concentration in the cell supernatant was assessed by ELISA; n = 3 (replicates from same cell line); one-way ANOVA, Dunnett's post hoc test. \* p < 0.05, \*\* p < 0.01, \*\*\* p < 0.001. The graphic in **(a)** was created with Biorender.com (self-created figure).

## 4 CONCLUSION and OUTLOOK

Within this thesis, I identified protective and disease-ameliorating effects of spermidine on key hallmarks of AD, namely neurotoxic soluble A $\beta$ , neuroinflammation and microglial activation, thus making spermidine a promising target to be further studied as a potential therapeutic agent (Fig. M8).

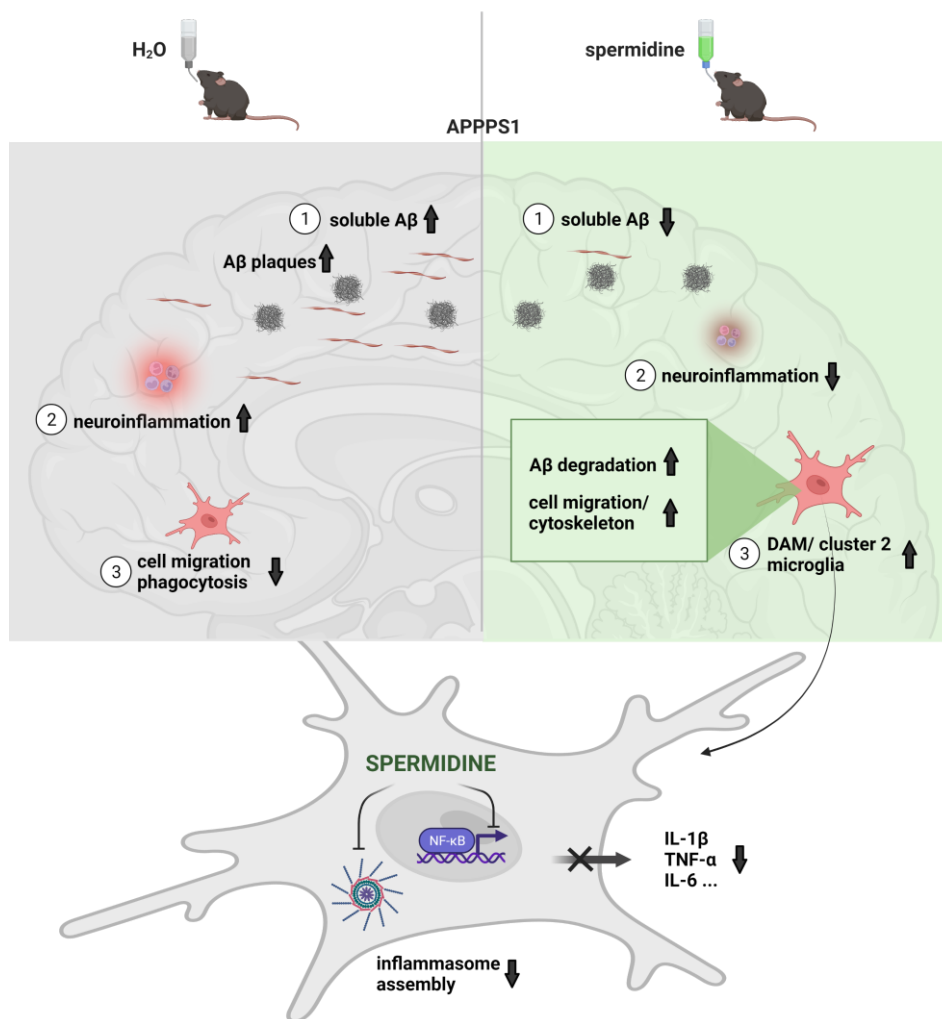


**Figure M8.** Graphical abstract of thesis findings. Differences regarding A $\beta$  levels, neuroinflammation and microglia changes found between spermidine-treated and H<sub>2</sub>O control APPPS1 mice are shown side-by-side. *In vitro* findings are summarized in the cell below showing the inhibitory effect of spermidine on the inflammasome assembly and NF- $\kappa$ B-mediated cytokine release. The figure was self-created with Biorender.com.

## 4.1 Limitations of this work and future questions

The effect of spermidine on AD pathology was investigated here using the mouse model APPPS1 exhibiting A $\beta$  plaque pathology and neuroinflammation. As every model organism, it bears the disadvantage of not modelling all aspects of AD. The effect of spermidine on tau pathology as well as on cognitive deficits could not be assessed using this mouse model. The effects of spermidine supplementation on tau pathology has not been investigated so far, however, dysregulated polyamine metabolism by overexpression of AZIN2 resulted in increasing tau pathology in PS19 mice, indicating that spermidine might also regulate tau pathology<sup>41</sup>. Even though cognitive impairment is one of the key symptoms of AD patients, data from our group revealed only very small changes in behavior and neurodegeneration in APPPS1 mice<sup>66,67</sup>. Thus, we chose to assess the most prevalent phenotypes, namely A $\beta$  pathology, neuroinflammation and glial changes. Additionally, neuronal and behavioral/cognitive assessment upon spermidine supplementation has been studied previously in non-AD-like mice<sup>38,40</sup>.

The APPPS1 mouse strain presents with a rather aggressive and fast A $\beta$  pathology. Spermidine specifically reduced soluble A $\beta$  without affecting plaque-based A $\beta$ . It is still highly debated whether plaque-based A $\beta$  is detrimental for the disease progression. Recent findings suggest that microglia might compact A $\beta$  in form of plaques as a protective measure to avoid neurotoxicity of soluble A $\beta$ <sup>26</sup>. In this context, any procedure resulting in a significant reduction of 40 % in soluble A $\beta$  as it occurs upon spermidine treatment in 120- and 290-day-old mice may be regarded as a promising tool to modulate A $\beta$  pathology, even though A $\beta$  plaques are not affected. Within this work, we provided many unknown mechanistic insights of spermidine including changes in DAM, oligodendrocytes, cell migration, phagocytic AXL levels, A $\beta$  degradation, inflammasome assembly and anti-inflammatory effects. While we determined the *in vitro* effects of spermidine to be autophagy dependent (Fig. S5), it remains to be elucidated whether the *in vivo* effects of spermidine are mediated by autophagy induction. Further experiments using autophagy-deficient APPPS1 mice e.g. BECN1<sup>flox/flox</sup>.CX3CR1<sup>CreERT2</sup> mice with a microglia specific deletion in BECN1 would be required to determine this dependence. These experiments will be part of future investigations.

All in all, we cannot rule out that spermidine exhibits systemic effects and influences the periphery as spermidine is orally administered. However, recent data using deuterium-labelled spermidine indicated that spermidine indeed crosses the blood-brain-barrier and reaches the brain<sup>38</sup>. Therefore, spermidine may act directly on glial cells and their

metabolism. As oral application brings major advantages for a potential clinical application, it was more meaningful to apply spermidine orally instead of using pumps for direct administration to the brain. For future experiments it may be of interest to determine whether the brain-driven changes mediated by spermidine are accountable for the disease-ameliorating effects or whether secondary peripheral effects may have an influence.

## 4.2 Significance of the work and clinical applications

One major challenge in AD research remains to halt, cure or prevent the disease. Even though the socioeconomic burden with around 6.5 Mio people suffering from AD worldwide is huge<sup>68</sup>, so far mostly symptomatic treatment is possible. As direct therapeutic targeting of A $\beta$  pathology remained largely unsuccessful, it may be more promising to target other hallmarks of AD, namely neuroinflammation or dysfunction of autophagy. Autophagy activating drugs such as rapamycin were assessed before, showing an amelioration of A $\beta$  and tau pathology as well as cognitive benefits<sup>69,70</sup>. However, these drugs have substantial side effects, severely hampering their application *in vivo* and/ or in clinical settings<sup>71</sup>. Thus, administration of such drugs pose obvious safety concerns and highlight the unmet need for assessing alternative tolerable and efficient autophagy activators. Additionally, the pathogenetically relevant mechanisms by which autophagy modulation affects AD pathology were yet largely unknown. Thus, we set out to investigate the effect of the well-tolerable polyamine spermidine on AD pathology and identified AD ameliorating effects of spermidine. Spermidine supplementation in various model organisms and in clinical trials did not reveal known side effects and bears the advantage of oral administration<sup>38,72-74</sup>, which would allow long-term treatment. The decline of spermidine levels with age<sup>27</sup> may result in dysfunctional autophagy which in turn may initiate the accumulation of A $\beta$ . Thus, supplementing spermidine in aging people may be a promising approach to counteract AD pathology.

Clinical studies using spermidine have not been conducted yet in the context of AD. However, the preliminary effects of spermidine supplementation on individuals with subjective cognitive decline<sup>38,72-74</sup>, in combination with our findings in an AD-like mouse model, are an ideal basis to encourage and extend clinical studies to AD patients.

## 5 REFERENCES

1. Selkoe, D. J. & Hardy, J. The amyloid hypothesis of Alzheimer's disease at 25 years. *EMBO Mol. Med.* **8**, 595–608 (2016).
2. Krstic, D., Madhusudan, A., Doehner, J., Vogel, P., Notter, T., Imhof, C., Manalastas, A., Hilfiker, M., Pfister, S., Schwerdel, C., Riether, C., Meyer, U., & Knuesel, I. Systemic immune challenges trigger and drive Alzheimer-like neuropathology in mice. *J. Neuroinflammation* **9**, (2012).
3. Sierra, A., Abiega, O., Shahraz, A. & Neumann, H. Janus-faced microglia: Beneficial and detrimental consequences of microglial phagocytosis. *Front. Cell. Neurosci.* **0**, 6 (2013).
4. Keren-Shaul, H., Spinrad, A., Weiner, A., Matcovitch-Natan, O., Dvir-Szternfeld, R., Ulland, T. K., David, E., Baruch, K., Lara-Astaiso, D., Toth, B., Itzkovitz, S., Colonna, M., Schwartz, M., & Amit, I. A Unique Microglia Type Associated with Restricting Development of Alzheimer's Disease. *Cell* **169**, 1276-1290.e17 (2017).
5. Smit, T., Deshayes, N. A. C., Borchelt, D. R., Kamphuis, W., Middeldorp, J., & Hol, E. M. Reactive astrocytes as treatment targets in Alzheimer's disease—Systematic review of studies using the APP<sup>swe</sup>PS1dE9 mouse model. *Glia* **69**, 1852–1881 (2021).
6. Cai, Z. & Xiao, M. International Journal of Neuroscience Oligodendrocytes and Alzheimer's disease Oligodendrocytes and Alzheimer's disease. *Int. J. Neurosci.* **126**, 97–104 (2016).
7. Funderburk, S. F., Marcellino, B. K. & Yue, Z. Cell "Self-Eating" (Autophagy) Mechanism in Alzheimer's Disease. *Mt. SINAI J. Med.* **77**, 59–68 (2010).
8. Klionsky, D. J. & Emr, S. D. Autophagy as a Regulated Pathway of Cellular Degradation. *Science* **290**, 1717 (2000).
9. Su, P., Zhang, J., Wang, D., Zhao, F., Cao, Z., Aschner, M., & Luo, W. The role of autophagy in modulation of neuroinflammation in microglia. *Neuroscience* **319**, 155–167 (2016).
10. He, C. & Levine, B. The Beclin 1 interactome. *Curr. Opin. Cell Biol.* **22**, 140 (2010).
11. Walczak, M. & Martens, S. Dissecting the role of the Atg12–Atg5–Atg16 complex during autophagosome formation. *Autophagy* **9**, 424 (2013).
12. Kakimura, J.-I., Kitamura, Y., Takata, K., Umeki, M., Suzuki, S., Shibagaki, K., Taniguchi, T., Nomura, Y., Gebicke-Haerter, P. J., Smith, M. A., Perry, G., & Shimohama, S. Microglial activation and amyloid-beta clearance induced by exogenous heat-shock proteins. *FASEB J.* **16**, 601–603 (2002).
13. Kabeya, Y., Mizushima, N., Ueno, T., Yamamoto, A., Kirisako, T., Noda, T., Kominami, E., Ohsumi, Y., & Yoshimori, T. LC3, a mammalian homologue of yeast Apg8p, is localized in autophagosome membranes after processing. *EMBO J.* **19**, 5720 (2000).
14. Jiang, P., Nishimura, T., Sakamaki, Y., Itakura, E., Hatta, T., Natsume, T., & Mizushima, N. The HOPS complex mediates autophagosome-lysosome fusion through interaction with syntaxin 17. **25**, (2014).
15. Boland, B., Kumar, A., Lee, S., Platt, F. M., Wegiel, J., Yu, W. H., & Nixon, R. A. Autophagy induction and autophagosome clearance in neurons: relationship to autophagic pathology in Alzheimer's disease. *J. Neurosci.* **28**, 6926–6937 (2008).
16. Nixon, R. A. & Yang, D. S. Autophagy Failure in Alzheimer's Disease – Locating the Primary Defect. *Neurobiol. Dis.* **43**, 38 (2011).
17. Pickford, F., Masliah, E., Britschgi, M., Lucin, K., Narasimhan, R., Jaeger, P. A., Small, S., Spencer, B., Rockenstein, E., Levine, B., & Wyss-Coray, T. The autophagy-related protein beclin 1 shows reduced expression in early Alzheimer disease and regulates amyloid  $\beta$  accumulation in mice. *J. Clin. Invest.* **118**, (2008).
18. Lachance, V., Wang, Q., Sweet, E., Choi, I., Cai, C. Z., Zhuang, X. X., Zhang, Y., Jiang, J. L., Blitzer, R. D., Bozdagi-Gunal, O., Zhang, B., Lu, J. H., & Yue, Z. Autophagy protein NRBF2 has reduced expression in Alzheimer's brains and modulates memory and amyloid-beta homeostasis in mice. *Mol. Neurodegener.* **14**, 1–13 (2019).
19. Uddin, M. S., Stachowiak, A., Al Mamun, A., Tzvetkov, N. T., Takeda, S., Atanasov, A. G., Bergantin, L. B., Abdel-Daim, M. M., & Stankiewicz, A. M. Autophagy and Alzheimer's disease: From molecular mechanisms to therapeutic implications. *Front. Aging Neurosci.* **10**, (2018).
20. Zhang, Z., Yang, X., Song, Y. Q. & Tu, J. Autophagy in Alzheimer's disease pathogenesis: Therapeutic potential and future perspectives. *Ageing Res. Rev.* **72**, 101464 (2021).
21. Nilsson, P., Loganathan, K., Sekiguchi, M., Matsuba, Y., Hui, K., Tsubuki, S., Tanaka, M., Iwata, N., Saito, T., & Saido, T. C. A $\beta$  secretion and plaque formation depend on autophagy. *Cell Rep.* **5**, 61–69 (2013).
22. Nilsson, P., Sekiguchi, M., Akagi, T., Izumi, S., Komori, T., Hui, K., Sörgjerd, K., Tanaka, M., Saito, T., Iwata, N., & Saido, T. C. Autophagy-related protein 7 deficiency in amyloid  $\beta$  (A $\beta$ ) precursor protein transgenic mice decreases A $\beta$  in the multivesicular bodies and induces A $\beta$  accumulation in the Golgi. *Am. J. Pathol.* **185**, 305–313 (2015).
23. Rocchi, A., Yamamoto, S., Ting, T., Fan, Y., Sadleir, K., Wang, Y., Zhang, W., Huang, S., Levine, B., Vassar, R., & He, C. A Becln1 mutation mediates hyperactive autophagic sequestration of amyloid oligomers and

- improved cognition in Alzheimer's disease. *PLoS Genet.* **13**, (2017).
24. Houtman, J., Freitag, K., Gimber, N., Schmoranzner, J., Heppner, F. L., & Jendrach, M. Beclin1-driven autophagy modulates the inflammatory response of microglia via NLRP3. *EMBO J.* **38**, (2019).
  25. Heckmann, B. L., Teubner, B. J. W., Tummers, B., Boada-Romero, E., Harris, L., Yang, M., Guy, C. S., Zakharenko, S. S., & Green, D. R. LC3-Associated Endocytosis Facilitates  $\beta$ -Amyloid Clearance and Mitigates Neurodegeneration in Murine Alzheimer's Disease. *Cell* **178**, 536-551.e14 (2019).
  26. Huang, Y., Happonen, K. E., Burrola, P. G., O'Connor, C., Hah, N., Huang, L., Nimmerjahn, A., & Lemke, G. Microglia use TAM receptors to detect and engulf amyloid  $\beta$  plaques. *Nat. Immunol.* **2021** *225* **22**, 586–594 (2021).
  27. Madeo, F., Eisenberg, T., Pietrocola, F. & Kroemer, G. Spermidine in health and disease. *Science* **359**, 6374 (2018).
  28. Pietrocola, F., Lachkar, S., Enot, D. P., Niso-Santano, M., Bravo-San Pedro, J. M., Sica, V., Izzo, V., Maiuri, M. C., Madeo, F., Mariño, G., & Kroemer, G. Spermidine induces autophagy by inhibiting the acetyltransferase EP300. *Cell Death Differ.* **22**, 509–516 (2015).
  29. Eisenberg, T., Abdellatif, M., Schroeder, S., Primessnig, U., Stekovic, S., Pendl, T., Harger, A., Schipke, J., Zimmermann, A., Schmidt, A., Tong, M., Ruckstuhl, C., Dammbroek, C., Gross, A. S., Herbst, V., Magnes, C., Trausinger, G., Narath, S., Meinitzer, A., Hu, Zehan, Kirsch, A., Eller, K., Carmona-Gutierrez, D., Büttner, S., Pietrocola, F., Knittelfelder, O., Schrepfer, E., Rockenfeller, P., Simonini, C., Rahn, A., Horsch, M., Moreth, K., Beckers, J., Fuchs, H., Gailus-Durner, V., Neff, F., Janik, D., Rathkolb, B., Rozman, J., De Angelis, M., Moustafa, T., Haemmerle, G., Mayr, M., Willeit, P., Von Frieling-Salewsky, M., Pieske, B., Scorrano, L., Pieber, T., Pechlaner, R., Willeit, J., Sigrist, S. J., Linke, W. A., Mühlfeld, C., Sadoshima, J., Dengjel, J., Kiechl, S., Kroemer, G., Sedej, S., Madeo, F. Cardioprotection and lifespan extension by the natural polyamine spermidine. *Nat. Med.* **2016** *2212* **22**, 1428–1438 (2016).
  30. Yue, F., Li, W., Zou, J., Jiang, X., Xu, G., Huang, H., & Liu, L. Prevention and Epidemiology Spermidine Prolongs Lifespan and Prevents Liver Fibrosis and Hepatocellular Carcinoma by Activating MAP1S-Mediated Autophagy. *Cancer Res.* **77**, 2938-2951 (2017).
  31. Filfan, M., Olaru, A., Udristoiu, I., Margaritescu, C., Petcu, E., Hermann, D. M., & Popa-Wagner, A. Long-term treatment with spermidine increases health span of middle-aged Sprague-Dawley male rats. *GeroScience* **42**, 937 (2020).
  32. Sharma, S., Kumar, P. & Deshmukh, R. Neuroprotective potential of spermidine against rotenone induced Parkinson's disease in rats. *Neurochem. Int.* **116**, 104–111 (2018).
  33. Xu, T. T., Li, H., Dai, Z., Lau, G. K., Li, B. Y., Zhu, W. L., Liu, X. Q., Liu, H. F., Cai, W. W., Huang, S. Q., Wang, Q., & Zhang, S. J. Spermidine and spermine delay brain aging by inducing autophagy in SAMP8 mice. *Aging (Albany, NY)*. **12**, 6401–6414 (2020).
  34. Yang, Q., Zheng, C., Cao, J., Cao, G., Shou, P., Lin, L., Velletri, T., Jiang, M., Chen, Q., Han, Y., Li, F., Wang, Y., Cao, W., & Shi, Y. Spermidine alleviates experimental autoimmune encephalomyelitis through inducing inhibitory macrophages. *Cell Death Differ.* **23**, 1850–1861 (2016).
  35. Choi, Y. H. & Park, H. Y. Anti-inflammatory effects of spermidine in lipopolysaccharide-stimulated BV2 microglial cells. *J. Biomed. Sci.* **19**, 1–8 (2012).
  36. Jeong, J. W., Cha, H. J., Han, M. H., Hwang, S. J., Lee, D. S., Yoo, J. S., Choi, I. W., Kim, S., Kim, H. S., Kim, G. Y., Hong, S. H., Park, C., Lee, H. J., & Choi, Y. H. Spermidine Protects against Oxidative Stress in Inflammation Models Using Macrophages and Zebrafish. *Biomol. Ther. (Seoul)*. **26**, 146 (2018).
  37. Gupta, V. K., Pech, U., Bhukel, A., Fulterer, A., Ender, A., Mauermann, S. F., Andlauer, T. F. M., Antwi-Adjei, E., Beuschel, C., Thriene, K., Maglione, M., Quentin, C., Bushow, R., Schwärzel, M., Mielke, T., Madeo, F., Dengjel, J., Fiala, A., & Sigrist, S. J. Spermidine Suppresses Age-Associated Memory Impairment by Preventing Adverse Increase of Presynaptic Active Zone Size and Release. *PLOS Biol.* **14**, e1002563 (2016).
  38. Schroeder, S., Hofer, S. J., Zimmermann, A., Pechlaner, R., Dammbroek, C., Pendl, T., Marcello, G. M., Pogatschnigg, V., Bergmann, M., Müller, M., Gschiel, V., Ristic, S., Tadic, J., Iwata, K., Richter, G., Farzi, A., Üçal, M., Schäfer, U., Poglitsch, M., Royer, P., Mekis, R., Agreiter, M., Tölle, R. C., Sótonyi, P., Willeit, J., Mairhofer, B., Niederkofler, H., Pallhuber, I., Rungger, G., Tilg, H., Defrancesco, M., Marksteiner, J., Sinner, F., Magnes, C., Pieber, T. R., Holzer, P., Kroemer, G., Carmona-Gutierrez, D., Scorrano, L., Dengjel, J., Madl, T., Sedej, S., Sigrist, S. J., Rácz, B., Kiechl, S., Eisenberg, T., Madeo, F. Dietary spermidine improves cognitive function. *Cell Rep.* **35**, 108985 (2021).
  39. Deng, K., He, H., Qiu, J., Lorber, B., Bryson, J. B., & Filbin, M. T. Increased Synthesis of Spermidine as a Result of Upregulation of Arginase I Promotes Axonal Regeneration in Culture and In Vivo. *J Neurosci.* **29**, 9545-9552 (2009).
  40. Maglione, M., Kochlamazashvili, G., Eisenberg, T., Rácz, B., Michael, E., Toppe, D., Stumpf, A., Wirth, A., Zeug, A., Müller, F. E., Moreno-Velasquez, L., Sammons, R. P., Hofer, S. J., Madeo, F., Maritzen, T., Maier, N., Ponimaskin, E., Schmitz, D., Haucke, V., & Sigrist, S. J. Spermidine protects from age-related synaptic alterations at hippocampal mossy fiber-CA3 synapses. *Sci. Reports* **2019** *91* **9**, 1–12 (2019).
  41. Sandusky-Beltran, L. A., Kovalenko, A., Placides, D. S., Ratnasamy, K., Ma, C., Hunt, J. B., Liang, H., Calahatian, J. I. T., Michalski, C., Fahnestock, M., Blair, L. J., Darling, A. L., Baker, J. D., Fontaine, S. N., Dickey, C. A., Gamsby, J. J., Nash, K. R., Abner, E., Selenica, M. L. B., & Lee, D. C. Aberrant AZIN2 and

- polyamine metabolism precipitates tau neuropathology. *J. Clin. Invest.* **131**, (2021).
42. Radde, R., Bolmont, T., Kaeser, S. A., Coomaraswamy, J., Lindau, D., Stoltze, L., Calhoun, M. E., Jäggi, F., Wolburg, H., Gengler, S., Haass, C., Ghetti, B., Czech, C., Hölscher, C., Mathews, P. M., & Jucker, M. A $\beta$ 42-driven cerebral amyloidosis in transgenic mice reveals early and robust pathology. *EMBO Rep.* **7**, 940–946 (2006).
  43. Freitag, K., Sterczyk, N., Wendlinger, S., Obermayer, B., Schulz, J., Farztdinov, V., Mülleder, M., Ralsler, M., Houtman, J., Fleck, L., Braeuning, C., Sansevrino, R., Hoffmann, C., Milovanovic, D., Sigrist, S. J., Conrad, T., Beule, D., Heppner, F. L., & Jendrach, M. Spermidine reduces neuroinflammation and soluble amyloid beta in an Alzheimer’s disease mouse model. *J. Neuroinflammation* **2022** *191* **19**, 1–19 (2022).
  44. Eede, P., Obst, J., Benke, E., Yvon-Durocher, G., Richard, B. C., Gimber, N., Schmoranzler, J., Böddrich, A., Wanker, E. E., Prokop, S., Heppner, F. L. Interleukin- 12 / 23 deficiency differentially affects pathology in male and female Alzheimer ’ s disease-like mice. *EMBO Rep.* **21**, 1–18 (2020).
  45. Schneider, C. A., Rasband, W. S. & Eliceiri, K. W. NIH Image to ImageJ: 25 years of image analysis. *Nat. Methods* **9**, 671–675 (2012).
  46. Otsu, N. A Threshold Selection Method from Gray-Level Histograms. *IEEE Trans Syst Man Cybern* **SMC-9**, 62–66 (1979).
  47. Ridler, T. W. & Calvard, S. Picture Thresholding Using an Iterative Selection Method. *IEEE Trans. Syst. Man Cybern.* **SMC-8**, 630–632 (1978).
  48. Wei, Z., Cai, L., Zhao, X., Jiang, X. & Li, X. Effects of Spermidine on Cell Proliferation, Migration, and Inflammatory Response in Porcine Enterocytes. *Front. Biosci.* **2022**, *27*(6), 194 **27**, 194 (2022).
  49. Franco-Bocanegra, D. K., George, B., Lau, L. C., Holmes, C., Nicoll, J. A. R., & Boche, D. Microglial motility in Alzheimer’s disease and after A $\beta$ 42 immunotherapy: a human post-mortem study. *Acta Neuropathol. Commun.* **7**, 174 (2019).
  50. Mosher, K. I. & Wyss-Coray, T. Microglial dysfunction in brain aging and Alzheimer’s disease. *Biochem. Pharmacol.* **88**, 594–604 (2014).
  51. Park, C. R., You, D. J., Park, S., Mander, S., Jang, D. E., Yeom, S. C., Oh, S. H., Ahn, C., Lee, S. H., Seong, J. Y., & Hwang, J. I. The accessory proteins REEP5 and REEP6 refine CXCR1-mediated cellular responses and lung cancer progression. *Sci. Reports* **2016** *61* **6**, 1–13 (2016).
  52. Kenigsbuch, M., Bost, P., Halevi, S., Yehuda, H. Ben, Hajbi, R., Schwikowski, B., Peles, E., Amit, I., & Schwartz, M. A shared oligodendrocyte activation state associated with neuroinflammation and neurodegeneration. *BASIC Sci. Pathog.* (2021).
  53. Belgrad, J., de Pace, R. & Douglas Fields, R. Autophagy in Myelinating Glia. *J. Neurosci.* **40**, 256–266 (2020).
  54. Wu, Y., Guo, Z., Yao, K., Miao, Y., Liang, S., Liu, F., Wang, Y., & Zhang, Y. The Transcriptional Foundations of Sp110-mediated Macrophage (RAW264.7) Resistance to Mycobacterium tuberculosis H37Ra. *Sci. Rep.* **6**, (2016).
  55. Zheng, C. B., Gao, W. C., Xie, M., Li, Z., Ma, X., Song, W., Luo, D., Huang, Y., Yang, J., Zhang, P., Huang, Y., Yang, W., & Yao, X. Ang II Promotes Cardiac Autophagy and Hypertrophy via Orai1/STIM1. *Front. Pharmacol.* **12**, (2021).
  56. She, H., Yang, Q., Shepherd, K., Smith, Y., Miller, G., Testa, C., & Mao, Z. Direct regulation of complex I by mitochondrial MEF2D is disrupted in a mouse model of Parkinson disease and in human patients. *J. Clin. Invest.* **121**, 930–940 (2011).
  57. Mao, Z., Bonni, A., Xia, F., Nadal-Vicens, M. & Greenberg, M. E. Neuronal Activity-Dependent Cell Survival Mediated by Transcription Factor MEF2. *Science* **286**, 785–790 (1999).
  58. Akhtar, M. W., Kim, M. S., Adachi, M., Morris, M. J., Qi, X., Richardson, J. A., Bassel-Duby, R., Olson, E. N., Kavalali, E. T., & Monteggia, L. M. In vivo analysis of MEF2 transcription factors in synapse regulation and neuronal survival. *PLoS One* **7**, (2012).
  59. Chang, T. Y., Yamauchi, Y., Hasan, M. T. & Chang, C. Thematic Review Series: ApoE and Lipid Homeostasis in Alzheimer’s Disease: Cellular cholesterol homeostasis and Alzheimer’s disease. *J. Lipid Res.* **58**, 2239 (2017).
  60. Zhao, Y. & Xu, H. Microglial lactate metabolism as a potential therapeutic target for Alzheimer’s disease. *Mol. Neurodegener.* **17**, 1–3 (2022).
  61. Messerer, J., Wrede, C., Schipke, J., Brandenberger, C., Abdellatif, M., Eisenberg, T., Madeo, F., Sedej, S., & Mühlfeld, C. Spermidine supplementation influences mitochondrial number and morphology in the heart of aged mice. *J. Anat.* **00**, 1–11 (2021).
  62. Hofer, S. J., Liang, Y., Zimmermann, A., Schroeder, S., Dengjel, J., Kroemer, G., Eisenberg, T., Sigrist, S. J., & Madeo, F. Spermidine-induced hypusination preserves mitochondrial and cognitive function during aging) Spermidine-induced hypusination preserves mitochondrial and cognitive function during aging. (2021).
  63. Heneka, M. T., Kummer, M. P., Stutz, A., Delekate, A., Schwartz, S., Vieira-Saecker, A., Griep, A., Axt, D., Remus, A., Tzeng, T. C., Gelpi, E., Halle, A., Korte, M., Latz, E., & Golenbock, D. T. NLRP3 is activated in Alzheimer’s disease and contributes to pathology in APP/PS1 mice. *Nature* **493**, 674 (2013).
  64. Ising, C., Venegas, C., Zhang, S., Scheiblich, H., Schmidt, S. V., Vieira-Saecker, A., Schwartz, S., Albasset, S., McManus, R. M., Tejera, D., Griep, A., Santarelli, F., Brosseron, F., Opitz, S., Stunden, J., Merten, M.,

- Kayed, R., Golenbock, D. T., Blum, D., Latz, E., Buée, L., Heneka, M. T. NLRP3 inflammasome activation drives tau pathology. *Nature* **575**, 669 (2019).
65. Wang, X., Wang, W., Li, L., Perry, G., Lee, H. gon, & Zhu, X. Oxidative stress and mitochondrial dysfunction in Alzheimer's disease. *Biochim. Biophys. Acta* **1842**, 1240–1247 (2014).
  66. vom Berg, J., Prokop, S., Miller, K. R., Obst, J., K, R. E., Lopategui-Cabezas, I., Wegner, A., Mair, F., Schipke, C. G., Peters, O., Winter, Y., Becher, B., & Heppner, F. L. Inhibition of IL-12/IL-23 signaling reduces Alzheimer's disease-like pathology and cognitive decline. *Nat. Med.* **12**, 1812-9 (2012).
  67. Wagner, L. K., Gilling, K. E., Schormann, E., Kloetzel, P. M., Heppner, F. L., Krüger, E., & Prokop, S. Immunoproteasome deficiency alters microglial cytokine response and improves cognitive deficits in Alzheimer's disease-like APPPS1 mice. *Acta Neuropathol. Commun.* **5**, 52 (2017).
  68. Alzheimer's Association. More Than Normal Aging: Understanding Mild Cognitive Impairment. *Alzheimer's Dis. Facts Fig.* (2022).
  69. Majumder, S., Richardson, A., Strong, R. & Oddo, S. Inducing Autophagy by Rapamycin Before, but Not After, the Formation of Plaques and Tangles Ameliorates Cognitive Deficits. *PLoS One* **6**, (2011).
  70. Caccamo, A., De Pinto, V., Messina, A., Branca, C. & Oddo, S. Genetic Reduction of Mammalian Target of Rapamycin Ameliorates Alzheimer's Disease-Like Cognitive and Pathological Deficits by Restoring Hippocampal Gene Expression Signature. *J. Neurosci.* **34**, 7988 (2014).
  71. Salmon, A.B. About-face on the metabolic side effects of rapamycin. *Oncotarget* **6**, 2585-6 (2015).
  72. Wirth, M., Benson, G., Schwarz, C., Köbe, T., Grittner, U., Schmitz, D., Sigrist, S. J., Bohlken, J., Stekovic, S., Madeo, F., & Flöel, A. The effect of spermidine on memory performance in older adults at risk for dementia: A randomized controlled trial. *Cortex*. **109**, 181–188 (2018).
  73. Wirth, M., Schwarz, C., Benson, G., Horn, N., Buchert, R., Lange, C., Köbe, T., Hetzer, S., Maglione, M., Michael, E., Märschenz, S., Mai, K., Kopp, U., Schmitz, Di., Grittner, U., Sigrist, S. J., Stekovic, S., Madeo, F., & Flöel, A. Effects of spermidine supplementation on cognition and biomarkers in older adults with subjective cognitive decline (SmartAge)-study protocol for a randomized controlled trial. *Alzheimers. Res. Ther.* **11**, (2019).
  74. Schwarz, C., Horn, N., Benson, G., Wrachtrup Calzado, I., Wurdack, K., Pechlaner, R., Grittner, U., Wirth, M., & Flöel, A. Spermidine intake is associated with cortical thickness and hippocampal volume in older adults. *Neuroimage* **221**, (2020).

## 6 EIDESSTATTLICHE VERSICHERUNG

„Ich, Kiara Freitag, versichere an Eides statt durch meine eigenhändige Unterschrift, dass ich die vorgelegte Dissertation mit dem Thema: „Spermidine-induced autophagy and its effect on Alzheimer´s disease pathogenesis in mice/ Die Auswirkung der Spermidin-induzierten Autophagie auf die Pathogenese der Alzheimer Erkrankung im Mausmodell“ selbstständig und ohne nicht offengelegte Hilfe Dritter verfasst und keine anderen als die angegebenen Quellen und Hilfsmittel genutzt habe.

Alle Stellen, die wörtlich oder dem Sinne nach auf Publikationen oder Vorträgen anderer Autoren/innen beruhen, sind als solche in korrekter Zitierung kenntlich gemacht. Die Abschnitte zu Methodik (insbesondere praktische Arbeiten, Laborbestimmungen, statistische Aufarbeitung) und Resultaten (insbesondere Abbildungen, Graphiken und Tabellen) werden von mir verantwortet.

Ich versichere ferner, dass ich die in Zusammenarbeit mit anderen Personen generierten Daten, Datenauswertungen und Schlussfolgerungen korrekt gekennzeichnet und meinen eigenen Beitrag sowie die Beiträge anderer Personen korrekt kenntlich gemacht habe (siehe Anteilserklärung). Texte oder Textteile, die gemeinsam mit anderen erstellt oder verwendet wurden, habe ich korrekt kenntlich gemacht.

Meine Anteile an etwaigen Publikationen zu dieser Dissertation entsprechen denen, die in der untenstehenden gemeinsamen Erklärung mit dem/der Erstbetreuer/in, angegeben sind. Für sämtliche im Rahmen der Dissertation entstandenen Publikationen wurden die Richtlinien des ICMJE (International Committee of Medical Journal Editors; [www.icmje.org](http://www.icmje.org)) zur Autorenschaft eingehalten. Ich erkläre ferner, dass ich mich zur Einhaltung der Satzung der Charité – Universitätsmedizin Berlin zur Sicherung Guter Wissenschaftlicher Praxis verpflichte.

Weiterhin versichere ich, dass ich diese Dissertation weder in gleicher noch in ähnlicher Form bereits an einer anderen Fakultät eingereicht habe.

Die Bedeutung dieser eidesstattlichen Versicherung und die strafrechtlichen Folgen einer unwahren eidesstattlichen Versicherung (§§156, 161 des Strafgesetzbuches) sind mir bekannt und bewusst.“

---

Datum

---

Unterschrift

## 7 ANTEILSERKLÄRUNG

### Ausführliche Anteilserklärung an der erfolgten Publikation als Top-Journal im Rahmen der Promotionsverfahren zum PhD

Kiara Freitag hatte die folgenden Anteile an der nachfolgenden Publikation:

**Freitag K**, Sterczyk N, Wendlinger S, Obermayer B, Schulz J, Farztdinov V, Mülleder M, Ralser M, Houtman J, Fleck L, Braeuning C, Sansevrino R, Hoffmann C, Milovanovic D, Sigrist SJ, Conrad T, Beule D, Heppner FL, Jendrach M: Spermidine reduces neuroinflammation and soluble amyloid beta in an Alzheimer's disease mouse model. *J Neuroinflammation*. 2022 Jul 2;19(1):172. doi: 10.1186/s12974-022-02534-7.

Kiara Freitag war gemeinsam mit Prof. Dr. Frank Heppner und PD Dr. Marina Jendrach maßgeblich an der Entwicklung des Studiendesigns beteiligt. Durch ihre Initiative wurden neue Kollaborationen mit der Genomics Core Facility (Dr. Caroline Braeuning, Dr. Thomas Conrad) und der Core Unit Bioinformatics (Dr. Benedikt Obermayer, Dr. Dieter Beule) für die Einzelzellsequenzierung sowie mit der High-Throughput mass spectrometry Core Facility (Dr. Vadim Farztdinov, Dr. Michael Mülleder, Prof. Dr. Markus Ralser) für die Proteomanalyse mittels Massenspektrometrie gebildet. Sie war der Hauptansprechpartner für die Kollaborationen und hat die Koordination der Experimente und Analysen übernommen.

Außerdem hat Kiara Freitag die Kohortenplanung, Behandlung sowie die Gewebeentnahme und Mikroglia-Isolation aller Spermidin und Wasser behandelten Mäuse übernommen (Fig. 1-3, Fig. S1-S3). Die Messung vom A $\beta$  (Fig. 1a) sowie Zytokine-Gehalt (Fig. 3f) im Gehirn von Spermidin-behandelten Mäusen wurde ebenfalls von Kiara Freitag mit Hilfe von Nele Sterczyk durchgeführt, welche als Bachelorstudentin von Kiara Freitag betreut wurde. Zudem hat Kiara Freitag die Nuclei-Isolation durchgeführt, welche danach von der Genomics Core Facility (Dr. Caroline Braeuning, Dr. Thomas Conrad) für die Einzelzellsequenzierung genutzt wurden. In enger Zusammenarbeit mit der Core Unit Bioinformatics (Dr. Benedikt Obermayer, Dr. Dieter Beule) hat Kiara Freitag die Abbildungen Fig. 1b-f, Fig. 2a-b und Fig. S2a-g entwickelt. Dr. Benedikt Obermayer hat die bioinformatische Analyse übernommen, während Kiara Freitag Kandidatengene sowie Signalwege definiert hat. Für die Proteomanalyse isolierte Kiara Freitag Mikroglia, welche durch die High-Throughput mass spectrometry Core Facility (Dr. Vadim Farztdinov, Dr. Michael Mülleder, Prof. Dr. Markus Ralser) aufgearbeitet wurden. Zusammen mit dem Bioinformatiker Dr. Vadim Farztdinov hat Kiara Freitag die Abbildungen Fig. 3b-e und Fig. S3 zusammengestellt.

Die *in vitro* und *in vivo* Validierung der Einzelzellsequenzierungskandidaten (Fig. 1h-i, Fig. 2c, Fig. S2h-m) wurde von Sarah Wendlinger mithilfe von Kiara Freitag durchgeführt. Kiara Freitag betreute die Masterarbeit von Sarah Wendlinger. Zudem etablierte Kiara Freitag die Stimulation von akuten Hirnschnitten mit LPS und ATP sowie die Kultur von isolierten adulten Mikroglia und nutze diese um die Wirkung von Spermidin auf die Zytokinausschüttung zu analysieren (Fig. 4a, fig. S4d-h). Kiara Freitag hat zusammen mit Nele Sterczyk alle Experimente mit poly I:C als Stimulus sowie alle Experimente mit neonatalen Astrozyten durchgeführt (Fig. 4, Fig. S4, S5). Die Wirkung von Spermidin auf LPS/ATP-stimulierte Mikroglia und den Inflammasompathway wurde von PD Dr. Marina Jendrach und Julia Schulz untersucht (Fig. 4b, Fig. 5, Fig. S6). Kiara Freitag schrieb zudem zusammen mit PD Dr. Marina Jendrach das Manuskript für die Publikation.

---

Unterschrift der Doktorandin

## 8 AUSZUG JOURNAL SUMMARY LIST

Journal Data Filtered By: **Selected JCR Year: 2020** Selected Editions: SCIE,SSCI  
 Selected Categories: **"NEUROSCIENCES"** Selected Category Scheme: WoS  
**Gesamtanzahl: 273 Journale**

Rank	Full Journal Title	Total Cites	Journal Impact Factor	Eigenfactor Score
1	NATURE REVIEWS NEUROSCIENCE	49,897	34.870	0.048890
2	NATURE NEUROSCIENCE	73,709	24.884	0.128020
3	TRENDS IN COGNITIVE SCIENCES	33,482	20.229	0.036270
4	NEURON	111,115	17.173	0.175220
5	ACTA NEUROPATHOLOGICA	28,031	17.088	0.036970
6	MOLECULAR PSYCHIATRY	28,622	15.992	0.046220
7	Molecular Neurodegeneration	6,772	14.195	0.011650
8	TRENDS IN NEUROSCIENCES	22,858	13.837	0.019470
9	Nature Human Behaviour	5,549	13.663	0.023120
10	BRAIN	64,627	13.501	0.061550
11	BIOLOGICAL PSYCHIATRY	50,155	13.382	0.045540
12	JOURNAL OF PINEAL RESEARCH	12,492	13.007	0.008170
13	BEHAVIORAL AND BRAIN SCIENCES	11,610	12.579	0.007760
14	Annual Review of Neuroscience	14,699	12.449	0.010490
15	PROGRESS IN NEUROBIOLOGY	15,161	11.685	0.010300
16	SLEEP MEDICINE REVIEWS	11,218	11.609	0.014840
17	ANNALS OF NEUROLOGY	43,728	10.422	0.039960
18	NEUROSCIENCE AND BIOBEHAVIORAL REVIEWS	36,525	8.989	0.048970
19	Brain Stimulation	9,206	8.955	0.015960
20	npj Parkinsons Disease	1,093	8.651	0.003040
21	FRONTIERS IN NEUROENDOCRINOLOGY	5,338	8.606	0.005050
22	Neurology-Neuroimmunology & Neuroinflammation	3,863	8.485	0.008390
23	Journal of Neuroinflammation	19,657	8.322	0.027070
24	NEUROPATHOLOGY AND APPLIED NEUROBIOLOGY	4,791	8.090	0.004640
25	NEURAL NETWORKS	18,837	8.050	0.019420

## 9 PUBLIKATION

**Freitag K**, Sterczyk N, Wendlinger S, Obermayer B, Schulz J, Farztdinov V, Mülleder M, Ralser M, Houtman J, Fleck L, Braeuning C, Sansevrino R, Hoffmann C, Milovanovic D, Sigrist SJ, Conrad T, Beule D, Heppner FL, Jendrach M: Spermidine reduces neuroinflammation and soluble amyloid beta in an Alzheimer's disease mouse model. *J Neuroinflammation*. 2022 Jul 2;19(1):172. doi: 10.1186/s12974-022-02534-7.

RESEARCH

Open Access



# Spermidine reduces neuroinflammation and soluble amyloid beta in an Alzheimer's disease mouse model

Kiara Freitag<sup>1,2</sup>, Nele Sterczyk<sup>1</sup>, Sarah Wendlinger<sup>1,3</sup>, Benedikt Obermayer<sup>4</sup>, Julia Schulz<sup>1</sup>, Vadim Farztdinov<sup>5</sup>, Michael Müller<sup>5</sup>, Markus Ralser<sup>6,7</sup>, Judith Houtman<sup>1</sup>, Lara Fleck<sup>1</sup>, Caroline Braeuning<sup>8,12</sup>, Roberto Sansevrino<sup>9</sup>, Christian Hoffmann<sup>9</sup>, Dragomir Milovanovic<sup>9</sup>, Stephan J. Sigrist<sup>2,10,11</sup>, Thomas Conrad<sup>8,12</sup>, Dieter Beule<sup>4</sup>, Frank L. Heppner<sup>1,2,10†</sup> and Marina Jendrach<sup>1\*†</sup>

## Abstract

**Background:** Deposition of amyloid beta (A $\beta$ ) and hyperphosphorylated tau along with glial cell-mediated neuroinflammation are prominent pathogenic hallmarks of Alzheimer's disease (AD). In recent years, impairment of autophagy has been identified as another important feature contributing to AD progression. Therefore, the potential of the autophagy activator spermidine, a small body-endogenous polyamine often used as dietary supplement, was assessed on A $\beta$  pathology and glial cell-mediated neuroinflammation.

**Results:** Oral treatment of the amyloid prone AD-like APPS1 mice with spermidine reduced neurotoxic soluble A $\beta$  and decreased AD-associated neuroinflammation. Mechanistically, single nuclei sequencing revealed AD-associated microglia to be the main target of spermidine. This microglia population was characterized by increased AXL levels and expression of genes implicated in cell migration and phagocytosis. A subsequent proteome analysis of isolated microglia confirmed the anti-inflammatory and cytoskeletal effects of spermidine in APPS1 mice. In primary microglia and astrocytes, spermidine-induced autophagy subsequently affected TLR3- and TLR4-mediated inflammatory processes, phagocytosis of A $\beta$  and motility. Interestingly, spermidine regulated the neuroinflammatory response of microglia beyond transcriptional control by interfering with the assembly of the inflammasome.

**Conclusions:** Our data highlight that the autophagy activator spermidine holds the potential to enhance A $\beta$  degradation and to counteract glia-mediated neuroinflammation in AD pathology.

**Keywords:** Alzheimer's disease, Neuroinflammation, Microglia, Astrocytes, Autophagy, Spermidine, Dietary supplement, Single nuclei sequencing, Liquid chromatography tandem mass spectrometry, Phagocytosis

## Background

Alzheimer's disease (AD) is the most common neurodegenerative disease and the leading cause of dementia worldwide. Pathologically, AD is defined by the following hallmarks: extracellular plaques containing amyloid-beta (A $\beta$ ), neurofibrillary tangles consisting of hyperphosphorylated microtubule-associated protein tau, loss of neurons and neuroinflammation. Over the last decade, a large body of evidence revealed a substantial involvement

<sup>†</sup>Frank L. Heppner and Marina Jendrach contributed equally to this work

\*Correspondence: marina.jendrach@charite.de

<sup>1</sup> Department of Neuropathology, Charité, Universitätsmedizin Berlin, corporate member of Freie Universität Berlin, Humboldt-Universität Zu Berlin, Berlin Institute of Health, Berlin, Germany  
Full list of author information is available at the end of the article



© The Author(s) 2022. **Open Access** This article is licensed under a Creative Commons Attribution 4.0 International License, which permits use, sharing, adaptation, distribution and reproduction in any medium or format, as long as you give appropriate credit to the original author(s) and the source, provide a link to the Creative Commons licence, and indicate if changes were made. The images or other third party material in this article are included in the article's Creative Commons licence, unless indicated otherwise in a credit line to the material. If material is not included in the article's Creative Commons licence and your intended use is not permitted by statutory regulation or exceeds the permitted use, you will need to obtain permission directly from the copyright holder. To view a copy of this licence, visit <http://creativecommons.org/licenses/by/4.0/>. The Creative Commons Public Domain Dedication waiver (<http://creativecommons.org/publicdomain/zero/1.0/>) applies to the data made available in this article, unless otherwise stated in a credit line to the data.

of microglia, the brain's intrinsic myeloid cells, in regulating and potentially driving AD pathogenesis. Microglia are essential for maintaining brain homeostasis and respond to AD pathology by transforming into disease-associated microglia (DAM) [1], an activated and transcriptionally distinct state, which is associated with alterations in proliferation, phagocytic behavior and increased cytokine production [2]. Similarly, astrocytes produce cytokines upon activation with A $\beta$  [3, 4]. The link between neuroinflammation and neurodegenerative diseases is strengthened by the profound effects of maternal immune activation (e.g., by poly I:C injections) on the development of neurodegenerative diseases [5–7], thus demonstrating a crucial role of inflammatory events in the initiation of a vicious cycle of neuropathological alterations.

A growing set of data, including those derived from genome-wide association studies of various human diseases by the Wellcome Trust Case Control Consortium [8], indicates that autophagy, one of the main degradation and quality control pathways of the cell, is dysregulated in AD patients and AD mouse models [9, 10]. Autophagy may interfere with AD pathology either by regulating A $\beta$  degradation and/or by modulating neuroinflammatory processes. For both interference points, the mechanisms and target cells are still not fully understood. Mice deficient in the autophagic protein ATG16L1 exhibited a specific increase of Interleukin (IL)-1 $\beta$  and IL-18 in macrophages and severe colitis, which was ameliorated by anti-IL-1 $\beta$  and IL-18 antibody administration [11]. Recently, we could show that a reduction of the key autophagic protein Beclin1 (BECN1), which is also decreased in AD patients [12, 13], resulted in an enhanced release of IL-1 $\beta$  and IL-18 by microglia [14]. The multimeric NLRP3 inflammasome complex, responsible for processing Pro-IL-1 $\beta$  and Pro-IL-18 into its mature forms by activated Caspase-1 (CASP1) [15], was shown to be degraded by autophagy [14, 16]. Lack of the NLRP3–inflammasome axis resulted in amelioration of neuroinflammation and disease pathology in several neurodegenerative mouse models [17–19], thus emphasizing that activation of autophagy presents an intriguing therapeutic target to counteract neuroinflammation.

The small endogenous polyamine and nutritional supplement spermidine is known to induce autophagy by inhibiting different acetyltransferases [20, 21] and to extend the life span of flies, worms and yeast [21–24]. In addition, spermidine supplementation improved clinical scores and neuroinflammation in mice with experimental autoimmune encephalomyelitis (EAE) [24, 25], protected dopaminergic neurons in a Parkinson's disease rat model [26], and exhibited neuroprotective effects and anti-inflammatory properties in a murine model of

accelerated aging [27]. Consistent with these observations, spermidine decreased the inflammatory response of macrophages and the microglial cell line BV2 upon LPS stimulation in vitro [28–30]. Recent data showed that polyamines improved age-impaired cognitive function and tau-mediated memory impairment in mice [31, 32] and impaired COVID-19 virus particle production [33]. These findings led us to investigate the yet unknown potential of spermidine to interfere with AD pathology and chronic neuroinflammation.

Here, we show that spermidine treatment of the AD-like APPPS1 mice reduced soluble A $\beta$  species. Applying single nuclei sequencing and liquid chromatography tandem mass spectrometry, crucial underlying changes in microglia, namely, the DAM marker AXL and pathways associated with cell migration, phagocytosis, autophagy and anti-neuroinflammation were identified. At later stages of disease pathology, spermidine reduced a CNS-wide AD-associated neuroinflammation in vivo, which correlates with targeting key inflammatory signaling pathways in vitro. We, therefore, provide evidence that spermidine enhances degradation of A $\beta$  and subsequently counteracts microglia-mediated neuroinflammation.

## Materials and methods

### Mice and spermidine treatment

APPPS1<sup>+/-</sup> mice [34] were used as an Alzheimer's disease-like mouse model. *Casp1*<sup>-/-</sup> mice were a kind gift from F. Knäuf and M. Reichel, Medizinische Klinik m.S. Nephrologie und Internistische Intensivmedizin, Charité Berlin. *Beclin1*<sup>fllox/fllox</sup> mice were a kind gift from Tony Wyss-Coray (Stanford University School of Medicine/USA).

APPPS1<sup>+/-</sup> mice and littermate wild type control (WT) mice were treated with 3 mM spermidine dissolved in their drinking water (changed twice a week) from an age of 30 days until an age of either 120 days or 290 days. Control mice received only water (H<sub>2</sub>O). Prior to each exchange of the drinking bottles, the weight of the bottles was determined and used to calculate the average volume consumed per animal per day. Animals were kept in individually ventilated cages with a 12 h light cycle with food and water ad libitum. All animal experiments were conducted in accordance with animal welfare acts and were approved by the regional office for health and social service in Berlin (LaGeSo).

### Tissue preparation

Mice were anesthetized with isoflurane, euthanized by CO<sub>2</sub> exposure and transcardially perfused with PBS. Brains were removed from the skull and sagittally divided. The left hemisphere was fixed with 4% paraformaldehyde for 24 h at 4 °C and subsequently immersed in 30%

sucrose until sectioning for immunohistochemistry was performed. The right hemisphere was snap-frozen in liquid nitrogen and stored at  $-80^{\circ}\text{C}$  for a 3-step protein extraction using buffers with increasing stringency as described previously [35]. In brief, the hemisphere was homogenized in Tris-buffered saline (TBS) buffer (20 mM Tris, 137 mM NaCl, pH=7.6) to extract soluble proteins, in Triton-X buffer (TBS buffer containing 1% Triton X-100) for membrane-bound proteins and in SDS buffer (2% SDS in ddH<sub>2</sub>O) for the SDS-soluble fraction of A $\beta$ , which we here refer to as insoluble A $\beta$ . The protein fractions were extracted by ultracentrifugation at 100,000 g for 45 min after initial homogenization with a tissue homogenizer and a 1 ml syringe with G26 canulas. The respective supernatants were collected and frozen at  $-80^{\circ}\text{C}$  for downstream analysis. Protein concentration was determined using the Quantipro BCA Protein Assay Kit (Pierce) according to the manufacturer's protocol with a Tecan Infinite<sup>®</sup> 200 Pro (Tecan Life Sciences).

#### Quantification of A $\beta$ levels and pro-inflammatory cytokines

A $\beta$ 40 and A $\beta$ 42 levels of brain protein fractions were measured using the 96-well MultiSpot V-PLEX A $\beta$  Peptide Panel 1 (6E10) Kit (MesoScale Discovery, K15200E-1). While the TBS and TX fraction were not diluted, the SDS fraction was diluted 1:500 with Diluent 35. Cytokine concentrations were measured in the undiluted TBS fraction or in the cell supernatant using the V-PLEX Pro-inflammatory Panel 1 (MesoScale Discovery, K15048D1). For all samples, duplicates were measured and concentrations in the TBS fraction normalized to BCA values.

#### Histology

Paraformaldehyde-fixed and sucrose-treated hemispheres were frozen and cryosectioned coronally at 40  $\mu\text{m}$  using a cryostat (Thermo Scientific HM 560). Details for the different staining procedures are described in the Additional file 2.

#### Brain slice culture

The brains of C57Bl/6J and APPPS1 mice were harvested, the cerebellum removed and the hemispheres mounted on a cutting disk using a thin layer of superglue. Hemispheres were cut using the Vibratome platform submerged in chilled medium consisting of DMEM medium (Invitrogen, 41966-029) supplemented with 1% penicillin/streptomycin (Sigma, P0781-20ML). Coronal slicing was performed from anterior to posterior after discarding the first 1 mm of tissue generating 10  $\times$  300  $\mu\text{m}$  sequential slices per brain with vibrating frequency set to

10 and speed to 3. Brain slices were cultured in pairs in 1 ml culture medium at 35  $^{\circ}\text{C}$ , 5% CO<sub>2</sub> in 6-well plates. Pre-treatment with the indicated spermidine concentrations was started immediately for 2 h. Subsequently, LPS (10  $\mu\text{g}/\text{ml}$ ) was added to the medium for 3 h followed by the addition of ATP (5 mM) for an additional 3 h. Afterwards, the culture medium was frozen for subsequent analyses.

#### Isolation and culture of adult microglia

Adult microglia were isolated from the hemispheres of 160-day-old C57BL/6 J mice by magnetic activated cell sorting (MACS). The manufacturer's protocols were followed. In brief, mice were transcardially perfused with PBS and tissue dissociated with the Neural Tissue Dissociation kit (P) (Miltenyi Biotec, 130-092-628) in C-tubes (Miltenyi, 130-096-334) on a gentleMACS Octo Dissociator with Heaters (Miltenyi Biotec, 130-096-427). Afterwards, the cell suspension was labelled with CD11b microbeads (Miltenyi Biotec, 130-093-634) and passed through LS columns (Miltenyi Biotec, 130-042-401) placed on an OctoMACS<sup>™</sup> manual separator. Subsequently, microglia were collected by column flushing and cultured in DMEM medium (Invitrogen, 41966-029) supplemented with 10% FBS (PAN-Biotech, P40-37500) and 1% penicillin/streptomycin (Sigma, P0781-20ML). Medium was changed every 3 days until adult microglia were treated as indicated after 8 days in vitro (DIV).

#### Cell culture of neonatal microglia and astrocytes

Newborn mice (1–4 days) were sacrificed by decapitation. Mixed glial cultures were prepared as described previously [14]. In brief, brains were dissected, meninges removed and brains mechanically and enzymatically homogenized with 0.005% trypsin/EDTA. Cells were cultured in complete medium consisting of DMEM medium (Invitrogen, 41966-029) supplemented with 10% FBS (PAN-Biotech, P40-37500) and 1% penicillin/streptomycin (Sigma, P0781-20ML) at 37  $^{\circ}\text{C}$  with 5% CO<sub>2</sub>. From 7 DIV on, microglia proliferation was induced by adding 5 ng/ml GM-CSF (Miltenyi Biotec, 130-095-746) to the complete medium. Microglia were harvested at 10–13 DIV by manually shaking flasks for 6 min. Cells were treated after a settling time of 24 h. Neonatal BECN1<sup>fllox/fllox</sup>.CX3CR1<sup>CreERT2</sup> microglia were treated with (Z)-4-Hydroxytamoxifen (Sigma #7904) after 5 DIV and assessed 7 days after Tamoxifen treatment.

After isolating neonatal microglia, neonatal astrocytes were separated by MACS. Neonatal astrocytes were detached with 0.05% trypsin, pelleted by centrifugation and incubated with CD11b microbeads (Miltenyi Biotec, 130-093-634) for 15 min at 4  $^{\circ}\text{C}$  to negatively isolate astrocytes. Afterwards, the cell suspension

was passed through LS columns (Miltenyi Biotec, 130-042-401) placed on an OctoMACS™ manual separator and the flow-through containing the astrocytes was collected. Subsequently, astrocytes were cultured in complete medium for 2 days before being treated. For all experiments, 100,000 cells were seeded on 24 well plates if not stated otherwise.

#### Cell treatment

For pro-inflammatory stimulation, cells were either treated with LPS (1 µg/ml, Sigma, L4391-1MG) for 3 h followed by ATP (2 mM, Sigma Aldrich, A6419-5 g; 4 mM for ASC speck/inflammasome formation) for 45 min, with poly I:C (50 µg/ml, InVivoGen, tlrpicw-250) for 6 h or with oligomeric Aβ (5 µM, Cayman Chemicals) for 24 h if not stated otherwise. Spermidine trihydrochloride (Sigma, S2501-5G) diluted in complete medium was added as indicated. For the ARPC3 western blot, cells were pretreated with spermidine for 6 h and subsequently stimulated with LPS (1 µg/ml) for 6 h followed by ATP (2 mM) for 45 min. Autophagy was activated by keeping cells in HBSS for 2 h prior to treatment (24020-091, Invitrogen) and blocked by addition of 3-MA (Sigma-Aldrich, M9282, final concentration 10 mM). The ASC oligomerization inhibitor MCC950 (inh-mcc, Invivogen) was used with a final concentration of 300 nM.

#### Cell migration/chemotaxis assay

Cell migration was assessed using the Cell Migration/Chemotaxis Assay Kit (96-well, 8 µm) (ab235673). The manufacturer's instructions were followed, and a standard of dyed cells was prepared for each biological replicate. Cell numbers were proportional to the fluorescence at Ex/Em = 530/590 measured with an Infinite® 200 Pro (Tecan Life Sciences) plate reader. As migration inducing stimulus ATP (300 µM, Sigma Aldrich, A6419-5 g) was used in the bottom chamber. Cells were seeded at a density of 50,000 cells per well in the top chamber and if treated, supplemented with 10 µM spermidine trihydrochloride (Sigma, S2501-5G). In both chambers DMEM medium (Invitrogen, 41966-029) supplemented with 1% penicillin/streptomycin (Sigma, P0781-20ML) was used. After an incubation of approximately 20 h at 37 °C with 5% CO<sub>2</sub> the cells remaining on top of the membrane were removed with a cotton swab and cells that adhered on the bottom were dissociated. The number of cells migrated through the semipermeable membrane of the Boyden chamber was calculated based on the measured fluorescence and the generated linear regression standard curve with a range of 0–12,500 cells.

#### Wound healing/scratch assay

Cells were seeded at a density of 300,000 cells/well of a 24-well plate. After 8 h of adherence, cells were treated with 3 µM or 10 µM spermidine trihydrochloride (Sigma, S2501-5G) in complete medium. After 15 h of incubation, the cell layer was scratched with a 200 µl pipette tip. Images were taken with a Zeiss Axio Observer Z1 Inverted Phase Contrast Fluorescence Microscope using the Zen 2 blue software for 72 h at the indicated timepoints. Acquired images were analyzed using ImageJ by defining the gap area right after scratching (0 h) as region of interest. The threshold was set to include every cell inside the region of interest, the area fraction in percent was measured and normalized to the respective value at 0 h.

#### Western blot

For ASC crosslinking, 1 mM DSS (Thermo, A39267) was added to freshly harvested microglia in PBS for 30 min. All cell pellets were lysed in protein sample buffer containing 0.12 M Tris-HCl (pH 6.8), 4% SDS, 20% glycerol, 5% β-mercaptoethanol. Proteins were separated by Tris-Tricine polyacrylamide gel electrophoresis (PAGE) and transferred by wet blotting onto a nitrocellulose membrane. After blocking with 1% skim milk in Tris-buffered saline with 0.5% Tween20 (TBST), primary antibodies were added (Additional file 2). For signal detection the SuperSignal West Femto Maximum Sensitivity Substrate (ThermoFisher, 34096) was used. Western blots were analyzed by quantifying the respective intensities of each band using ImageJ. All samples were normalized to ACTIN levels or whole protein content in the supernatant.

#### Quantitative real-time PCR

For total RNA isolation, the RNeasy Mini kit (Qiagen, 74104) was used and cells were directly lysed in the provided RLT lysis buffer in the cell culture plate. Reverse transcription into cDNA was performed using the High-Capacity cDNA Reverse Transcription kit (ThermoFisher, 4368813). The manufacturer's instructions for both kits were followed. Quantitative PCR was conducted on a QuantStudio 6 Flex Real-Time PCR System (Applied Biosystems) using 12 ng cDNA per reaction. Gene expression was analyzed in 384 well plates using the TaqMan Fast Universal Master Mix (Applied Biosystems, 4364103) and TaqMan primers as described in the Additional file 2. With the Double delta Ct method, values were normalized to the house keeping gene *Actin* and non-treated controls.

## ELISA

Cytokine concentrations in the supernatant of cultured cells were measured using the IL-1 $\beta$  (eBioscience, 88701388), IL-18 (Thermo Fisher, 88-50618-22), TNF- $\alpha$  (eBioscience, 88723477) and IL-6 (eBioscience, 88706488) enzyme-linked immunosorbent assay (ELISA) kit according to manufacturer's instructions. The absorption was read at a wavelength of 450 nm and a reference length of 570 nm with the microplate reader Infinite<sup>®</sup> 200 Pro (Tecan Life Sciences) and analyzed using the Magellan Tecan Software.

## Immunocytochemistry and confocal microscopy

Cells were seeded at a density of 50,000 cells per well on 12 mm coverslips. After treatment, cells were fixed with 4% paraformaldehyde for 20 min, permeabilized with 0.1% Triton X-100 in PBS for another 20 min and blocked with 3% bovine serum in PBS for 1 h. The primary antibodies (anti-ASC, AdipoGen, AG-25B-0006, 1:500; anti-IBA1, Wako 019-19741, 1:1000) were added overnight at 4 °C. Subsequently, cells were incubated with the fluorescent secondary antibodies (Alexa Fluor 568-conjugated anti-rabbit IgG, 1:500, Invitrogen, A11011; 488-conjugated anti-rabbit IgG, Invitrogen A21206) for 3 h at room temperature. Cell nuclei were counterstained with DAPI (Roche, 10236276001) and coverslips embedded in fluorescent mounting medium (Dako, S3023). Images were acquired using Leica TCS SP5 confocal laser scanning microscope controlled by LAS AF scan software (Leica Microsystems, Wetzlar, Germany). Z-stacks were taken and images presented as the maximum projection of the z-stack. The number and size of ASC specks was assessed using ImageJ software as described before [14].

## A $\beta$ preparation

**Labeling.** A $\beta$  1–42 peptides (Cayman Chemicals) were resuspended in hexafluoroisopropanol to obtain 1 mM solution, evaporated and stored as aliquots. For each preparation, 125  $\mu$ g of amyloid- $\beta$  was dissolved in 2  $\mu$ L DMSO, sonicated for 10 min in the waterbath and supplemented with 3  $\times$  molar excess of NHS-ester ATTO647N dye (Sigma) in 1  $\times$  PBS (phosphate buffer saline, Gibco) and pH was adjusted to 9 with sodium bicarbonate. After 1 h of labeling reaction in the dark at room temperature, the labeled peptides were separated using spin columns (Mobicol, Mobitec) and loaded with 0.7 mL of Sephadex G25 beads (Cytiva). Clean, chromatography-grade H<sub>2</sub>O (LiChrosolv LC-MS grade, Merck) was used for washing, equilibration and elution. Peptide concentrations were determined using 15% SDS-PAGE gels and comparing the band intensities of the input with the eluted fractions.

**Maturation.** A $\beta$  peptides were matured according to [36]. In short, to obtain oligomeric forms, A $\beta$  was resuspended in the final concentration of 1  $\times$  PBS and incubated at 4 °C overnight. Turbidity measurements and ThT aggregation assay were performed on Synergy H1 Hybrid Multi-Mode Microplate Reader (BioTek instruments) to determine the formation of A $\beta$  oligomers and fibrils, as described in [37].

## Phagocytosis assay

Neonatal microglia (50,000 cells/ 24 well) were seeded on coverslips and pre-treated for 18 h with spermidine. 0.5  $\mu$ M 647-labelled A $\beta$  was added and after 24 h cells were fixed and counterstained with anti-IBA1 (Wako 019-19741, 1:1000). Quantification of Z-stacks taken at the confocal microscope with constant settings was performed with Image J: a mask was created for each IBA1 stained cell body and the intensity of the A $\beta$  signal in every cell was determined. The mean intensity/phagocytic cell was calculated as well as the number of A $\beta$ -containing phagocytic cells.

## Single nuclei sequencing (snRNA-seq)

Nuclei preparation, single nuclei sequencing and single nuclei sequencing analysis are described in the Additional file 2. The dataset has been deposited in the GEO database, GSE206202.

## Proteomics analysis

Sample preparation, Liquid chromatography mass spectrometry and data analysis are described in the Additional file 2. The mass spectrometry proteomics data have been deposited with the ProteomeXchange Consortium via the PRIDE partner repository with the dataset identifier PXD034638.

## Data analysis

All values are presented as mean  $\pm$  SEM (standard error of the mean). All data sets were tested for normality using the Shapiro–Wilk test. For normally distributed data, parametric tests were used: the student's *t* test for pairwise comparisons or a one-way ANOVA using the indicated post hoc test for multiple comparisons. If the data distribution was not normal, the corresponding non-parametric tests Mann–Whitney *U* test or Kruskal–Wallis test with Dunn's multiple comparison test were applied. As a reference for the Dunnett's post hoc test or the Dunn's multiple comparison either LPS/ATP, poly I:C or A $\beta$  samples were used. Outlier testing was performed

using the ROUT method ( $Q=0.5\%$ ). Statistically significant values were determined using the GraphPad Prism software and are indicated as follows:  $*p < 0.05$ ,  $**p < 0.01$  and  $***p < 0.001$ .

## Results

### Spermidine reduced soluble A $\beta$ in APPPS1 mice

To assess the potential of spermidine on AD pathology, we investigated its effects on APPPS1 mice. This AD-like mouse model, which harbors transgenes for the human amyloid precursor protein (APP) bearing the Swedish mutation as well as a presenilin 1 mutation, develops a strong A $\beta$  pathology including neuroinflammation. APPPS1 mice were treated with 3 mM spermidine via their drinking water [31], starting prior to disease onset (namely, substantial A $\beta$  deposition), at the age of 30 days (Fig. 1a). Compared to control APPPS1 mice that received pure water (H<sub>2</sub>O), spermidine-supplemented animals showed no differences in fluid uptake per day (Additional file 1: Fig. S1a).

A $\beta$  deposition was analyzed at an intermediate disease state (120 days) and at 290 days, when pathology is known to have reached a plateau. After consecutive protein extractions, soluble and insoluble/SDS soluble A $\beta$ 40 and A $\beta$ 42 were measured by electrochemiluminescence (MesoScale Discovery panel). Spermidine supplementation significantly reduced soluble A $\beta$ 40 in both 120- and 290-day-old APPPS1 mice by 40% and soluble A $\beta$ 42 in 290-day-old mice by 49% (Fig. 1a) while not affecting insoluble A $\beta$  (Additional file 1: Fig. S1b). These findings were further substantiated by the fact that no differences in A $\beta$  plaque covered area or plaque size were observed after staining tissue sections with the fluorescent dye pFTAA (Additional file 1: Fig. S1c). Mechanistically,

spermidine treatment did neither affect APP production and cleavage nor BACE1 abundance in whole hemisphere lysates or in proximity to 4G8-positive A $\beta$  plaques (Additional file 1: Fig. S1d–f). As the A $\beta$ -degrading enzyme IDE (insulin-degrading enzyme) was also not altered by spermidine treatment (Additional file 1: Fig. S1g), we concluded that spermidine might target soluble A $\beta$  by altering its phagocytosis and/or degradation.

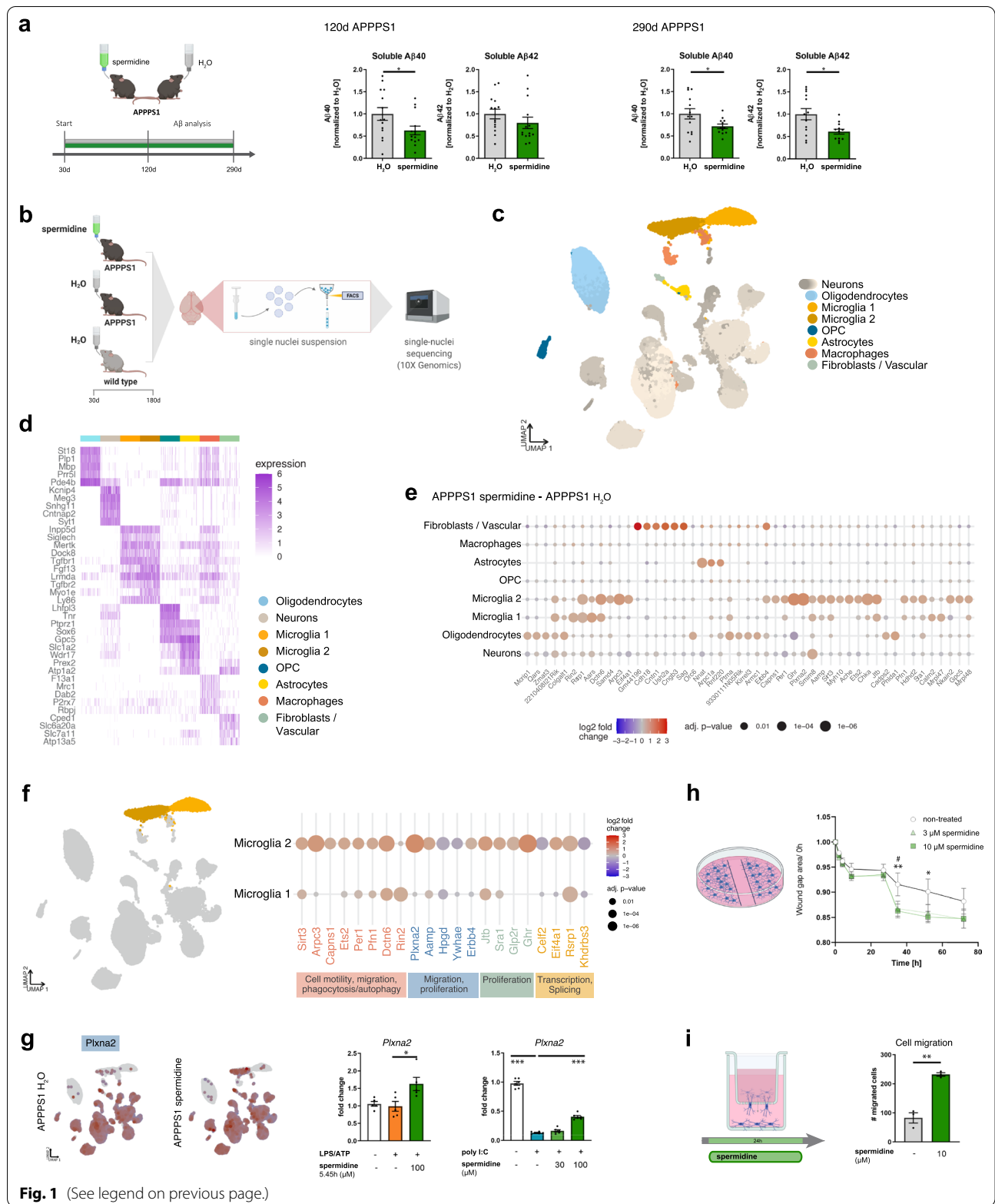
### Spermidine treatment of APPPS1 mice induced transcriptomic alterations in microglia

To gain insights into the molecular mechanisms mediating the reduced soluble A $\beta$  levels and the cell populations affected by spermidine, comparative single nuclei sequencing (snRNA-seq) was performed. Hemispheres of three male spermidine-treated APPPS1 mice, H<sub>2</sub>O-treated APPPS1 control as well as wild type (WT) mice were analyzed at the age of 180 days, representing a midpoint in the course of pathology in this AD-like mouse model (Fig. 1b). Using fluorescence-activated cell sorted single nuclei and the 10xGenomics platform (Additional file 1: Fig. S2a), between 6500 and 10,000 cells per mouse at a median depth of 1400–1700 genes could be detected. Automated clustering revealed 34 clusters, which were grouped into 7 major cell types, namely, neurons, oligodendrocytes, microglia, oligodendrocyte precursors (OPC), astrocytes, macrophages and fibroblasts/vascular cells, using label transfer from a previously published mouse brain reference data set [38] (Fig. 1c, d).

Interestingly, the strongest transcriptional changes were found in microglia. Fewer genes were altered in oligodendrocytes, neurons, and astrocytes, while OPC and macrophages remained almost unaffected (Fig. 1e, Additional file 1: Fig. S2f). In agreement with previous

(See figure on next page.)

**Fig. 1** Spermidine reduced soluble A $\beta$  and induced transcriptomic alterations in microglia of APPPS1 mice. **a** APPPS1 mice were treated with 3 mM spermidine via their drinking water starting at 30 days (d) until mice reached an age of 120 days or 290 days according to the depicted treatment scheme. Spermidine-treated APPPS1 mice were compared to non-treated controls (H<sub>2</sub>O). The A $\beta$ 40 and A $\beta$ 42 content was measured in the TBS (soluble) fraction of brain homogenates of 120-day-old or 290-day-old spermidine-treated mice and water controls (mixed sex) using electrochemiluminescence (MesoScale Discovery panel). Values were normalized to water controls. 120d APPPS1 H<sub>2</sub>O ( $n=14$ ), 120d APPPS1 spermidine ( $n=14$ ), 290d APPPS1 H<sub>2</sub>O ( $n=14$ ), 290d APPPS1 spermidine ( $n=12$ ); two-tailed *t*-test, A $\beta$ 42 in 120d mice: Mann–Whitney *U* test. **b** Single nuclei sequencing of hemispheres harvested from 180-day-old male spermidine-treated APPPS1, H<sub>2</sub>O APPPS1 and H<sub>2</sub>O control mice was performed of FACS-sorted DAPI-stained nuclei using the 10xGenomics platform ( $n=3$ ). **c** UMAP embedding and clustering of the snRNA-seq data, together with annotation of the major cell types. **d** Heatmap showing the top 5 marker genes for 300 cells in each of the major cell types. **e** Dot plot for the top 50 genes in a cell-type-specific differential expression analysis between spermidine-treated APPPS1 and H<sub>2</sub>O APPPS1 mice. Color scale indicates log<sub>2</sub> fold change, dot size indicates adjusted *p* value. **f** Same as e, for selected genes differentially expressed in microglia clusters 1 or 2. Associated pathways are color-coded. **g** Expression of *Plxna2* in APPPS1 spermidine and APPPS1 H<sub>2</sub>O mice. Color scale indicates normalized expression, grey dots represent no data (left panels). For validation, neonatal microglia were treated with the indicated concentrations of spermidine in combination with LPS (1  $\mu$ g/ml) and ATP (2 mM) or with poly I:C (50  $\mu$ g/ml) and the gene expression was assessed by RT-qPCR (right panels). *Plxna2* expression was normalized to *Actin* and displayed as fold change compared to non-treated control cells;  $n=5-6$ , one-way ANOVA, Dunnett's post hoc test. **h** Neonatal microglia were pre-treated with 3 or 10  $\mu$ M spermidine for 15 h. The confluent cell layer was scratched and the scratch area was imaged for 72 h at the indicated timepoints. The gap area normalized to timepoint 0 h is displayed;  $n=5-6$ , two-way ANOVA, Dunnett's post hoc test. **i** Neonatal microglia were non-treated or treated with 10  $\mu$ M spermidine and their migration towards 300  $\mu$ M ATP was quantified after 24 h using a transwell migration assay; two-tailed *t*-test.  $*p < 0.05$ ,  $**p < 0.01$ ,  $***p < 0.001$



single cell transcriptomic analyses of APPPS1 mice [1], two microglia subpopulations were detected. The microglia 2 cluster appeared only in APPPS1 but not in WT mice, thus presenting an AD-associated activated microglia phenotype, which was largely equivalent to the classical DAM published by Keren-Shaul et al. [1] (Additional file 1: Fig. S2b–d). To discover the main characteristics of both microglia clusters, differential gene expression followed by gene set enrichment analysis between these populations was performed. Compared to cluster 1, the AD-associated cluster 2 revealed a downregulation of genes involved in phagocytosis, endocytosis, cell adhesion and cell polarity while upregulating neuroinflammatory responses, cell cycle transition and autophagy (Additional file 1: Fig. S2e).

Next, genes differentially expressed in spermidine-treated APPPS1 mice compared to H<sub>2</sub>O-treated controls were specifically assessed in microglia clusters 1 and 2. Among the top differentially expressed genes in microglia were genes associated with cell motility/ cell migration (*Arpc3*, *Capns1*, *Pfn1*, *Plxna2*, *Aamp*, *ErbB4*, *Ywhae*, *Hpgd*), phagocytosis (*Arpc3*, *Capns1*, *Pfn1*, *Dctn6*, *Rin2*), autophagy (*Arpc3*, *Capns1*, *Ets2*, *Per1*, *Ghr*), proliferation (*Aamp*, *Ets2*, *ErbB4*, *Hpgd*, *Glp2r*, *Ghr*, *Jtb*, *Sra1*, *Ywhae*), transcription and alternative splicing (*Celf2*, *Eif4a1*, *Rsrp1*, *Khdrbs3*) (Fig. 1f; Additional file 1: Fig. S2g). Gene set enrichment analysis correspondingly revealed the following Gene Ontology terms to be significantly regulated by spermidine: glial cell migration, microtubule organization center localization, cell matrix adhesion and the semaphorin–plexin signaling pathway (Additional file 3).

To validate these changes, neonatal microglia were isolated and either activated with LPS followed by ATP, inducing the TLR4 pathway, or with the viral dsRNA poly I:C stimulating the TLR3 pathway (Fig. 4b, c). Indeed, spermidine treatment upregulated Plexin A2 (*Plxna2*) expression of activated microglia (Fig. 1g). On the functional level, spermidine treatment of neonatal microglia increased the migration in a scratch wound healing assay (Fig. 1h, Additional file 1: Fig. S2h) and towards ATP in a transwell migration assay (Fig. 1i), correlating well with the snRNA-seq changes of cell migration genes. Furthermore, spermidine augmented the expression of the autophagy-associated gene *Ets2* in vitro (Additional file 1: Fig. S2i). Also, distinct anti-inflammatory-associated genes, *Pfn1* [39], *Glp2r* [40], *Per1* [41] and *Sirt3* [42, 43], were upregulated by spermidine in the AD-associated microglia cluster 2. This upregulation of the anti-inflammatory NAD-dependent deacetylase *Sirt3* was confirmed in activated neonatal microglia in vitro (Additional file 1: Fig. S2j).

We, therefore, hypothesize that spermidine prolongs and expands the early activated state of microglia, characterized by increased phagocytosis, cell motility, migration and proliferation, thus maintaining the surveillance mode of microglia and thereby reducing soluble A $\beta$ .

### Spermidine altered AD-associated microglia and their capacity to degrade A $\beta$

Next, the abundance of cell types was compared between spermidine and H<sub>2</sub>O APPPS1 mice. Interestingly, spermidine significantly increased the abundance of microglia cluster 2 (Fig. 2a), which correlates well with the induction of proliferation-associated genes by spermidine, and reduced levels of the anti-proliferatory gene *Hpgd* after acute spermidine treatment in vitro (Additional file 1: Fig. S2k).

To validate that spermidine indeed altered the DAM/ microglia cluster 2, APPPS1 mice treated with spermidine were stained for the established cluster 2 marker and receptor tyrosine kinase AXL (Fig. 2b). In line with the snRNA-seq, the AXL intensity normalized to the IBA1 area was significantly increased in spermidine-treated mice (Fig. 2c). As the AXL-GAS6 signaling pathway was shown to promote phagocytosis and reduce A $\beta$  load [44], the effect of spermidine on phagocytosis of A $\beta$  was assessed in vitro. Spermidine pre-treatment of neonatal microglia significantly decreased the mean A $\beta$  signal per phagocytic cell after 24 h, indicating enhanced A $\beta$  degradation, while the percentage of phagocytic cells was not altered (Fig. 2d). In line with this, spermidine treatment increased the expression of the phagocytosis-associated actin nucleation gene *Arpc3* in APPPS1 mice, which could be validated on mRNA and protein level in spermidine-treated neonatal microglia in vitro (Additional file 1: Fig. S2l). Accordingly, spermidine reduced the expression of the transcriptional regulator *Celf2* (Fig. 1f), which negatively regulates the phagocytic receptor TREM2 [45] and preserved the levels of *Trem2* in activated neonatal microglia in vitro (Additional file 1: Fig. S2m).

Correlating well with the observed reduction in soluble A $\beta$  in spermidine-treated APPPS1 mice, these results show that spermidine indeed alters phagocytosis and degradation of A $\beta$ .

### Spermidine treatment reduced progressive neuroinflammation in APPPS1 mice

A $\beta$  pathology and its associated changes in microglia are a generally accepted and crucial driver of neuroinflammation [2, 8]. To complement the observed transcriptomic changes, we performed an unbiased proteome screening using liquid chromatography tandem mass

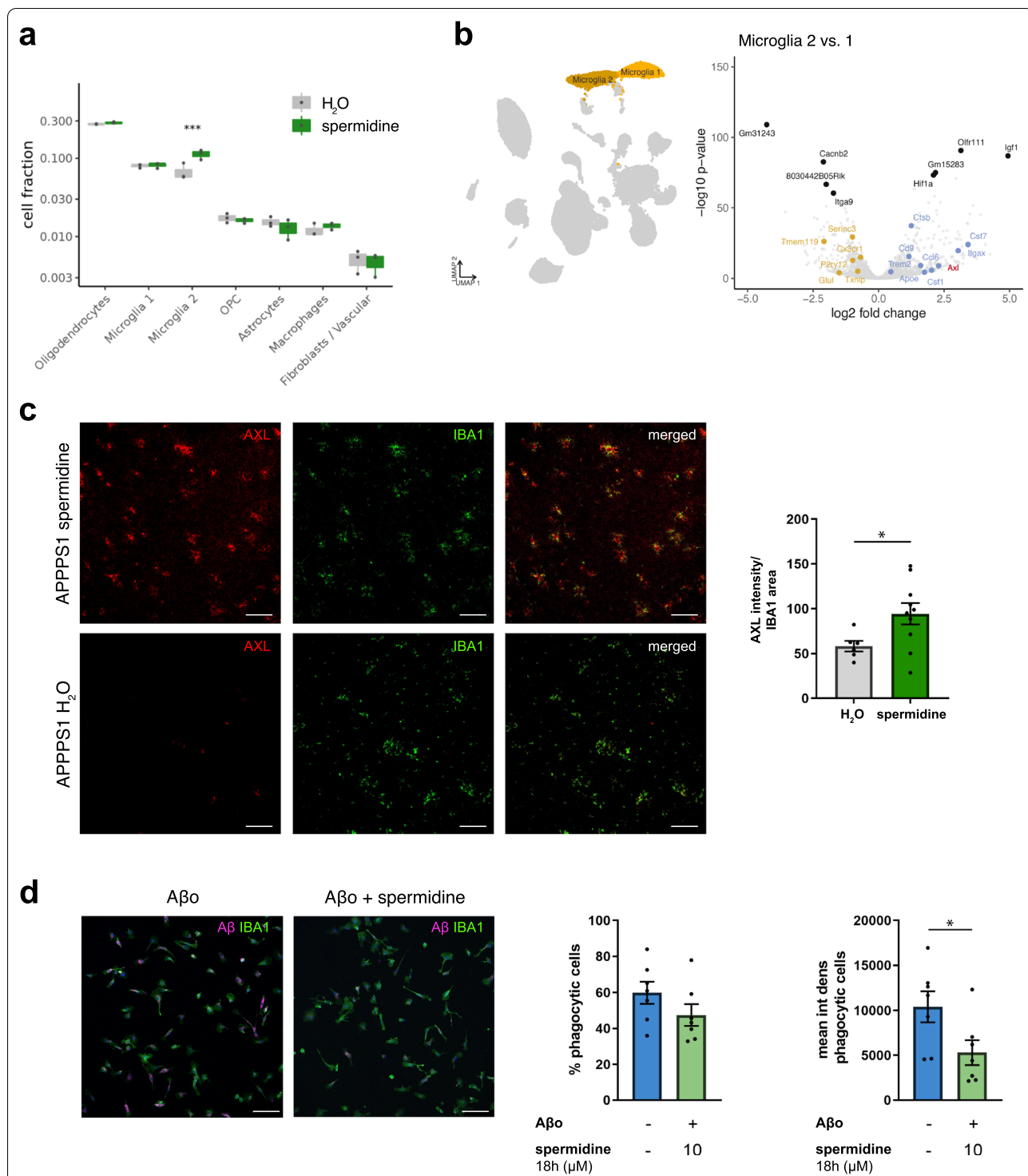


**Fig. 2** Spermidine altered AD-associated microglia and their capacity to degrade Aβ. **a** Cluster abundance in snRNA-seq of male spermidine-treated APPS1 and H<sub>2</sub>O APPS1 mice with *p* values from mixed-effects binomial model. **b** Volcano plot of genes differentially expressed in microglia cluster 2 vs. 1. The top 5 up- and down-regulated genes are indicated as well as previously published markers for homeostatic (yellow) and disease-associated (blue) microglia [1]. Significance threshold of adj. *p* value < 0.01 was used. *Axl* as a gene of interest is highlighted in red. **c** Tissue sections of male 180-day-old mice were stained for the microglia cluster 2 marker AXL (red) and IBA1 (green). The AXL intensity normalized to the IBA1 area was determined by ImageJ analysis; *n* = 6–10, two-tailed *t*-test. **d** Neonatal microglia were pre-treated for 18 h with 10 μM spermidine and fluorescently labelled oligomeric (Aβ) Aβ (magenta) was added for further 24 h. Microglia cells were stained for IBA1 (green). The percentage of phagocytic cells and the Aβ mean intensity density per phagocytic cell was assessed by confocal microscopy. Representative images are shown; *n* = 7, two-tailed *t*-test. \**p* < 0.05, \*\**p* < 0.01, \*\*\**p* < 0.001

spectrometry of microglia isolated from 180-day-old APPPS1 mice treated with spermidine or H<sub>2</sub>O as well as WT controls (Fig. 3a). To reveal the effect of spermidine on AD pathology, we applied linear modelling integrating the information of proteins changing upon spermidine treatment of APPPS1 as well as between WT and APPPS1 mice [(APPPS1 spermidine + WT H<sub>2</sub>O)/2 – APPPS1 H<sub>2</sub>O]. The 72 differentially expressed proteins ( $\alpha = 0.04$ ,  $fdr < 0.3$ ) were inversely correlated (slope =  $-0.77$ ,  $R^2 = 0.85$ ), when comparing APPPS1 against spermidine (Fig. 3b). The opposite regulation highlights the beneficial effects of spermidine on AD-associated changes. No proteins were found to be regulated into the same direction, e.g., amplifying potentially disease-driving protein changes, indicating no adverse effects of spermidine on AD pathology (Fig. 3b, Additional file 1: Fig. S3a). To assess whether those proteins can discriminate the spermidine-treated groups from the controls, a principal component analysis (PCA) and hierarchical clustering was performed, resulting in a clear separation based on spermidine treatment (Additional file 1: Fig. S3b).

To consider also coordinated changes, which did not pass significance criteria on the single-protein level, we performed gene-set enrichment analysis (GSEA), a functional analysis with a special focus on biological process (GO:BP) and pathways (REACTOME) terms related to inflammation and neurodegeneration. In line with the transcriptomic results, spermidine treatment increased pathways involved in “microtubule cytoskeleton organization”, “regulation of actin filament binding” and “regulation of actin binding”, thus supporting the observed microglial migration changes upon spermidine treatment

(Fig. 3c). While the transcriptomics analysis only revealed a few anti-inflammatory genes to be regulated by spermidine, a clear downregulation of many inflammatory pathways including “acute inflammatory response” as one of the top downregulated pathways, as well as IL-1 and IL-6 signaling and inflammasome pathways were found (Fig. 3c). Among the downregulated pathway clusters within a REACTOME enrichment map was a big cluster of IL signaling-related pathways indicating anti-inflammatory effects of spermidine. Matching previous studies [20, 46], spermidine also upregulated the pathway cluster “autophagy”. Furthermore, spermidine affected ubiquitin-associated pathways and SUMOylation (Fig. 3d). Comparing the pathways altered in APPPS1 mice with those found to be affected by spermidine revealed a clear reversal of the AD-associated induction of inflammation and oxidative phosphorylation and the downregulation of cytoskeletal pathways (Fig. 3e). Thus, we conclude that spermidine reverted AD-mediated effects in APPPS1 mice.

To assess whether these microglia-specific anti-inflammatory effects interfered with neuroinflammation later in the pathology, ten cytokines were quantified by electrochemiluminescence in brain homogenates of 290-day-old male spermidine-treated APPPS1 mice. Spermidine supplementation significantly reduced the AD-relevant pro-inflammatory cytokines IL-6, TNF- $\alpha$ , IL-12, IL-4 and IL-5 in 290-day-old mice (Fig. 3f), while not altering IL-1 $\beta$  (combined measurement of Pro-IL-1 $\beta$  and IL-1 $\beta$ ), IFN- $\gamma$ , IL-2, IL-10 and KC/GRO (Additional file 1: Fig. S3c), revealing indeed anti-inflammatory effects of spermidine in the CNS at late stages of disease pathology.

(See figure on next page.)

**Fig. 3** Spermidine treatment reduced progressive neuroinflammation in APPPS1 mice. **a** Male APPPS1 mice were treated with 3 mM spermidine via their drinking water starting at 30 days (d) until mice reached an age of 180 days. Microglia were isolated by MACS and the proteome assessed by mass spectrometry. **b** Scatterplot of protein regulation in Contrast2 (APPPS1 spermidine—APPPS1 H<sub>2</sub>O, y axis) vs. its regulation in Contrast1 (APPPS1 H<sub>2</sub>O,—WT H<sub>2</sub>O, x axis). Contrast 2 shows regulation due to spermidine effect, Contrast 1 shows the regulation of proteins by Alzheimer disease. Proteins that are regulated by spermidine and show significant anti-APPPS1 effect were marked in red. As such we selected proteins that show significant ( $\alpha = 0.04$ ) regulation due to spermidine in APPPS1 mice (Contrast2) and simultaneously, show significant ( $\alpha = 0.04$ ) effect in Contrast5 = (Contrast2 – Contrast1)/2, in the direction, opposite to the effect of the AD-like model. **c** Volcano plot of GSEA enrichment of GO BP terms. x-axis shows normalized enrichment score of functional term, y-axis represent the  $-\log_{10}$  of its false discovery rate. Labelled are only terms that have relation to neurodegeneration and inflammation. As such we selected terms that have in their names following strings: neuro, inflamm, Clathrin, interleukin, Caspase, TNF, ubiquitin, SUMO, Alzheimer, Parkinson, Huntington, lipoprotein, autophagy, cell migration, cell motility, microtubule, actin, actin-, glia, amyloid. Not all labels appear due to strong overlap, especially at high  $fdr > \sim 0.5$  ( $-\log_{10}(fdr) < \sim 0.3$ ). Long term names are truncated to 50 characters. **d** GSEA enrichment map using top 50 REACTOME terms from list of neurodegeneration and inflammation terms. As such we selected terms that have in their names following strings: neuro, inflamm, Clathrin, interleukin, Caspase, TNF, ubiquitin, SUMO, Alzheimer, Parkinson, Huntington, lipoprotein, autophagy, cell migration, cell motility, microtubule, actin, actin-, glia, amyloid. **e** Dot plot of selected functional terms related to neuroinflammation and degeneration. **f** APPPS1 mice were treated with 3 mM spermidine via their drinking water starting at 30 days until mice reached an age of 290 days. The content of the indicated pro-inflammatory cytokines was measured in the TBS (soluble) fraction of brain homogenates of male spermidine-treated mice and water controls using electrochemiluminescence (MesoScale Discovery panel). Values were normalized to water controls. 290d APPPS1 H<sub>2</sub>O ( $n = 14$ ), 290d APPPS1 spermidine ( $n = 12$ ); two-tailed  $t$ -test. \* $p < 0.05$ , \*\* $p < 0.01$ , \*\*\* $p < 0.001$

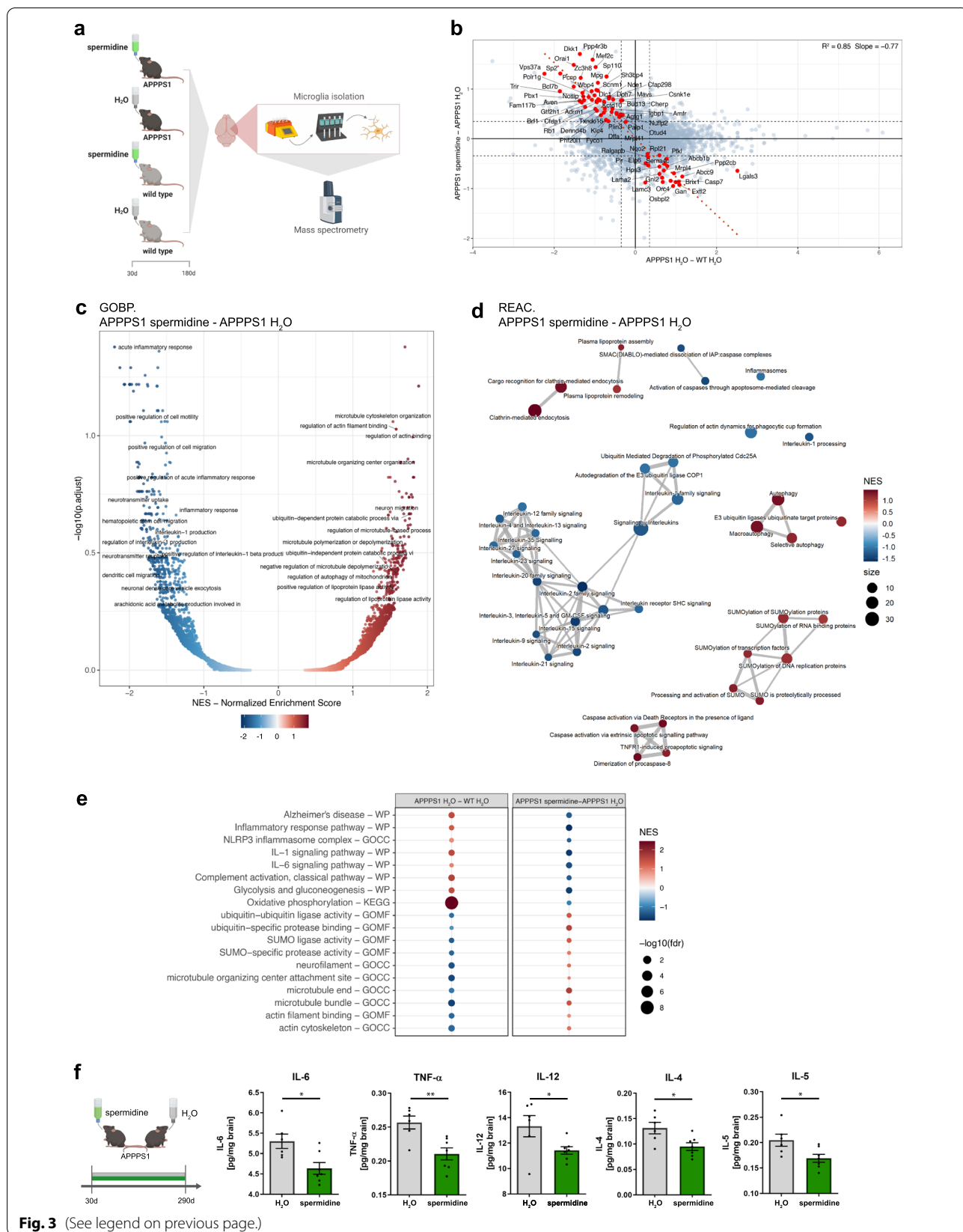


**Fig. 3** (See legend on previous page.)

### Spermidine exhibits direct anti-inflammatory effects on microglia

To assess whether spermidine influenced neuroinflammation in a direct manner or whether its effects on neuroinflammation were secondary, acute whole hemisphere slice cultures derived from 200-day-old WT or APPPS1 mice were treated with spermidine and subsequently stimulated with LPS and ATP (Fig. 4a). LPS/ATP treatment of APPPS1 slice cultures resulted in a massive release of IL-1 $\beta$  and IL-6 compared to slices from WT mice. Spermidine significantly reduced their levels in both genotypes (Fig. 4a), underlining that spermidine could directly influence neuroinflammation in APPPS1 mice.

To pinpoint which cytokine-producing glial cell accounts for the anti-inflammatory effects of spermidine, both neonatal microglia and astrocytes were activated either with LPS followed by ATP (Fig. 4b), with poly I:C (Fig. 4c) or oligomeric A $\beta$  (Fig. 4d). The presence of spermidine reduced the LPS/ATP-induced release of IL-6, TNF- $\alpha$ , IL-5, IL-1 $\beta$ , IL-18, IL-10, IL-12, KC/GRO and IL-2 into the cell supernatant of microglia dose-dependently (Fig. 4b, Additional file 1: Fig. S4a). In addition, spermidine treatment reduced the poly I:C-induced release of IL-6, TNF- $\alpha$ , IL-10, IL-12, IL-4 and KC/GRO in neonatal microglia and astrocytes (Fig. 4c, Additional file 1: Fig. S4b, c). These anti-inflammatory effects were also confirmed in adult microglia (Additional file 1: Fig. S4d–h). Furthermore, spermidine reduced the IL-6 and TNF- $\alpha$  release by neonatal microglia upon treatment with oligomeric A $\beta$  (Fig. 4d), also indicating a direct effect of spermidine on A $\beta$ -induced neuroinflammation.

Mechanistically, spermidine reduced the gene expression of the A $\beta$ -induced or LPS/ATP-induced AD-relevant cytokines *Il-6*, *Tnf- $\alpha$*  and *Il-1 $\beta$*  in neonatal microglia dose-dependently (Fig. 4e, Additional file 1: Fig. S4i, j). Also, poly I:C-induced gene expression of *Il-6* and *Tnf- $\alpha$*  was decreased by spermidine in both neonatal microglia

and astrocytes (Additional file 1: Fig. S4k, l). Reduced phosphorylation of NF- $\kappa$ B upon spermidine treatment might account for these gene expression changes (Fig. 4f, Additional file 1: Fig. S4m).

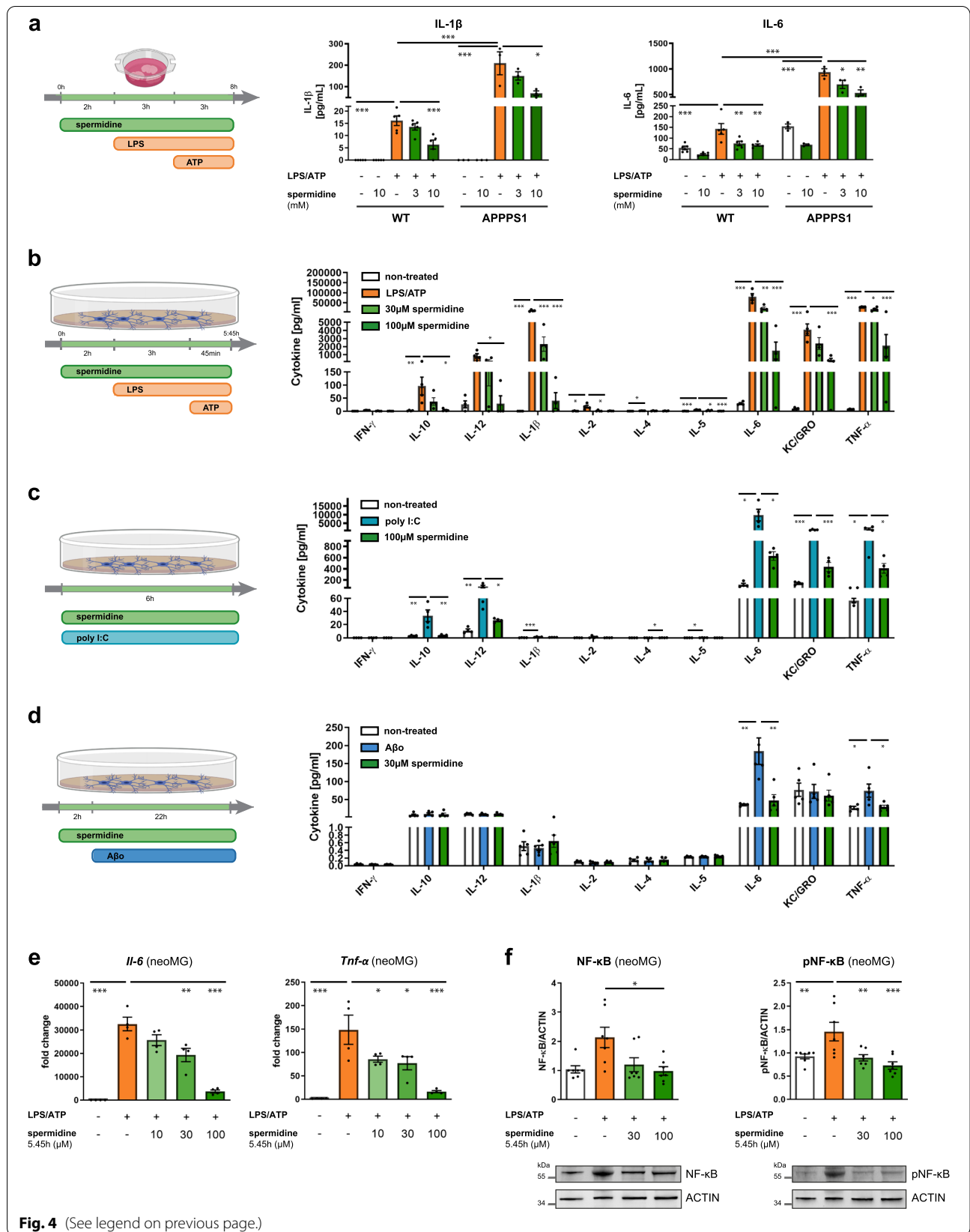
Correlating with the induction of autophagy as shown in the proteomic analysis of spermidine-treated APPPS1 mice, the anti-inflammatory effects of spermidine in vitro were autophagy-mediated. Spermidine induced expression of autophagic proteins significantly (Additional file 1: Fig. S5a–d) and no effects of spermidine treatment were measured upon autophagy activation with HBSS (Additional file 1: Fig. S5e–f). Impairment of autophagy by 3-MA or using primary microglia with BECN1 knock-out (Tamoxifen-treated BECN1<sup>flox/flox</sup>.CX3CR1<sup>CreERT2</sup> cultures) on the other hand, abolished spermidine-mediated effects (Additional file 1: Fig. S5g–i). Therefore, we concluded that spermidine exerts direct anti-inflammatory effects on microglia and astrocytes in an autophagy-dependent manner, correlating with the observed reduced neuroinflammation in 290-day-old APPPS1 mice.

### Spermidine regulates neuroinflammation beyond transcription by interfering with inflammasome assembly

As recent studies and our proteome analysis showed that spermidine mediates some of its effects solely on protein level [20, 22, 31], the effects of spermidine on neuroinflammation beyond transcriptional control were studied by treating microglia with spermidine after activating/priming them with LPS (Fig. 5a). Interestingly, post-LPS spermidine treatment (1.45 h) reduced only the release of IL-1 $\beta$  and IL-18 into the cell supernatant (Fig. 5b, c) while not altering the release of all other measured cytokines (Additional file 1: Fig. S6a–c). *Il-1 $\beta$* , *Il-6* and *Tnf- $\alpha$*  gene expression revealed no alterations by this spermidine treatment scheme (Additional file 1: Fig. S6d). However, increased protein levels of Pro-IL-1 $\beta$  and uncleaved

(See figure on next page.)

**Fig. 4** Spermidine exhibits direct anti-inflammatory effects on microglia. **a** Hemispheres of wild type (WT) and APPPS1 mice were coronally sliced and treated with the indicated spermidine concentration, LPS (10  $\mu$ g/ml) and ATP (5 mM) as depicted. The IL-1 $\beta$  and IL-6 concentration in the supernatant was determined by ELISA;  $n = 3–5$ , two-way ANOVA, Tukey's post hoc test. **b–f** Neonatal microglia (neoMG) were either treated with LPS (1  $\mu$ g/ml) and ATP (2 mM), with poly I:C (50  $\mu$ g/ml) or with oligomeric A $\beta$  (A $\beta$ , 5  $\mu$ M) and the indicated spermidine concentrations as depicted in the schemes. **b–d** Amount of cytokines in the cell supernatant was determined by electrochemiluminescence (MesoScale Discovery panel);  $n = 4–5$ . **b** IFN- $\gamma$ , IL-10, IL-12, IL-2: Kruskal–Wallis, Dunn's multiple comparison; IL-1 $\beta$ , IL-4, IL-5, IL-6, KC/GRO, TNF- $\alpha$ : one-way ANOVA, Dunnett's post hoc test. **c** INF- $\gamma$ , IL-2, IL-4: Kruskal–Wallis, Dunn's multiple comparison; IL-10, IL-12, IL-1 $\beta$ , IL-5, IL-6, KC/GRO, TNF- $\alpha$ : one-way ANOVA, Dunnett's post hoc test. **d** IL-10, IL-12, IL-4, KC/GRO: Kruskal–Wallis, Dunn's multiple comparison; INF- $\gamma$ , IL-1 $\beta$ , IL-2, IL-5, IL-6, TNF- $\alpha$ : one-way ANOVA, Dunnett's post hoc test. **e** The gene expression of *Tnf- $\alpha$*  and *Il-6* was assessed by RT-qPCR after treatment of neonatal microglia as depicted in **b**. Their expression was normalized to *Actin* and displayed as fold change compared to non-treated control cells;  $n = 4$ . *Il-6*: one-way ANOVA, Dunnett's post hoc test; *Tnf- $\alpha$* : Kruskal–Wallis, Dunn's multiple comparison. **f** Levels of phosphorylated NF- $\kappa$ B (pNF- $\kappa$ B) and NF- $\kappa$ B were determined by western blot in neonatal microglia treated as depicted in **b**. Representative images are shown and protein levels are displayed as fold changes compared to non-treated controls normalized to ACTIN;  $n = 7$ . NF- $\kappa$ B: Kruskal–Wallis, Dunn's multiple comparison; pNF- $\kappa$ B: one-way ANOVA, Dunnett's post hoc test. \* $p < 0.05$ , \*\* $p < 0.01$ , \*\*\* $p < 0.001$



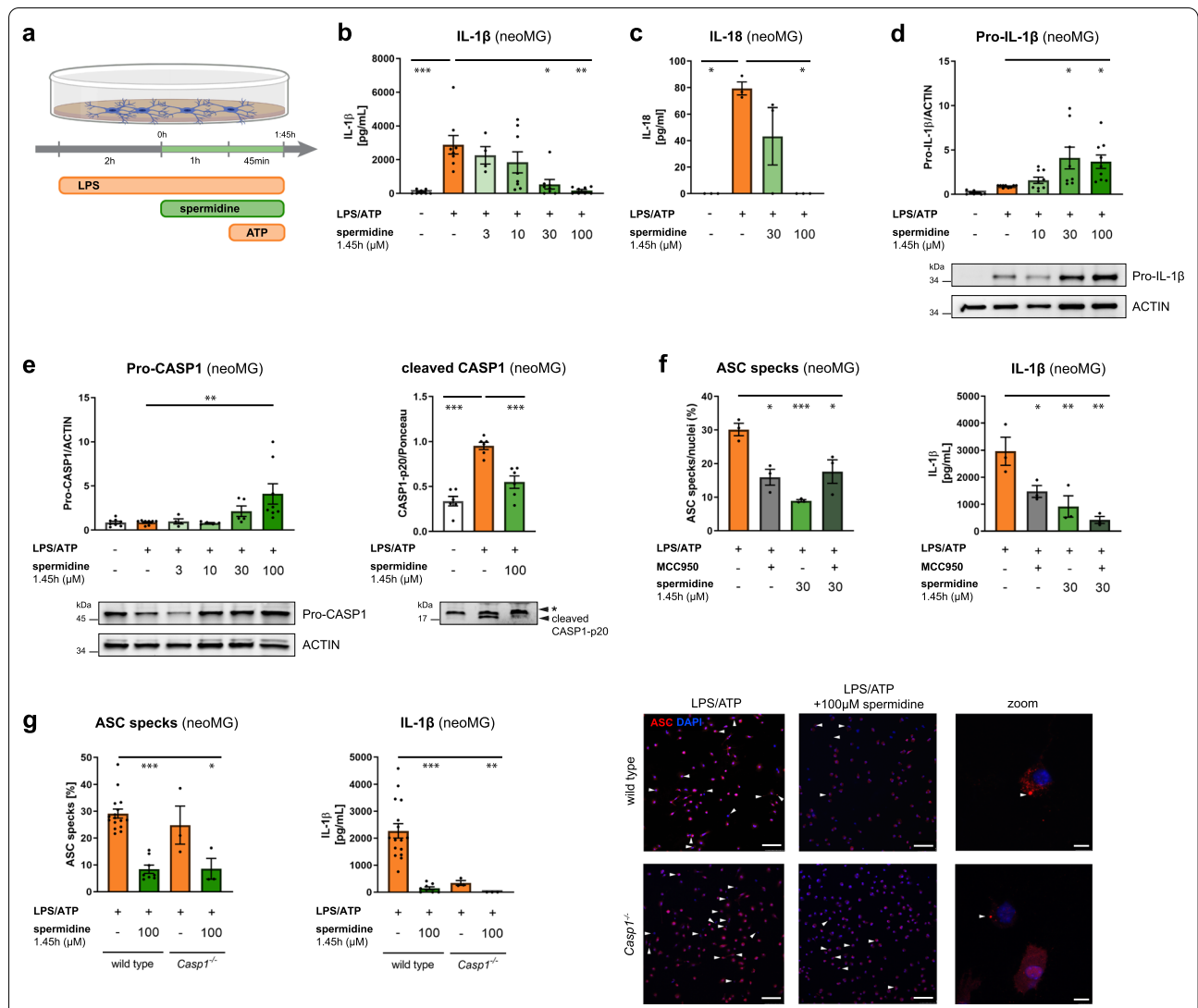


**Fig. 5** Spermidine regulates neuroinflammation beyond transcription by interfering with inflammasome assembly. Neonatal microglia (neoMG) were treated with LPS (1 μg/ml) and spermidine at indicated concentrations for 1.45 h and ATP (2 mM) as depicted in the scheme (a). **b** IL-1β concentration in the cell supernatant was determined by ELISA;  $n = 4-8$ ; Kruskal–Wallis, Dunn’s multiple comparison. **c** IL-18 concentration in the cell supernatant was determined by ELISA;  $n = 3$ ; Kruskal–Wallis, Dunn’s multiple comparison. **d** Pro-IL-1β protein levels were determined by western blot and normalized to ACTIN. Representative images are shown and values are displayed as fold changes compared to LPS/ATP-treated cells;  $n = 8-9$ ; Kruskal–Wallis, Dunn’s multiple comparison. **e** Cellular Pro-CASP1 and cleaved CASP1 p20 levels in the supernatant were determined by western blot (\* non-specific band). Pro-CASP1 was normalized to ACTIN ( $n = 4-8$ ) and CASP1 p20 was normalized to whole protein content determined by Ponceau S staining ( $n = 3$ ). Values are displayed as fold changes compared to LPS/ATP-treated cells; Pro-CASP1: Kruskal–Wallis, Dunn’s multiple comparison; cleaved CASP1: one-way ANOVA, Dunnett’s post hoc test. **f** Neonatal microglia were stimulated as shown in a and MCC950 was added 15 min before addition of ATP. Cells were stained for ASC to visualize inflammasomes and with DAPI for nuclear staining. The percentage of ASC specks in respect to the number of total cells (DAPI positive cells) was determined (left). The IL-1β concentration in the cell supernatant was assessed by ELISA (right);  $n = 3$ ; one-way ANOVA, Dunnett’s post hoc test. **g** Neonatal WT and *Casp1*<sup>-/-</sup> microglia were stimulated as shown in a but with 4 mM ATP to increase the number of inflammasomes. Cells were stained for ASC (red) to visualize inflammasomes and with DAPI (blue) for nuclear staining as shown in the representative images (scale bar = 100 μm). Arrowheads highlight ASC specks within microglia. The percentage of ASC specks in respect to the number of total cells (DAPI positive cells) was determined (left). The IL-1β concentration in the cell supernatant was assessed by ELISA (right); WT:  $n = 8-16$ ; *Casp1*<sup>-/-</sup>:  $n = 3$ . Kruskal–Wallis, Dunn’s multiple comparison. \* $p < 0.05$ , \*\* $p < 0.01$ , \*\*\* $p < 0.001$

Pro-CASP1 were found (Fig. 5d, e), indicating reduced processing at the NLRP3 inflammasome. This correlated with a reduction of cleaved and activated CASP1 and Gasdermin D (GSDMD), another substrate of CASP1, in the supernatant (Fig. 5e, Additional file 1: Fig. S6e).

While NLRP3 expression was not altered on the mRNA or protein level by spermidine (Additional file 1: Fig. S6f), staining and quantification of ASC specks/inflammasomes revealed that spermidine treatment reduced the number of ASC specks significantly (Fig. 5f, g). A similar reduction was also detected in *Casp1*<sup>-/-</sup> microglia (Fig. 5g), indicating that spermidine did not directly interfere with Pro-CASP1 cleavage but rather with inflammasome formation. To test this hypothesis, the ASC-oligomerization inhibitor MCC950 [47] was added prior to adding ATP. No additive effects of MCC950 to the spermidine-mediated effects could be detected, underlining that spermidine was indeed interfering with ASC-oligomerization and inflammasome formation (Fig. 5f). Consistent with this hypothesis, western blot analysis for ASC after chemical crosslinking showed reduced appearance of ASC oligomers in spermidine-treated cells (Additional file 1: Fig. S6g), while the amount of ASC monomers was not altered (Additional file 1: Fig. S6h). Thus, spermidine treatment of activated microglia reduced IL-1 $\beta$  processing by interfering with the oligomerization of ASC-positive inflammasomes.

Taken together, we elucidated a novel regulatory mechanism of spermidine in addition to targeting NF- $\kappa$ B-mediated transcription of pro-inflammatory genes. Thus, spermidine targets multifarious pathways, such as degradation of A $\beta$ , proliferation and active reduction of inflammatory signaling, which stabilizes a presumably protective microglia population.

## Discussion

Delaying AD progression still presents an urgent unmet clinical need. Based on recent advances in our understanding of AD pathogenesis that resulted in the appreciation of the impact of neuroinflammation and autophagy, we assessed the therapeutic effects of the autophagic activator spermidine on A $\beta$  pathology in APPPS1 mice.

Interestingly, spermidine treatment significantly increased A $\beta$  degradation and reduced soluble A $\beta$  levels in vivo, while A $\beta$  plaque burden and size were not altered. Whereas the effects of spermidine on AD pathology have not been assessed so far, De Risi et al. [48] reported that spermidine decreased soluble A $\beta$  and  $\alpha$ -synuclein in a mouse model with mild cognitive impairment. Despite the fact that the toxicity and importance of soluble vs. insoluble A $\beta$  in AD pathology is still a matter of debate, there is clear evidence that soluble A $\beta$  causes more synaptotoxicity than plaque-bound insoluble A $\beta$ . It was

shown to alter synaptic transmission and to mediate synaptic loss and neuronal death [49–51], thus suggesting that targeting soluble A $\beta$  might suffice to ameliorate AD. In line with this, recent data suggest that microglia create core plaques as a protective measure to shield the brain from soluble A $\beta$ . The DAM marker AXL is thought to contribute to this formation [52]. In addition, the AXL-GAS6 pathway has been shown to not only suppress the microglial inflammatory response but also to mediate A $\beta$  phagocytosis [44]. Thus, the increased AXL levels in spermidine-treated APPPS1 mice as well as the in vitro phagocytosis experiments underline that spermidine affects microglial phagocytosis and degradation of A $\beta$ . As the APPPS1 mouse model exhibits a fast disease progression with a strong genetically driven A $\beta$  pathology appearing at 60 days, the substantial effect of spermidine on soluble A $\beta$  highlights its potential to interfere with AD progression. Since neuroinflammation is a known driver for plaque formation [5, 6], the additional anti-inflammatory effects of spermidine may have a beneficial effect on insoluble A $\beta$  and plaques in mice older than those we analyzed within the frame of this work (namely, older than 290 days).

Notably, previous studies assessing the effect of autophagy activation on AD pathology also revealed reduced A $\beta$  pathology [53–56]; however, the mechanisms by which autophagy modulation targets AD pathology had not been elucidated so far. By applying snRNA-seq to 180-day-old spermidine-treated APPPS1 mice, we revealed microglia as the main glial cell type to be targeted by spermidine. The most profound effects of spermidine on the transcriptome level were seen in the AD-associated microglia cluster 2, which was characterized by increased migration, cell motility, phagocytosis and cell proliferation. While acute activation of microglia in early disease pathology induces microglial phagocytosis and migration towards plaques, later stages of AD pathology and chronic priming of microglia with A $\beta$  have adverse effects [57, 58]. In accordance, microglial motility in the presence of A $\beta$  plaques was found to be decreased in APPPS1 mice compared to control mice when a focal laser lesion was induced [59].

A common denominator of the transcriptome and proteome analysis was that spermidine prevented AD-associated cytoskeletal changes and thus, might increase microglial migration and cell motility, as demonstrated in vitro. Accordingly, spermidine was found to promote cell migration in neural cells and keratinocytes as well as wound healing processes ex vivo and in vivo [60]. In line with previous publications [61], the proteomics analysis revealed that spermidine also preserved the energy metabolism in microglia from APPPS1 mice by affecting oxidative phosphorylation, glycolysis and

gluconeogenesis. By promoting genes and proteins involved in cell motility, migration and phagocytosis, spermidine seems to delay the onset of the late-stage AD-associated microglial population.

Interestingly, some of those changes might be exerted by SUMOylation. SUMOylation is, similar to ubiquitination, a post-translational modification regulating transcription, cell proliferation and protein stability and turnover. To our knowledge this is the first time that an effect of spermidine on SUMOylation is described and it may also contribute to autophagy induction and/or protein degradation. In correlation, recent publications on the post-translational modification called hypusination [31, 32] indicate that spermidine can exert some of its function on the post-transcriptional levels.

In addition, spermidine also increased the abundance of microglia cluster 2. Although it is still under discussion whether proliferation of microglia in AD is beneficial or detrimental [62], spermidine mediated the enlargement of a microglial subpopulation showing increased phagocytosis and cell motility including *Axl* expression as described above. Several regulated genes, such as *Arpc3* [63], *Glp2r* [64], *Sirt3* [65] and *Per1* [66, 67] have been reported to exert protective effects in neurodegenerative diseases or reverse memory deficits in various models, underlining the observed protective effects of spermidine. For instance, SIRT3 was shown to target similar pathways as spermidine, such as inflammation, including the IL-1 $\beta$  processing pathway [42, 43] and microglial migration [68]. Even though microglia were the main glial cells to be affected by spermidine on transcriptional level at 180 days, our in vitro analyses revealed that spermidine also reduced cytokine production in astrocytes, indicating that astrocytes might also be altered at later stages of AD pathology. While only few anti-inflammatory effects of spermidine were found by snRNA-seq, the proteomics analysis of microglia isolated from spermidine-treated APPPS1 revealed a clear downregulation of inflammatory pathways. These changes might pave the path for the brain-wide reduction in cytokines mediated by spermidine at 290 days, when APPPS1 mice are known to exhibit profound neuroinflammation. Of note, while spermidine was found to target the IL-1 $\beta$  processing pathway at 180 days and in vitro, no changes in IL-1 $\beta$  cytokine levels were found in 290-day-old APPPS1 mice. This might be due to the fact that the MSD cytokine panel does not distinguish between Pro-IL-1 $\beta$  and cleaved IL-1 $\beta$ . Next to the in vitro effects of spermidine on transcription of cytokines by modulating the NF- $\kappa$ B signaling pathway, which was previously described in BV2 and macrophages [29, 30], we identified a novel spermidine-modulated post-translational mechanism. Spermidine interfered with the ASC assembly of the NLRP3

inflammasome and thereby reduced the production of IL-1 $\beta$ . This pathway was also found to be downregulated in the proteomics analysis of spermidine-treated APPPS1 microglia, again indicating that spermidine acts beyond modulation of transcription.

## Conclusions

Activators of autophagy such as fasting or caloric restriction, exercise, rapamycin, an inhibitor of the mechanistic target of rapamycin (mTOR), and metformin were shown to prolong the life span of several species and to reduce A $\beta$  deposition in different mouse models [53–56], yet most of these drugs—in contrast to the orally applicable spermidine—were problematic in terms of tolerability and/or administration. Therefore, the body-endogenous substance spermidine seems to be an attractive therapeutic dietary supplement as it attenuated AD-relevant neuroinflammation, reduced synaptotoxic soluble A $\beta$  and reverted AD-associated proteomic changes with no adverse effects. Since spermidine supplementation is already tested in humans, the extension of spermidine supplementation from individuals with subjective cognitive decline [32, 69–71] to clinical trials aimed at testing spermidine efficacy in AD patients appears to be a tempting approach.

## Abbreviations

AD: Alzheimer's disease; A $\beta$ : Amyloid  $\beta$ ; APP: Amyloid precursor protein; DAM: Disease-associated microglia; IL: Interleukin; LPS: Lipopolysaccharide; neoMG: Neonatal microglia; AdMG: Adult microglia; neoAC: Neonatal astrocytes; snRNA-seq: Single nuclei sequencing; WT: Wild type.

## Supplementary Information

The online version contains supplementary material available at <https://doi.org/10.1186/s12974-022-02534-7>.

**Additional file 1.** Supplementary figures.

**Additional file 2.** Supplementary methods.

**Additional file 3.** Supplementary Table 1.

## Acknowledgements

This work was supported by the Deutsche Forschungsgemeinschaft (DFG, German Research Foundation) under Germany's Excellence Strategy—EXC-2049—390688087, as well as under JE-278/6-1 to MJ and SFB TRR 43, SFB TRR 167 and HE 3130/6-1 to F.L.H., by the German Center for Neurodegenerative Diseases (DZNE) Berlin, and by the European Union (PHAGO, 115976; Innovative Medicines Initiative-2; FP7-PEOPLE-2012-ITN: NeuroKine). Furthermore, this project has received funding from Ministry of Education and Research (BMBF) as part of the National Research Node 'Mass spectrometry in Systems Medicine (MSCoreSys) under grant agreement 031L0220 (to MR), the German Research Foundation (INST 335/797-1) and the Berlin University Alliance (501\_Massenspektrometrie, 501\_Linklab. We are grateful to Alexander Haake and Julia Bertram for excellent technical support. Treatment images were created with Biorender.com. Computation has been performed on the HPC for Research cluster of the Berlin Institute of Health.

### Author contributions

KF, SS, FH and MJ designed experiments; KF, NS and JH treated and analyzed the mice; KF, NS, SW and LF performed experiments and analyzed data for the TLR3 pathway and astrocytes; JS, SW and MJ performed experiments and analyzed data for the TLR4 pathway and the phagocytosis; KF, NS, JS and MJ assessed autophagy; RS, CH, and DM prepared the chemically defined A $\beta$  for in vitro phagocytosis assays. KF, BO and VF prepared the figures. BO performed sequencing data analysis. MM and VF performed the mass spectrometry analysis. All authors wrote, revised and approved the manuscript. All authors read and approved the final manuscript.

### Funding

Open Access funding enabled and organized by Projekt DEAL. This work was supported by the Deutsche Forschungsgemeinschaft (DFG, German Research Foundation) under Germany's Excellence Strategy—EXC-2049—390688087, as well as under JE-278/6-1 to MJ and SFB TRR 43, SFB TRR 167 and HE 3130/6-1 to F.L.H., by the German Center for Neurodegenerative Diseases (DZNE) Berlin, and by the European Union (PHAGO, 115976; Innovative Medicines Initiative-2; FP7-PEOPLE-2012-ITN: NeuroKine).

### Availability of data and materials

Data generated and analyzed during this study are included in this published article and its additional information files. The snRNA-seq dataset has been deposited in the GEO database with the accession identifier GSE206202: <https://www.ncbi.nlm.nih.gov/geo/query/acc.cgi?acc=GSE206202>. The mass spectrometry proteomics dataset has been deposited with the ProteomeXchange Consortium via the PRIDE partner repository with the dataset identifier PXD034638.

### Declarations

#### Ethical approval and consent to participate

All animal experiments were conducted in accordance with animal welfare acts and were approved by the regional office for health and social service in Berlin (LaGeSo).

#### Consent for publication

Not applicable.

#### Competing interests

The authors declare that they have no competing interests.

#### Author details

<sup>1</sup>Department of Neuropathology, Charité, Universitätsmedizin Berlin, corporate member of Freie Universität Berlin, Humboldt-Universität Zu Berlin, Berlin Institute of Health, Berlin, Germany. <sup>2</sup>German Center for Neurodegenerative Diseases (DZNE) within the Helmholtz Association, Berlin, Germany. <sup>3</sup>Department of Biosciences, University of Salzburg, Salzburg, Austria. <sup>4</sup>Core Unit Bioinformatics, Berlin Institute of Health at Charité, Universitätsmedizin Berlin, Charitéplatz 1, Berlin, Germany. <sup>5</sup>Core Facility, High-Throughput Mass Spectrometry, Charité, Universitätsmedizin Berlin, corporate member of Freie Universität Berlin and Humboldt-Universität Zu Berlin, Berlin, Germany. <sup>6</sup>Molecular Biology of Metabolism Laboratory, The Francis Crick Institute, London, UK. <sup>7</sup>Department of Biochemistry, Charité, Universitätsmedizin Berlin, corporate member of Freie Universität Berlin and Humboldt-Universität Zu Berlin, Berlin, Germany. <sup>8</sup>Genomics Technology Platform, Max Delbrück Center for Molecular Medicine in the Helmholtz Association (MDC), Berlin, Germany. <sup>9</sup>Laboratory of Molecular Neuroscience, German Center for Neurodegenerative Diseases (DZNE) within the Helmholtz Association, Berlin, Germany. <sup>10</sup>Cluster of Excellence, NeuroCure, Berlin, Germany. <sup>11</sup>Institute for Biology and Genetics, Freie Universität Berlin, Berlin, Germany. <sup>12</sup>Berlin Institute of Health (BIH), Berlin, Germany.

Received: 9 March 2022 Accepted: 16 June 2022

Published online: 02 July 2022

### References

- Keren-Shaul H, Spinrad A, Weiner A, Matcovitch-Natan O, Dvir-Szternfeld R, Ulland TK, et al. A unique microglia type associated with restricting development of Alzheimer's disease. *Cell*. 2017;169(7):1276–90.e17.
- Heppner FL, Ransohoff RM, Becher B. Immune attack: the role of inflammation in Alzheimer disease. *Nat Rev Neurosci*. 2015;16(6):358–72.
- LaRocca TJ, Cavalier AN, Roberts CM, Lemieux MR, Ramesh P, Garcia MA, et al. Amyloid beta acts synergistically as a pro-inflammatory cytokine. *Neurobiol Dis*. 2021;159: 105493.
- Montoliu-Gaya L, Mulder SD, Herrebout MAC, Baayen JC, Villegas S, Veerhuis R. A $\beta$ -oligomer uptake and the resulting inflammatory response in adult human astrocytes are precluded by an anti-A $\beta$  single chain variable fragment in combination with an apoE mimetic peptide. *Mol Cell Neurosci*. 2018;89:49–59.
- Vuillermot S, Joodmardi E, Perlmann T, Ove Ögren S, Feldon J, Meyer U. Prenatal immune activation interacts with genetic <em>Nurr1</em> deficiency in the development of attentional impairments. *J Neurosci*. 2012;32(2):436–51.
- Krstic D, Knuesel I. Deciphering the mechanism underlying late-onset Alzheimer disease. *Nat Rev Neurol*. 2013;9(1):25–34.
- Krstic D, Madhusudan A, Doehner J, Vogel P, Notter T, Imhof C, et al. Systemic immune challenges trigger and drive Alzheimer-like neuropathology in mice. *J Neuroinflammation*. 2012;9:151.
- Genome-wide association study of 14,000 cases of seven common diseases and 3,000 shared controls. *Nature*. 2007;447(7145):661–78.
- Li Q, Liu Y, Sun M. Autophagy and Alzheimer's disease. *Cell Mol Neurobiol*. 2017;37(3):377–88.
- Ulland TK, Song WM, Huang SC, Ulrich JD, Sergushichev A, Beatty WL, et al. TREM2 maintains microglial metabolic fitness in Alzheimer's disease. *Cell*. 2017;170(4):649–63.e13.
- Saitoh T, Fujita N, Jang MH, Uematsu S, Yang BG, Satoh T, et al. Loss of the autophagy protein Atg16L1 enhances endotoxin-induced IL-1 $\beta$  production. *Nature*. 2008;456(7219):264–8.
- Lucin KM, O'Brien CE, Bieri G, Czirr E, Mosher KI, Abbey RJ, et al. Microglial beclin 1 regulates retromer trafficking and phagocytosis and is impaired in Alzheimer's disease. *Neuron*. 2013;79(5):873–86.
- Pickford F, Masliah E, Britschgi M, Lucin K, Narasimhan R, Jaeger PA, et al. The autophagy-related protein beclin 1 shows reduced expression in early Alzheimer disease and regulates amyloid  $\beta$  accumulation in mice. *J Clin Investig*. 2008;118(6):2190–9.
- Houtman J, Freitag K, Gimber N, Schmoranzler J, Heppner FL, Jendrach M. Beclin1-driven autophagy modulates the inflammatory response of microglia via NLRP3. *Embo J*. 2019;38(4).
- Swanson KV, Deng M, Ting JP. The NLRP3 inflammasome: molecular activation and regulation to therapeutics. *Nat Rev Immunol*. 2019;19(8):477–89.
- Shi CS, Shenderov K, Huang NN, Kabat J, Abu-Asab M, Fitzgerald KA, et al. Activation of autophagy by inflammatory signals limits IL-1 $\beta$  production by targeting ubiquitinated inflammasomes for destruction. *Nat Immunol*. 2012;13(3):255–63.
- Heneka MT, Kummer MP, Stutz A, Delekate A, Schwartz S, Vieira-Saecker A, et al. NLRP3 is activated in Alzheimer's disease and contributes to pathology in APP/PS1 mice. *Nature*. 2013;493(7434):674–8.
- Ising C, Venegas C, Zhang S, Scheiblich H, Schmidt SV, Vieira-Saecker A, et al. NLRP3 inflammasome activation drives tau pathology. *Nature*. 2019;575(7784):669–73.
- Lee JW, Nam H, Kim LE, Jeon Y, Min H, Ha S, et al. TLR4 (toll-like receptor 4) activation suppresses autophagy through inhibition of FOXO3 and impairs phagocytic capacity of microglia. *Autophagy*. 2019;15(5):753–70.
- Eisenberg T, Knauer H, Schauer A, Büttner S, Ruckenstein C, Carmona-Gutierrez D, et al. Induction of autophagy by spermidine promotes longevity. *Nat Cell Biol*. 2009;11(11):1305–14.
- Pietrocola F, Lachkar S, Enot DP, Niso-Santano M, Bravo-San Pedro JM, Sica V, et al. Spermidine induces autophagy by inhibiting the acetyltransferase EP300. *Cell Death Differ*. 2015;22(3):509–16.
- Eisenberg T, Abdellatif M, Schroeder S, Primesnig U, Stekovic S, Pendl T, et al. Cardioprotection and lifespan extension by the natural polyamine spermidine. *Nat Med*. 2016;22(12):1428–38.

23. Madeo F, Eisenberg T, Pietrocola F, Kroemer G. Spermidine in health and disease. *Science* (New York, NY). 2018;359(6374).
24. Yang Q, Zheng C, Cao J, Cao G, Shou P, Lin L, et al. Spermidine alleviates experimental autoimmune encephalomyelitis through inducing inhibitory macrophages. *Cell Death Differ*. 2016;23(11):1850–61.
25. Guo X, Harada C, Namekata K, Kimura A, Mitamura Y, Yoshida H, et al. Spermidine alleviates severity of murine experimental autoimmune encephalomyelitis. *Invest Ophthalmol Vis Sci*. 2011;52(5):2696–703.
26. Sharma S, Kumar P, Deshmukh R. Neuroprotective potential of spermidine against rotenone induced Parkinson's disease in rats. *Neurochem Int*. 2018;116:104–11.
27. Xu TT, Li H, Dai Z, Lau GK, Li BY, Zhu WL, et al. Spermidine and spermine delay brain aging by inducing autophagy in SAMP8 mice. *Aging*. 2020;12(7):6401–14.
28. Liu R, Li X, Ma H, Yang Q, Shang Q, Song L, et al. Spermidine endows macrophages anti-inflammatory properties by inducing mitochondrial superoxide-dependent AMPK activation, Hif-1 $\alpha$  upregulation and autophagy. *Free Radical Biol Med*. 2020;161:339.
29. Choi YH, Park HY. Anti-inflammatory effects of spermidine in lipopolysaccharide-stimulated BV2 microglial cells. *J Biomed Sci*. 2012;19(1):31.
30. Jeong JW, Cha HJ, Han MH, Hwang SJ, Lee DS, Yoo JS, et al. Spermidine protects against oxidative stress in inflammation models using macrophages and zebrafish. *Biomolecules Therapeutics*. 2018;26(2):146–56.
31. Liang Y, Piao C, Beuschel CB, Toppe D, Kollipara L, Bogdanow B, et al. eIF5A hypusination, boosted by dietary spermidine, protects from premature brain aging and mitochondrial dysfunction. *Cell Rep*. 2021;35(2):108941.
32. Schroeder S, Hofer SJ, Zimmermann A, Pechlaner R, Dammbroeck C, Pendl T, et al. Dietary spermidine improves cognitive function. *Cell Rep*. 2021;35(2):108985.
33. Gassen NC, Papias J, Bajaj T, Emanuel J, Dethloff F, Chua RL, et al. SARS-CoV-2-mediated dysregulation of metabolism and autophagy uncovers host-targeting antivirals. *Nat Commun*. 2021;12(1):3818.
34. Radde R, Bolmont T, Kaeser SA, Coomaraswamy J, Lindau D, Stoltze L, et al. A $\beta$ 42-driven cerebral amyloidosis in transgenic mice reveals early and robust pathology. *EMBO Rep*. 2006;7(9):940–6.
35. Kawarabayashi T, Younkin LH, Saido TC, Shoji M, Ashe KH, Younkin SG. Age-dependent changes in brain, CSF, and plasma amyloid (beta) protein in the Tg2576 transgenic mouse model of Alzheimer's disease. *J Neurosci*. 2001;21(2):372–81.
36. Stine WB, Jungbauer L, Yu C, LaDu MJ. Preparing synthetic A $\beta$  in different aggregation states. *Methods Mol Biol* (Clifton, NJ). 2011;670:13–32.
37. Hoffmann C, Sanseverino R, Morabito G, Logan C, Vabulas RM, Ulusoy A, et al. Synapsin condensates recruit alpha-synuclein. *J Mol Biol*. 2021;433(12):166961.
38. Schneeberger S, Kim SJ, Eede P, Boltengagen A, Braeuning C, Andreadou M, et al. The neuroinflammatory interleukin-12 signaling pathway drives Alzheimer's disease-like pathology by perturbing oligodendrocyte survival and neuronal homeostasis. *bioRxiv*. 2021.04.25.441313.
39. George L, Winship A, Sorby K, Dimitriadis E, Menkhorst E. Profilin-1 is dysregulated in endometrioid (type I) endometrial cancer promoting cell proliferation and inhibiting pro-inflammatory cytokine production. *Biochem Biophys Res Commun*. 2020;531(4):459–64.
40. Amato A, Mulè F. Protective potential of glucagon like peptide 2 (GLP-2) against the neurodegeneration. *Neural Regen Res*. 2019;14(11):1901–2.
41. Wang T, Wang Z, Yang P, Xia L, Zhou M, Wang S, et al. PER1 prevents excessive innate immune response during endotoxin-induced liver injury through regulation of macrophage recruitment in mice. *Cell Death Dis*. 2016;7(4):e2176.
42. Sheng S, Kang Y, Guo Y, Pu Q, Cai M, Tu Z. Overexpression of Sirt3 inhibits lipid accumulation in macrophages through mitochondrial IDH2 deacetylation. *Int J Clin Exp Pathol*. 2015;8(8):9196–201.
43. Liu P, Huang G, Wei T, Gao J, Huang C, Sun M, et al. Sirtuin 3-induced macrophage autophagy in regulating NLRP3 inflammasome activation. *Biochimica et Biophysica Acta (BBA) Mol Basis Dis*. 2018;1864(3):764–77.
44. Owlett L, Olschowka JA, Elliott MR, O'Banion MK. AXL activation leads to reduced amyloid plaque deposition in APP/PS-1 mice. *Alzheimers Dement*. 2020;16(S2):e046330.
45. Yanaizu M, Washizu C, Nukina N, Satoh J-I, Kino Y. CELF2 regulates the species-specific alternative splicing of TREM2. *Sci Rep*. 2020;10(1):17995.
46. Bhukel A, Madeo F, Sigrist SJ. Spermidine boosts autophagy to protect from synapse aging. *Autophagy*. 2017;13(2):444–5.
47. Redondo-Castro E, Faust D, Fox S, Baldwin AG, Osborne S, Haley MJ, et al. Development of a characterised tool kit for the interrogation of NLRP3 inflammasome-dependent responses. *Sci Rep*. 2018;8(1):5667.
48. De Risi M, Torromino G, Tufano M, Moriceau S, Pignataro A, Rivagorda M, et al. Mechanisms by which autophagy regulates memory capacity in ageing. *Aging Cell*. 2020;19(9):e13189.
49. Busche MA, Konnerth A. Neuronal hyperactivity—a key defect in Alzheimer's disease? *BioEssays*. 2015;37(6):624–32.
50. De Strooper B, Karran E. The cellular phase of Alzheimer's disease. *Cell*. 2016;164(4):603–15.
51. Ben-Nejma IRH, Keliris AJ, Daans J, Ponsaerts P, Verhoye M, Van der Linden A, et al. Increased soluble amyloid-beta causes early aberrant brain network hypersynchronisation in a mature-onset mouse model of amyloidosis. *Acta Neuropathol Commun*. 2019;7(1):180.
52. Huang Y, Happonen KE, Burrola PG, O'Connor C, Hah N, Huang L, et al. Microglia use TAM receptors to detect and engulf amyloid  $\beta$  plaques. *Nat Immunol*. 2021;22(5):586–94.
53. Patel NS, Paris D, Mathura V, Quadros AN, Crawford FC, Mullan MJ. Inflammatory cytokine levels correlate with amyloid load in transgenic mouse models of Alzheimer's disease. *J Neuroinflammation*. 2005;2:9.
54. Mouton PR, Chachich ME, Quigley C, Spangler E, Ingram DK. Caloric restriction attenuates amyloid deposition in middle-aged dtg APP/PS1 mice. *Neurosci Lett*. 2009;464(3):184–7.
55. Farr SA, Roesler E, Niehoff ML, Roby DA, McKee A, Morley JE. Metformin improves learning and memory in the SAMP8 mouse model of Alzheimer's disease. *J Alzheimers Dis*. 2019;68(4):1699–710.
56. Kaeberlein M, Galvan V. Rapamycin and Alzheimer's disease: time for a clinical trial? *Sci Transl Med*. 2019;11(476).
57. Franco-Bocanegra DK, McAuley C, Nicoll JAR, Boche D. Molecular mechanisms of microglial motility: changes in ageing and Alzheimer's disease. *Cells*. 2019;8(6):639.
58. Anwar S, Rivest S. Alzheimer's disease: microglia targets and their modulation to promote amyloid phagocytosis and mitigate neuroinflammation. *Expert Opin Ther Targets*. 2020;24(4):331–44.
59. Krabbe G, Halle A, Matyash V, Rinnenthal JL, Eom GD, Bernhardt U, et al. Functional impairment of microglia coincides with beta-amyloid deposition in mice with Alzheimer-like pathology. *PLoS ONE*. 2013;8(4):e60921.
60. Ito D, Ito H, Ideta T, Kanbe A, Ninomiya S, Shimizu M. Systemic and topical administration of spermidine accelerates skin wound healing. *Cell Commun Signal*. 2021;19(1):36.
61. Li G, Ding H, Yu X, Meng Y, Li J, Guo Q, et al. Spermidine suppresses inflammatory DC function by activating the FOXO3 pathway and counteracts autoimmunity. *iScience*. 2020;23(1):100807.
62. Pepe G, De Maglie M, Minoli L, Villa A, Maggi A, Vegeto E. Selective proliferative response of microglia to alternative polarization signals. *J Neuroinflammation*. 2017;14(1):236.
63. Pelucchi S, Stringhri R, Marcello E. Dendritic spines in Alzheimer's disease: how the actin cytoskeleton contributes to synaptic failure. *Int J Mol Sci*. 2020;21(3):908.
64. Chi CL, Zhang SA, Liu Z, Chang MX, Wang H, Huang Y. Research on the role of GLP-2 in the central nervous system EPK signal transduction pathway of mice with vascular dementia. *Eur Rev Med Pharmacol Sci*. 2017;21(1):131–7.
65. Song S, Li B, Jia Z, Guo L. Sirtuin 3 mRNA expression is downregulated in the brain tissues of Alzheimer's disease patients: a bioinformatic and data mining approach. *Med Sci Monit*. 2020;26:e923547.
66. Sakai T, Tamura T, Kitamoto T, Kidokoro Y. A clock gene, period, plays a key role in long-term memory formation in *Drosophila*. *Proc Natl Acad Sci U S A*. 2004;101(45):16058–63.
67. Jilg A, Lesny S, Peruzki N, Schwegler H, Selbach O, Dehghani F, et al. Temporal dynamics of mouse hippocampal clock gene expression support memory processing. *Hippocampus*. 2010;20(3):377–88.
68. Cao R, Li S, Yin J, Guo L, Shi J. Sirtuin 3 promotes microglia migration by upregulating CX3CR1. *Cell Adh Migr*. 2019;13(1):228–34.
69. Wirth M, Benson G, Schwarz C, Kobe T, Grittner U, Schmitz D, et al. The effect of spermidine on memory performance in older adults at risk for dementia: a randomized controlled trial. *Cortex*. 2018;109:181–8.

70. Wirth M, Schwarz C, Benson G, Horn N, Buchert R, Lange C, et al. Effects of spermidine supplementation on cognition and biomarkers in older adults with subjective cognitive decline (SmartAge)-study protocol for a randomized controlled trial. *Alzheimer's Res Therapy*. 2019;11(1):36.
71. Schwarz C, Horn N, Benson G, Wrachtrup Calzado I, Wurdack K, Pechlaner R, et al. Spermidine intake is associated with cortical thickness and hippocampal volume in older adults. *Neuroimage*. 2020;221: 117132.

### **Publisher's Note**

Springer Nature remains neutral with regard to jurisdictional claims in published maps and institutional affiliations.

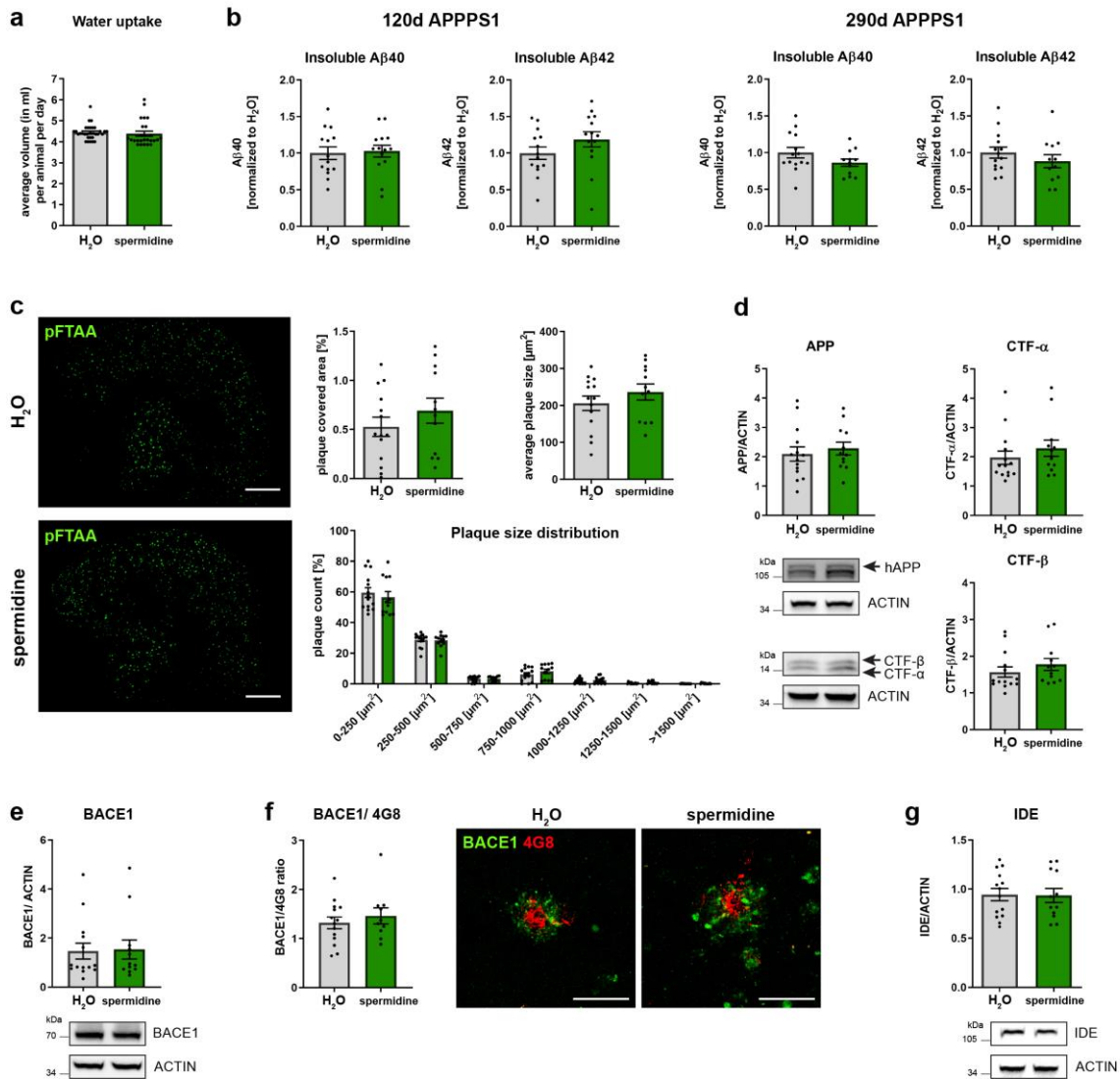
**Ready to submit your research? Choose BMC and benefit from:**

- fast, convenient online submission
- thorough peer review by experienced researchers in your field
- rapid publication on acceptance
- support for research data, including large and complex data types
- gold Open Access which fosters wider collaboration and increased citations
- maximum visibility for your research: over 100M website views per year

**At BMC, research is always in progress.**

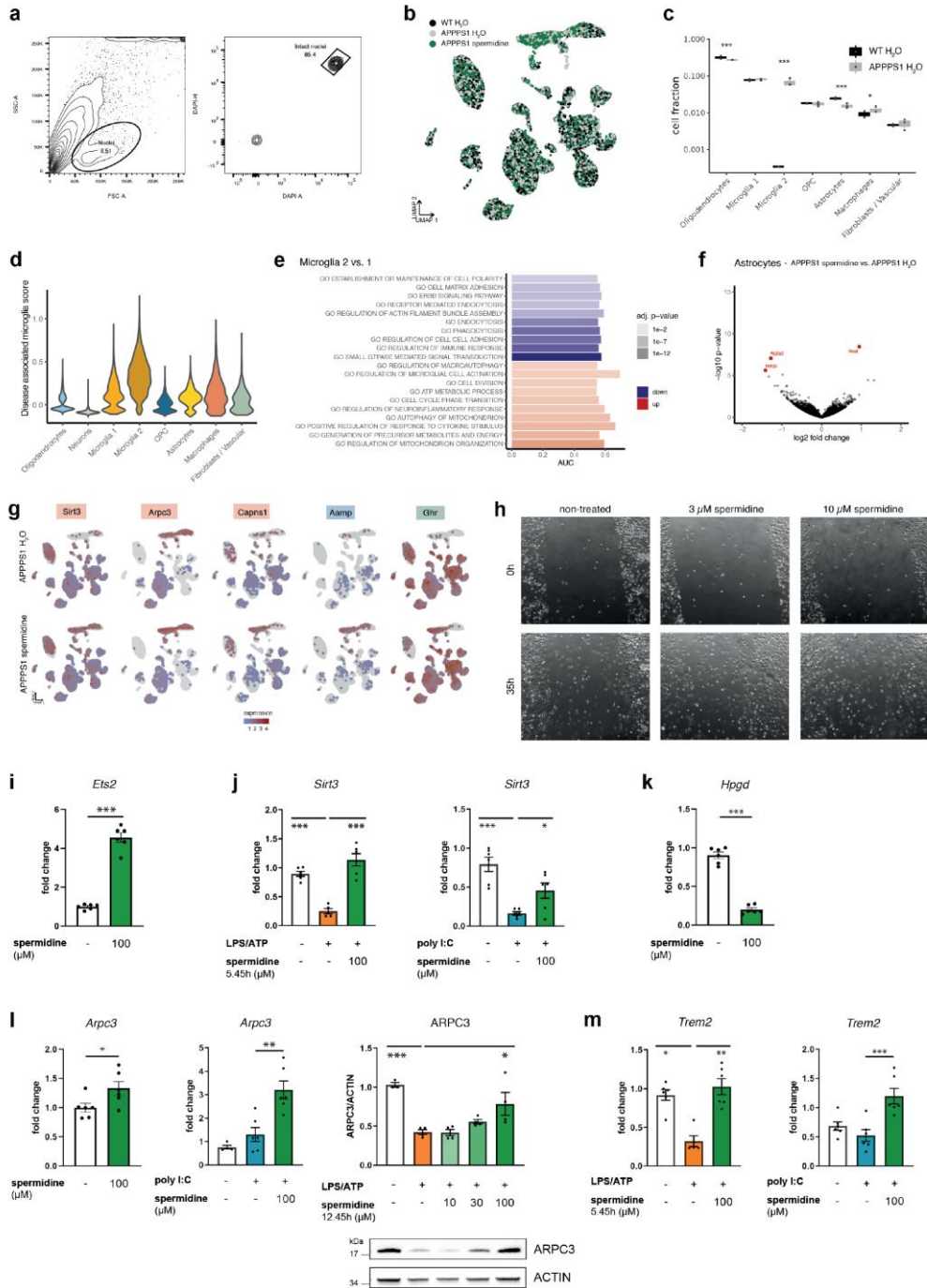
Learn more [biomedcentral.com/submissions](https://biomedcentral.com/submissions)





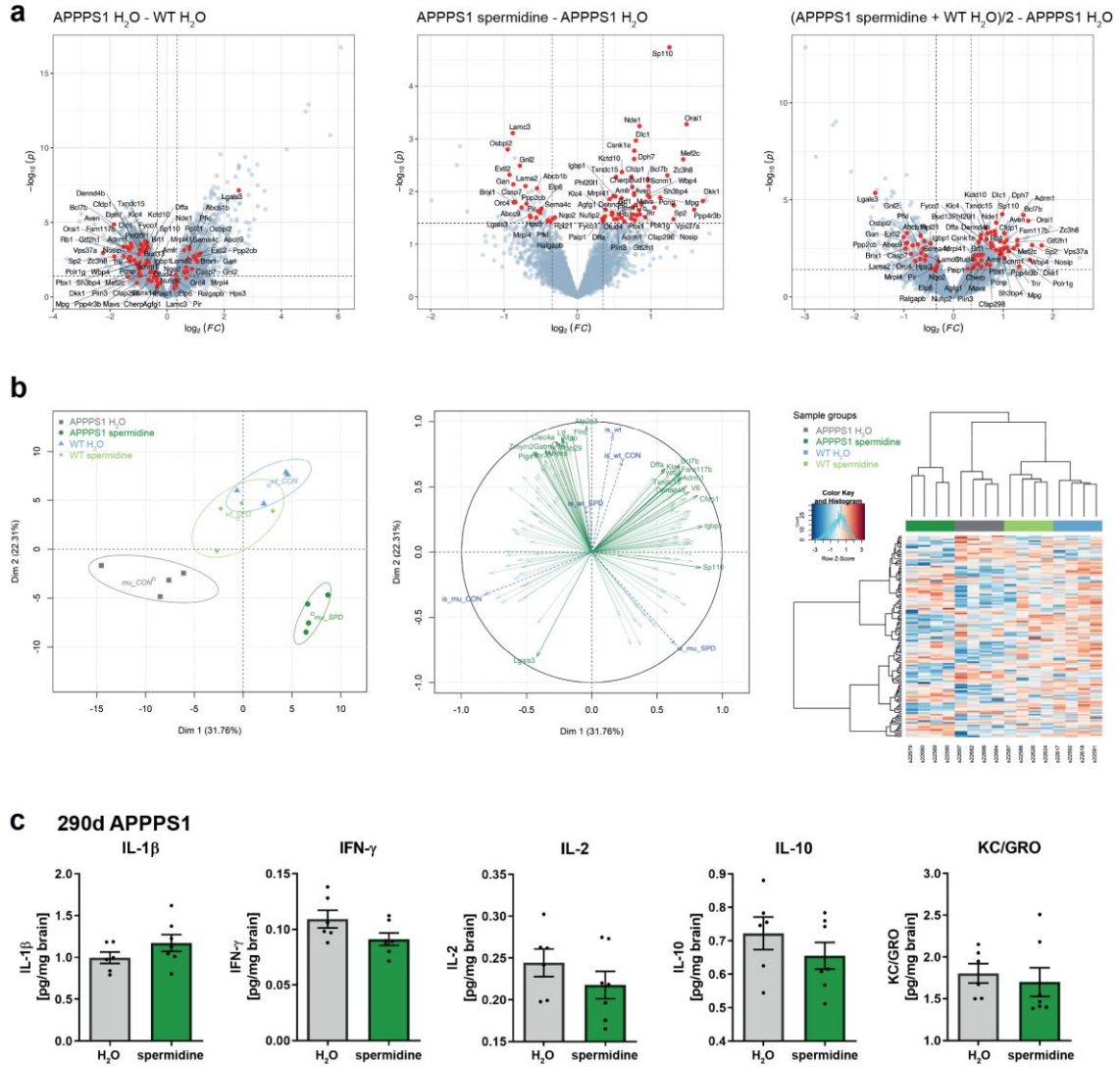
**Fig. S1**

APPPS1 mice were treated with 3 mM spermidine via their drinking water as depicted in Fig. 1a and analyzed at an age of 120 or 290 days (mixed sex). Spermidine-treated APPPS1 mice were compared to non-treated controls (H<sub>2</sub>O). **a** The average volume in ml per animal per day was calculated based on the volume that was drunk in an interval of 3.5 days per cage. APPPS1 H<sub>2</sub>O (n = 32), APPPS1 spermidine (n = 26); Mann-Whitney-U test. **b** The A $\beta$ 40 and A $\beta$ 42 content was measured in the SDS (insoluble) fraction of brain homogenates of 120- or 290-day-old spermidine-treated mice and water controls using electrochemiluminescence (MesoScale Discovery panel). Values were normalized to water controls. 120d APPPS1 H<sub>2</sub>O (n = 14), 120d APPPS1 spermidine (n = 14), 290d APPPS1 H<sub>2</sub>O (n = 14), 290d APPPS1 spermidine (n = 12); two-tailed t-test. **c** A $\beta$  plaques in tissue sections of 290-day-old mice were stained with pFTAA and the plaque covered area (%), the average plaque size and a plaque size distribution of the cortex was determined by ImageJ analysis; two-tailed t-test. The number of plaques of each indicated size is displayed as a percentage of the total number of plaques detected; Mann-Whitney-U test. APPPS1 H<sub>2</sub>O (n = 14), APPPS1 spermidine (n = 12). Scale bar = 1 mm. **d** The levels of APP, CTF- $\alpha$  and CTF- $\beta$  were determined by western blot of the TX (membrane-bound) protein fraction of 290-day-old spermidine-treated APPPS1 mice. Representative western blot images are shown. APPPS1 H<sub>2</sub>O (n = 14), APPPS1 spermidine (n = 12); Mann-Whitney-U test. **e** The levels of BACE1 were determined by western blot of the TX (membrane-bound) protein fraction of 290-day-old spermidine-treated APPPS1 mice. Representative western blot images are shown. APPPS1 H<sub>2</sub>O (n = 14), APPPS1 spermidine (n = 12); Mann-Whitney-U test. **f** Tissue sections of 290-day-old mice were stained for BACE1 (green) and 4G8-positive plaques (red). The BACE1-covered area normalized to 4G8-positive area was determined. Scale bar = 50  $\mu$ m. APPPS1 H<sub>2</sub>O (n = 14), APPPS1 spermidine (n = 12); two-tailed t-test. **g** The levels of IDE were determined by western blot of the TX (membrane-bound) protein fraction of 290-day-old spermidine-treated APPPS1 mice. Representative western blot images are shown. APPPS1 H<sub>2</sub>O (n = 14), APPPS1 spermidine (n = 12); two-tailed t-test.



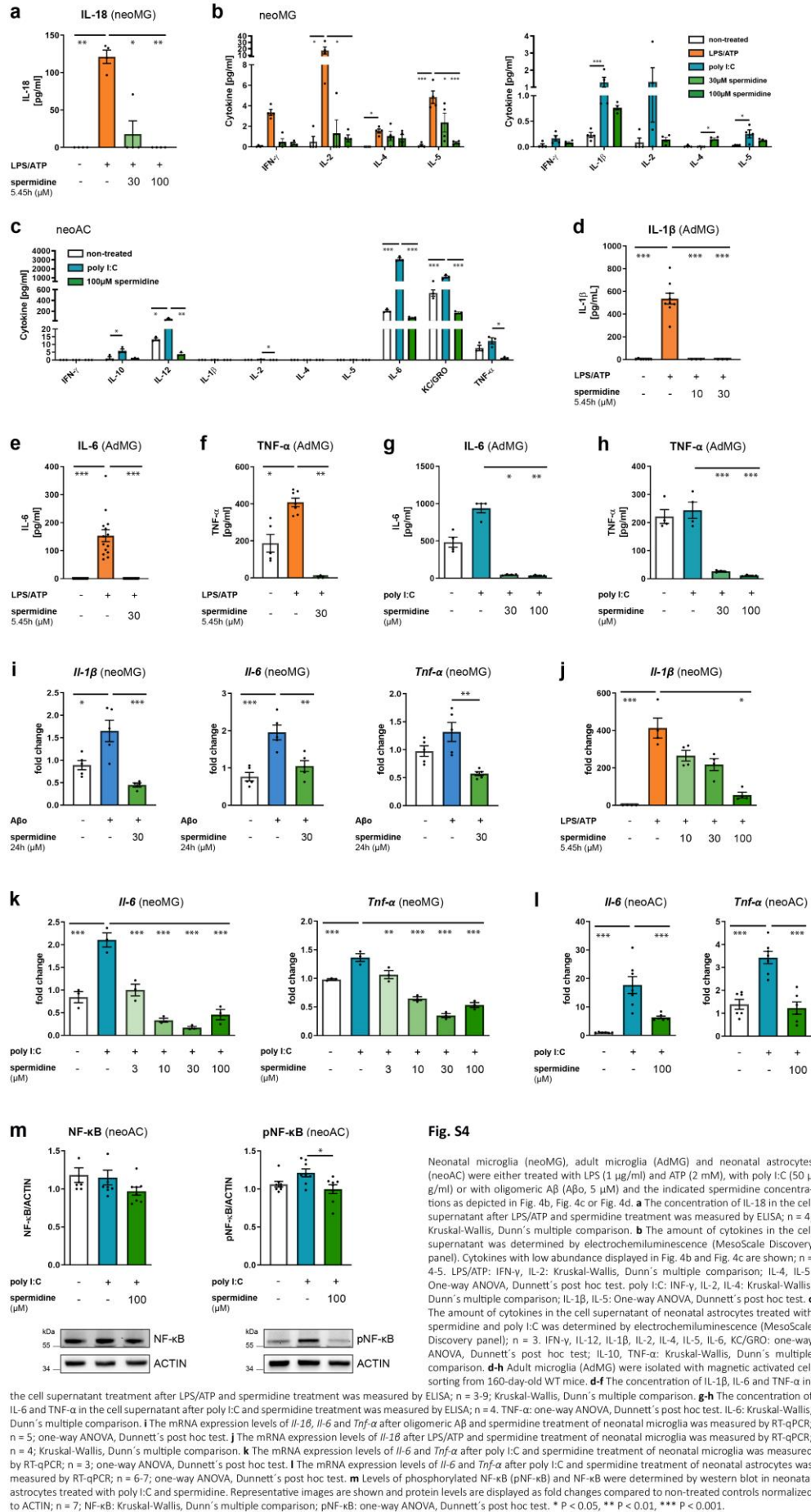
**Fig. S2**

Male APPPS1 mice were treated with 3 mM spermidine via their drinking water and analyzed at an age of 180 days. **a** Whole hemisphere homogenates were stained with DAPI and intact DAPI-stained nuclei were sorted using a FSC/SSC based gate to exclude debris followed by exclusion of damaged nuclei in a DAPI-A/DAPI-H for subsequent single nuclei sequencing. **b** UMAP embedding of the snRNAseq data with genotypes indicated. **c** Cluster abundance in APPPS1 H<sub>2</sub>O and WT H<sub>2</sub>O mice. P-values from mixed-effects binomial model. **d** Violin plot of a gene signature score for disease-associated microglia (using *ApoE*, *Axl*, *B2m*, *Ccl6*, *Ccl6*, *Ccl6*, *Cd9*, *Clec7a*, *Csf1*, *Cst7*, *Ctsb*, *Ctsd*, *Fth1*, *Irgax*, *Lyz2*, *Timp2*, *Trem2* and *Tyrbp*). **e** Selected terms from a gene set enrichment analysis of differential expression between microglia clusters 1 and 2 using tmod. **f** Volcano plot of genes differentially expressed in astrocytes of spermidine-treated APPPS1 versus H<sub>2</sub>O APPPS1 mice. Genes with adj. p-value < 0.01 are highlighted in red and top 5 up- and down-regulated genes are indicated. **g** Expression of *Sirt3*, *Arpc3*, *Capns1*, *Aamp* and *Ghr* in spermidine-treated APPPS1 (bottom) and H<sub>2</sub>O APPPS1 mice (top). Color scale indicates normalized expression, grey dots represent no data. **h** Representative images of a wound healing/scratch assay performed with spermidine-treated neonatal microglia at time point 0 h and 35 h. Quantification is shown in Fig. 1h. **i** Neonatal microglia were treated with 100 μM spermidine for 6 h and the gene expression of *Ets2* was assessed by RT-qPCR. Its expression was normalized to *Actin* and displayed as fold change compared to non-treated control cells; n = 6, two-tailed t-test. **j** Neonatal microglia were treated with the indicated concentrations of spermidine in combination with LPS (1 μg/ml) and ATP (2 mM) or with poly I:C (50 μg/ml) and *Sirt3* was assessed by RT-qPCR (right panels), normalized to *Actin* and displayed as fold change compared to non-treated control cells; n = 5-6, one-way ANOVA, Dunnett's post hoc test. **k** Neonatal microglia were treated with 100 μM spermidine for 6 h and the gene expression of *Hpgd* was assessed by RT-qPCR. Its expression was normalized to *Actin* and displayed as fold change compared to non-treated control cells; n = 6, two-tailed t-test. **l** Neonatal microglia were treated with the indicated amount of spermidine in combination with LPS (1 μg/ml) and ATP (2 mM) for 5.45 h for qPCR analysis and for 12.45 h for western blot analysis. The gene expression was assessed by RT-qPCR (left panels) and the *Arpc3* expression was normalized to *Actin* and displayed as fold change compared to non-treated control cells; n = 5-6. ARPC3 protein levels were determined by western blot and normalized to ACTIN. Representative images are shown and values are displayed as fold changes compared to non-treated cells; n = 4, one-way ANOVA, Dunnett's post hoc test. **m** Neonatal microglia were treated with the indicated concentrations of spermidine in combination with LPS (1 μg/ml) and ATP (2 mM) or with poly I:C (50 μg/ml) and the gene expression of *Trem2* was assessed by RT-qPCR. Its expression was normalized to *Actin* and displayed as fold change compared to non-treated control cells; n = 5-6. LPS/ATP: Kruskal-Wallis, Dunn's multiple comparison; poly I:C: one-way ANOVA, Dunnett's post hoc test. \* P < 0.05, \*\* P < 0.01, \*\*\* P < 0.001.



**Fig. S3**

**a** Volcano plots for three contrasts: contrast 1 = APPPS1 H<sub>2</sub>O – WT H<sub>2</sub>O (AD model effect, left panel), contrast 2 = APPPS1 spermidine – APPPS1 H<sub>2</sub>O (spermidine effect, central panel), and contrast 5 = (contrast 2 – contrast 1)/2 (spermidine anti-AD effect, right panel). On all three plots proteins that are simultaneously significantly regulated ( $\alpha = 0.04$ ) in two contrasts, contrast 2 (spermidine effect) and contrast 5 (spermidine anti-AD effect), are labelled. Dashed horizontal line shows the significance level use for feature selection. Vertical dashed lines show  $\log_2$ FC threshold = median SD of linear modelling. **b** Post hoc PCA analysis and hierarchical clustering using features significantly regulated ( $\alpha = 0.04$  and FC threshold = 1.27) in contrast 2 (spermidine effect). Left panel represents PCA score plot demonstrating clear separation of APPPS1 spermidine samples from APPPS1 H<sub>2</sub>O samples in the first two principal components (PCs). Middle panel represents the PCA loading plot and shows top 25 proteins correlation with the first two PCs. Right panel shows heatmap with results of hierarchical clustering of samples in the space of features regulated in contrast 2. **c** The content of the cytokines in the TBS (soluble) fraction of brain homogenates of male 290-day-old spermidine-treated APPPS1 mice was measured using electrochemiluminescence (MesoScale Discovery panel). APPPS1 H<sub>2</sub>O (n = 6), APPPS1 spermidine (n = 7). IL-1 $\beta$ , IFN- $\gamma$ , IL-2, IL-10: two-tailed t-test; KC/GRO: Mann-Whitney-U test.



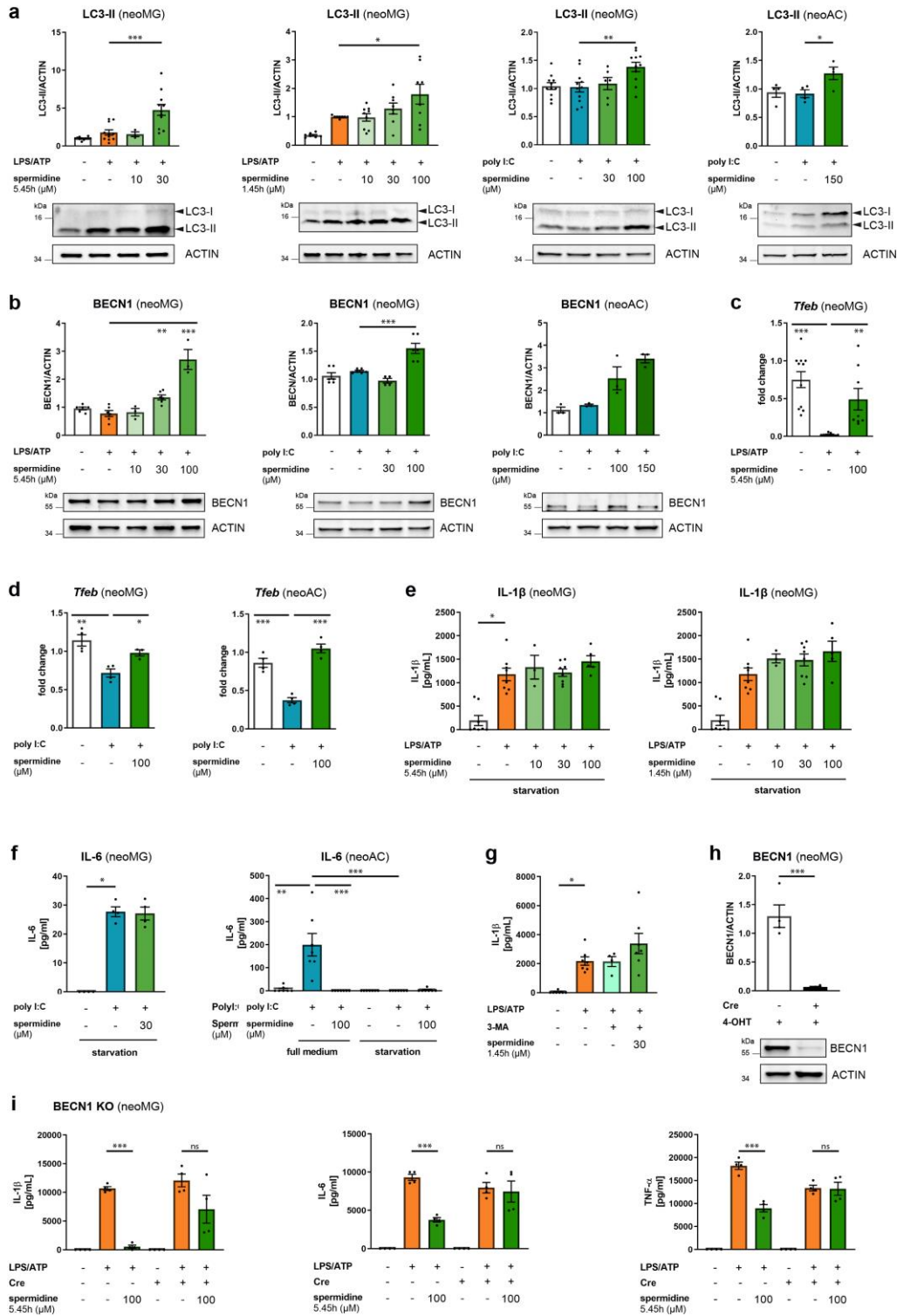


**Fig. S5**

Neonatal microglia (neoMG) and astrocytes (neoAC) were stimulated with LPS (1 μg/ml) and ATP (2 mM) or with poly I:C (50 μg/ml) and the indicated spermidine concentrations as depicted in Fig. 4b, 4c or 5a. **a** LC3-II levels were determined by western blot and normalized to ACTIN. Representative images are shown and values are displayed as fold changes compared to non-treated controls; microglia LPS/ATP 5.45h n = 3-11; microglia poly I:C n = 6-11; astrocytes poly I:C n = 4. One-way ANOVA, Dunnett's post hoc test. **b** BECN1 levels were determined by western blot and normalized to ACTIN. Representative images are shown and values are displayed as fold changes compared to non-treated controls; microglia LPS/ATP n = 3-6; microglia poly I:C n = 6; astrocytes poly I:C n = 3. neoMG: one-way ANOVA, Dunnett's post hoc test; neoAC: Kruskal-Wallis, Dunn's multiple comparison. **c-d** The gene expression of *Tfeb* was assessed by RT-qPCR. Its expression was normalized to *Actin* and displayed as fold change compared to non-treated control cells; microglia LPS/ATP n = 8-9; microglia poly I:C n = 3-4; astrocytes poly I:C n = 4. LPS/ATP: Kruskal-Wallis, Dunn's multiple comparison; poly I:C: one-way ANOVA, Dunnett's post hoc test. **e-f** Cells were stimulated in starvation medium HBSS and the IL-1β or IL-6 concentration in the cell supernatant was determined by ELISA; microglia LPS/ATP 5.45h n = 3-8; microglia LPS/ATP 1.45h n = 3-8; microglia poly I:C n = 4; astrocytes poly I:C n = 7. Kruskal-Wallis, Dunn's multiple comparison. **g** Neonatal microglia were stimulated as in Fig. 5a and 3-MA was added simultaneously with spermidine. The IL-1β concentration in the cell supernatant was determined by ELISA; n = 7; Kruskal-Wallis, Dunn's multiple comparison. **h** Neonatal BECN1<sup>fllox</sup>/CX3CR1<sup>CreERT2</sup> microglia positive or negative for Cre were treated with Tamoxifen and BECN1 levels were assessed by western blot and normalized to ACTIN. Representative images are shown and values are displayed as fold changes compared to non-treated controls; n = 4; two-tailed t-test. **i** Neonatal BECN1<sup>fllox</sup>/CX3CR1<sup>CreERT2</sup> microglia positive or negative for Cre were treated with Tamoxifen (4-OHT) and subsequently treated as depicted in Fig. 4b. The release of IL-1β, IL-6 and TNF-α was determined by ELISA; n = 3; two-tailed t-test. \* P < 0.05, \*\* P < 0.01, \*\*\* P < 0.001.

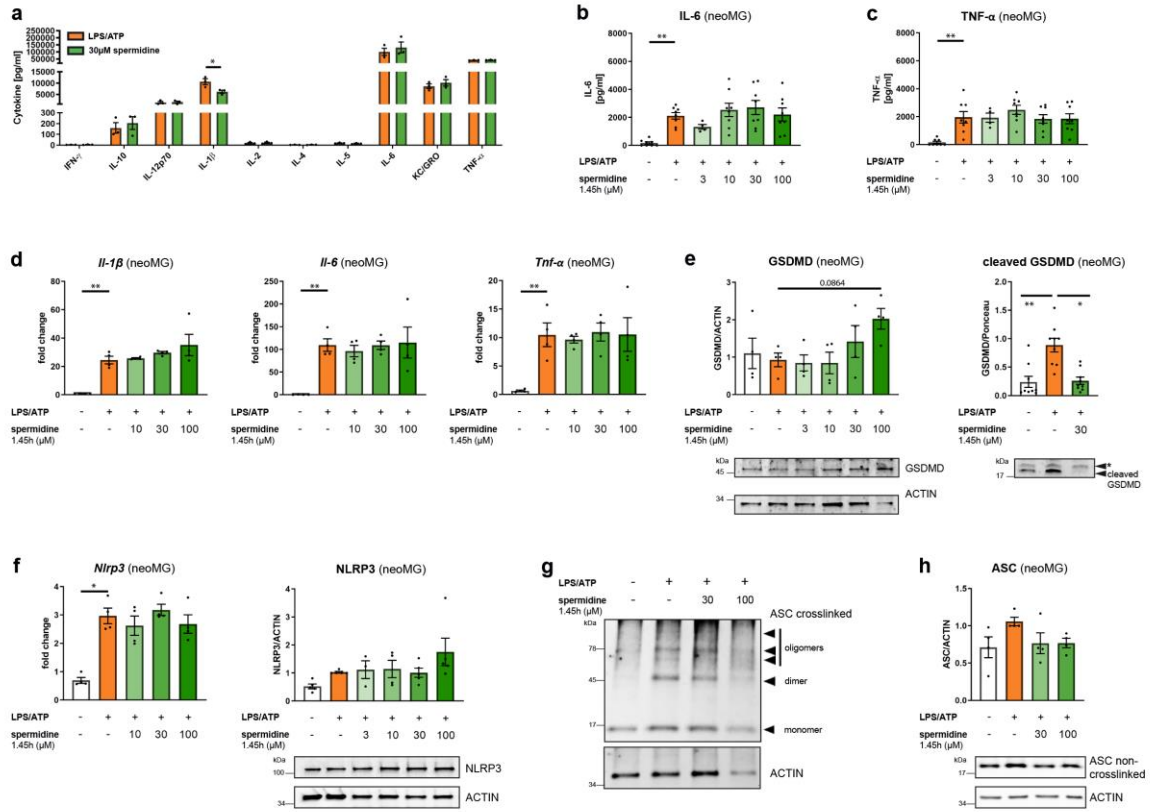


**Fig. S6**

Neonatal microglia (neoMG) were treated with LPS/ATP and spermidine as shown in Fig. 5a. **a** The amount of cytokines in the cell supernatant was determined by electrochemiluminescence (MesoScale Discovery panel);  $n = 3$ . IL-12, IL-1 $\beta$ , IL-2, IL-5, IL-6, KC/GRO, TNF- $\alpha$ : one-way ANOVA, Dunnett's post hoc test; IFN- $\gamma$ , IL-10, IL-4: Kruskal-Wallis, Dunn's multiple comparison. **b** The IL-6 concentration in the cell supernatant was determined by ELISA;  $n = 4-8$ ; Kruskal-Wallis, Dunn's multiple comparison. **c** The TNF- $\alpha$  concentration in the cell supernatant was determined by ELISA;  $n = 4-8$ ; Kruskal-Wallis, Dunn's multiple comparison. **d** The gene expression of *Il-1 $\beta$* , *Tnf- $\alpha$*  and *Il-6* was assessed by RT-qPCR. The expression was normalized to *Actin* and displayed as fold change compared to non-treated control cells;  $n = 4$ ; one-way ANOVA, Dunnett's post hoc test. **e** Cellular and cleaved GSDMD (C-terminal fragment) levels in the supernatant were determined by western blot (\* non-specific band). GSDMD was normalized to ACTIN ( $n = 4$ ) and the C-terminal fragment was normalized to whole protein content determined by Ponceau 5 staining ( $n = 9$ ). Values are displayed as fold changes compared to LPS/ATP-treated cells; one-way ANOVA, Dunnett's post hoc test for GSDMD and Kruskal-Wallis, Dunn's multiple comparison for cleaved GSDMD. **f** NLRP3 protein expression was determined by western blot and normalized to ACTIN. Representative images are shown and values are displayed as fold changes compared to LPS/ATP-treated cells;  $n = 3-5$ . The gene expression of *Nlrp3* was assessed by RT-qPCR. Its expression was normalized to *Actin* and displayed as fold change compared to non-treated control cells;  $n = 4$ ; Kruskal-Wallis, Dunn's multiple comparison. **g** Proteins were chemically cross-linked by DSS. ASC monomer and oligomers were visualized by western blot. **h** ASC monomer protein expression was determined by western blot and normalized to ACTIN. Representative images are shown and values are displayed as fold changes compared to LPS/ATP-treated cells;  $n = 4$ ; Kruskal-Wallis, Dunn's multiple comparison. \*  $P < 0.05$ , \*\*  $P < 0.01$ , \*\*\*  $P < 0.001$ .

## **10** LEBENSLAUF

Mein Lebenslauf wird aus datenschutzrechtlichen Gründen in der elektronischen Version meiner Arbeit nicht veröffentlicht.

# 11 PUBLIKATIONSLISTE

**Freitag K**, Sterczyk N, Wendlinger S, Obermayer B, Schulz J, Farztdinov V, Mülleder M, Ralser M, Houtman J, Fleck L, Braeuning C, Sansevrino R, Hoffmann C, Milovanovic D, Sigrist SJ, Conrad T, Beule D, Heppner FL, Jendrach M: Spermidine reduces neuroinflammation and soluble amyloid beta in an Alzheimer's disease mouse model. *J Neuroinflammation*. 2022 Jul 2;19(1):172. doi: 10.1186/s12974-022-02534-7. IF 9.6

**Freitag K**, Eede P, Ivanov A, Schneeberger S, Borodina T, Sauer S, Beule D, Heppner FL: Diverse but unique astrocytic phenotypes during embryonic stem cell differentiation, culturing and aging. *bioRxiv* 2021, submitted.08.02.454573; doi: <https://doi.org/10.1101/2021.08.02.454573>.

Preusse C, Eede P, Heinzeling L, **Freitag K**, Koll R, Froehlich W, Schneider U, Allenbach Y, Benveniste O, Schänzer A, Goebel HH, Stenzel W, Radke J: NanoString technology distinguishes anti-TIF-1<sub>+</sub> from anti-Mi-2<sub>+</sub> dermatomyositis patients. *Brain Pathol*. 2021 May;31(3):e12957. doi: 10.1111/bpa.12957. IF 7.6

Houtman J, **Freitag K**, Gimber N, Schmoranzler J, Heppner FL, Jendrach M: Beclin1-driven autophagy modulates the inflammatory response of microglia via NLRP3. *EMBO J*. 2019 Feb 15;38(4):e99430. doi: 10.15252/embj.201899430. Epub 2019 Jan 7. IF 9.9

Müller PM, Rademacher J, Bagshaw RD, Wortmann C, Barth C, van Unen J, Alp KM, Giudice G, Eccles RL, Heinrich LE, Pascual-Vargas P, Sanchez-Castro M, Brandenburg L, Mbamalu G, Tucholska M, Spatt L, Czajkowski MT, Welke RW, Zhang S, Nguyen V, Rustemi T, Trnka P, **Freitag K**, Larsen B, Popp O, Mertins P, Gingras AC, Roth FP, Colwill K, Bakal C, Pertz O, Pawson T, Petsalaki E, Rocks O. Systems analysis of RhoGEF and RhoGAP regulatory proteins reveals spatially organized RAC1 signalling from integrin adhesions. *Nat Cell Biol*. 2020 Apr;22(4):498-511. doi: 10.1038/s41556-020-0488-x. Epub 2020 Mar 23. IF 28.8

(Impact Factor = IF)

## 12 DANKSAGUNG

I would like to sincerely thank my first supervisor Frank Heppner for all his support, all motivational speeches whenever needed and all the trust along the way. Thanks for giving me the opportunity to develop a large technical and soft skill portfolio and for constantly supporting me in my scientific endeavors.

I would also like to express deep gratitude to my second supervisor Marina Jendrach for continuously working with me on this project and for all the fruitful discussions, all the scientific advice and for motivating me to grow beyond myself. Thanks for teaching me all the valuable scientific knowledge.

A huge thanks goes to my PhD girl team, Pascale Eede, Eileen Benke, Judith Houtman, Shirin Schneeberger and Alexander Haake for living with me through all ups and downs, for your continuous advice in any situation and all the fun moments in and outside the lab. Special thanks go to Alex for supporting me throughout my PhD, for all the mental support, for giving me an extra hand whenever I needed it, for making every joint experimental day a fun day and for all the excellent technical advice as well as all the adventures outside the lab. This endeavor would have not been the same without you.

I am also extremely grateful to all my students, especially Nele Sterczyk for working with me on this project for years but also to Sarah Wendlinger, Mascha Osang, Lara Fleck and Axel Fontanier for all your patience, motivation and hard work. You really inspired and motivated me every day. Thanks for always supporting even the craziest ideas I had.

A big thank you also to Paul and my family for supporting me in every step on the way to this PhD, for your continuous interest and encouragement and all the distractions whenever I needed them.

Many thanks also to all the people I have met along the way: all other lab members, collaborators and fellow PhD students, who sparked new ideas and made my scientific everyday life exciting and wonderful. All of you have made these years a unique and joyful experience.